NAVAL POSTGRADUATE SCHOOL

MONTEREY, CALIFORNIA

THESIS

AERODYNAMIC VALIDATION OF EMERGING PROJECTILE AND MISSILE CONFIGURATIONS

by

Tan Wei Chieh

December 2010

Thesis Advisor:	Max F. Platzer
Second Reader:	Garth V. Hobson

Approved for public release: distribution is unlimited

THIS PAGE INTENTIONALLY LEFT BLANK

REPORT DOCUMENTATION PAGE			*Form Approved OMB No. 0704-0188*
Public reporting burden for this collection of information is estimated to average 1 hour per response, including the time for reviewing instruction, searching existing data sources, gathering and maintaining the data needed, and completing and reviewing the collection of information. Send comments regarding this burden estimate or any other aspect of this collection of information, including suggestions for reducing this burden, to Washington headquarters Services, Directorate for Information Operations and Reports, 1215 Jefferson Davis Highway, Suite 1204, Arlington, VA 22202-4302, and to the Office of Management and Budget, Paperwork Reduction Project (0704-0188) Washington DC 20503.			
1. AGENCY USE ONLY ***(Leave blank)***	**2. REPORT DATE** December 2010	**3. REPORT TYPE AND DATES COVERED** Master's Thesis	
4. TITLE AND SUBTITLE Aerodynamic Validation of Emerging Projectile and Missile Configurations			**5. FUNDING NUMBERS**
6. AUTHOR(S) Tan Wei Chieh			
7. PERFORMING ORGANIZATION NAME(S) AND ADDRESS(ES) Naval Postgraduate School Monterey, CA 93943-5000			**8. PERFORMING ORGANIZATION REPORT NUMBER**
9. SPONSORING /MONITORING AGENCY NAME(S) AND ADDRESS(ES) N/A			**10. SPONSORING/MONITORING AGENCY REPORT NUMBER**
11. SUPPLEMENTARY NOTES The views expressed in this thesis are those of the author and do not reflect the official policy or position of the Department of Defense or the U.S. Government. IRB Protocol number ____N/A_____.			
12a. DISTRIBUTION / AVAILABILITY STATEMENT Approved for public release: distribution is unlimited			**12b. DISTRIBUTION CODE**
13. ABSTRACT (maximum 200 words) The M549 projectile has been analyzed using two different aerodynamic codes. The semi-empirical AP05 code has provided a very fast way to obtain results. The CFX code, based on the numerical solution of the full Navier-Stokes equations, took about four hours for one data point. The comparison between the AP05 and CFX computed total drag coefficient shows a difference of about 30 percent in the high subsonic range, good agreement in the transonic region, but a difference of 22 percent at M=1.2, decreasing to zero at M=3.			
14. SUBJECT TERMS Validation of emerging projectile and missile configurations			**15. NUMBER OF PAGES** 109
			16. PRICE CODE
17. SECURITY CLASSIFICATION OF REPORT Unclassified	**18. SECURITY CLASSIFICATION OF THIS PAGE** Unclassified	**19. SECURITY CLASSIFICATION OF ABSTRACT** Unclassified	**20. LIMITATION OF ABSTRACT** UU

NSN 7540-01-280-5500 Standard Form 298 (Rev. 2-89)
Prescribed by ANSI Std. 239-18

THIS PAGE INTENTIONALLY LEFT BLANK

Approved for public release: distribution is unlimited

AERODYNAMIC VALIDATION OF EMERGING PROJECTILE AND MISSILE CONFIGURATIONS

Tan Wei Chieh
Captain, Singapore Armed Forces
Electrical Engineer
National University of Singapore, 2000

Submitted in partial fulfillment of the
requirements for the degree of

MASTER OF SCIENCE IN MECHANICAL ENGINEERING

from the

NAVAL POSTGRADUATE SCHOOL
December 2010

Author: Tan Wei Chieh

Approved by: Max F. Platzer
Thesis Advisor

Garth V. Hobson
Second Reader

Knox T. Millsaps
Chairman, Department of Mechanical Engineering and Aeronautical Engineering

THIS PAGE INTENTIONALLY LEFT BLANK

ABSTRACT

The M549 projectile has been analyzed using two different aerodynamic codes. The semi-empirical AP05 code has provided a very fast way to obtain results. The CFX code, based on the numerical solution of the full Navier-Stokes equations, took about four hours for one data point. The comparison between the AP05 and CFX computed total drag coefficient shows a difference of about 30 percent in the high subsonic range, good agreement in the transonic region, but a difference of 22 percent at M=1.2, decreasing to zero at M=3.

THIS PAGE INTENTIONALLY LEFT BLANK

TABLE OF CONTENTS

LIST OF FIGURES

LIST OF ACRONYMS AND ABBREVIATIONS

a = speed of sound

C_{Df} = skin friction drag coefficient

c_p = specific heat at constant pressure

c_v = specific heat at constant volume

d = diameter of body

$\hat{e}_t$ = internal energy

h = altitude

$\hat{i}$ = unit vector in x direction

$\hat{j}$ = unit vector in y direction

$\hat{k}$ = unit vector in z direction

k = coefficient of heat conductivity

k_T = eddy coefficient of heat conductivity

M = Mach number

p = pressure

q_x = heat transfer in x direction

q_y = heat transfer in y direction

R = gas constant

R_e = Reynolds number

T = temperature

u = velocity in x direction

v = velocity in y direction

w = velocity in z direction

x, y, z = orthogonal coordinate axis system with x fixed along body centerline

- = indicates mean or average

‘ = indicates variation of flow quantity from mean value of flow variable

τ_{xy} = shear stress in y direction in plane normal to x axis

τ_{yx} = shear stress in x direction in plane normal to y axis

ρ = fluid density

μ = coefficient of viscosity

THIS PAGE INTENTIONALLY LEFT BLANK

ACKNOWLEDGMENTS

I am very grateful to my thesis advisor, Professor Max F. Platzer, for his dedication, guidance and support in the development of this thesis. His phenomenal knowledge and experience in this field of studies have enabled me to gain valuable insights and lessons that are applicable in my future endeavors. I would also like to thank Professor G. Hobson for his excellent inputs and recommendations in the CFD areas that have enabled me to overcome numerous challenges and develop an appreciation for CFD modeling. I am also thankful to Professor A. Gannon for his unyielding support that has greatly aided my CFD learning experience.

Lastly, I would like to thank my wife, Zhaoling, for her love, support, and understanding in the completion of this thesis.

THIS PAGE INTENTIONALLY LEFT BLANK

I. INTRODUCTION

The flight of projectiles ranges from transonic to supersonic speeds. The ability to predict the projectile's aerodynamic behavior is critical for the design of new projectile shapes. The conventional approach to predict this aerodynamic behavior is through wind tunnel testing and in shooting range. This trial and error approach is potentially time and cost-intensive. Alternatively, as Computational Fluid Dynamics (CFD) software and computational resources progress, numerous computational codes offer the capability to accurately predict the aerodynamic loads on projectile bodies at high speed. The primary numerical solution techniques employed in CFD are based on the Reynolds-averaged Navier-Stokes and Euler equations. One of the most widely used semi-empirical prediction codes is Aeroprediction Code 2005 (AP05). The present study focus is to verify the ability and accuracy of AP05 using existing software and data.

Aerodynamic drag constitutes a major force on all airborne projectiles. In particular, the M549, a standard 155mm caliber artillery shell, is extensively investigated and has a comparatively large amount of aerodynamic data compiled by the U.S. Army Ballistics Research Laboratory (ARL) using various codes such as MC Drag [1] and Reynolds-averaged Navier-Stokes techniques [1]. This provides an excellent opportunity to benchmark the AP05.

The total drag of a projectile consists of three major parts, namely, base drag, pressure drag, and viscous drag. The comparison focuses on subsonic, transonic, and supersonic flows. Transonic flow occurs during a critical transition period where subsonic and supersonic flow exist concurrently over the projectile. Hence, the aerodynamic coefficients vary drastically in the Mach number range 0.9 to 1.2. The usual behavior of the aerodynamic coefficients is characterized by a sharp increase near M=1.0 and a subsequent drop off at higher Mach numbers [2]. In this study, we investigate all three drag components using AP05 and the CFX-ANSYS Navier-Stokes code.

THIS PAGE INTENTIONALLY LEFT BLANK

II. AERODYNAMIC DRAG

Aerodynamic drag refers to the aerodynamic force that acts opposite to the relative motion of a body through a fluid. It is one of the major aerodynamic forces that hinders all moving bodies. The drag force consists of two parts, namely, the pressure drag, which is caused by normal forces acting perpendicular to the boundary surface, and the viscous drag, which is caused by the tangential forces acting parallel to the boundary surface.

A. PRESSURE DRAG

The pressure distribution over the body's surface exerts normal forces, which when summed and projected in the free-stream direction, are referred to as pressure drag. Pressure drag is caused by the air flowing over the moving object. Flow separation results in the formation of low- and high-pressure pockets that leave a wake behind the moving body. This opposes the forward motion of the body. This drag is also called form drag, as the drag is formed due to the form of the moving body [3] and [4].

B. SKIN FRICTION DRAG

All fluids have viscosity, which causes the shearing of one fluid layer over another. The build-up of this viscous shearing force over the whole moving body is called skin friction drag [3] and [4].

C. WAVE DRAG

Wave drag is a form of pressure drag. When a body flies at transonic and supersonic speed, a shock wave forms that causes a sudden increase in pressure at the nose tip of the body. The lost energy from the compression process of the shock wave is called wave drag [3] and [4].

D. BASE DRAG

Base drag is another pressure drag. When a projectile flies through a fluid, a separated flow region forms downstream of the projectile base, which causes the pressure of the base to be lower than the ambient pressure. The pressure difference between the forward part of the projectile and the base causes a net force that acts in an opposite direction to the motion of the projectile. This retarding force is called base drag. Base drag is a major contributor to the projectile's total drag.

III. SOLUTION TECHNIQUE

A. GOVERNING EQUATIONS

The equations governing compressible viscous fluid flows are the Navier-Stokes equations. At the Ballistics Research Laboratories, the Reynolds-averaged equations were solved by adopting the thin-layer approximation [5] and [6].

In this thesis, we use the complete equations as given in the CFX-ANSYS code [18].

B. BOUNDARY CONDITIONS

An adiabatic wall boundary condition is used on the projectile surfaces. The no-slip boundary condition is used at all the projectile walls. Free-stream boundary conditions are used at the inflow and outflow boundaries. A symmetry boundary condition is used at the center line axis of the projectile. The flow field is set to free-stream initial conditions.

C. TURBULENCE MODELING

For turbulent flow calculations, two turbulence models are being explored. They are the standard k-epsilon (k- ε) and Shear Stress Transport (SST) models.

The standard k-ε model is a robust and reasonably accurate turbulence prediction model for most turbulent flow calculations. However, when encountering a non-equilibrium boundary layer, the model behaves inadequately. It underpredicts the amount of separation and also predicts the onset of separation at a much later stage. Separation influences the pressure drag and wall heat transfer and predictions [7].

On the other hand, the SST model provides a more accurate prediction of non-equilibrium turbulent boundary layer flow. The model works by solving a turbulence/frequency-based k-omega (k-ω) model at the wall and standard k-epsilon (k-ε) in the bulk free-stream flow. The use of k-ω in the inner parts of the boundary layer

makes the model usable from the wall through the viscous sub-layer, causing the SST model to be used as a low-Reynolds turbulence model without additional dampings. The switch to k-ε in the free stream reduces the sensitivity of inlet free-stream turbulence properties. Furthermore, SST exploits the robust near-wall formulation of the k-ω model and switches automatically from a low-Reynolds number formulation to a wall function treatment based on grid density. This gives better heat transfer prediction for a flat-plate boundary layer on grids with different near-wall spacing; however, the SST model has a tendency to produce more pronounced turbulence levels in areas with large normal strain than a standard k-ε model [7].

IV. EXISTING DESIGN CODES

A. NSWCAP

The NSWCAP code [8] and [9] is a semi-empirical and analytical technique that provides fast predictions of static and dynamic coefficients of projectile shapes at transonic and low-to-moderate supersonic velocities.

The total drag is obtained by a linear superposition of pressure drag, skin friction drag and base drag. The pressure drag is based on empirical as well as experimental data at transonic speeds. The boattail pressure drag is based upon a small disturbance potential flow solution. The estimation of nose drag and boattail drag at supersonic speeds is based on the Van Dyke second-order theory [10].

The skin friction component of the drag is computed using the model of Van Driest [11]. The base drag component is empirical. It is assumed that the boattail is located after a relatively long afterbody so that the approaching external flow is at free-stream conditions. The base drag is determined by the expression

$$C_{AB} = -C_{p_{BA}}(M_\infty)\left(\frac{R_B}{R_{ref}}\right)^3 \qquad \textbf{(1)}$$

where $C_{p_{BA}}(M_\infty)$ is the base pressure coefficient for a long afterbody with no boattail. R_B is the base radius and R_{ref} is the reference body radius. $C_{p_{BA}}$ is based on the data for a long cylindrical afterbody and a fully turbulent boundary layer ahead of the base [8] and [9].

B. MCDRAG

MCDRAG is a program based on a semi-empirical technique that is used for estimating the drag of a projectile in the Mach number range of 0.5 to 5.0 [12]. The total drag is determined by the following expression

$$CD_0 = CD_P + CD_V + CD_B \qquad \textbf{(2)}$$

where CD_0 is the total drag coefficient at zero angle of attack, CD_P is the pressure drag coefficient, CD_V is the viscous drag coefficient and CD_B is the base drag coefficient.

The pressure drag consists of drag due to the projectile nose, boattail and driving band. The prediction of the projectile nose drag is based on analytical theories at supersonic speeds. The prediction of the transonic drag is based on correlations with experimental data. The effect of leading edge bluntness is accounted for in estimating the nose drag. The effect of boattail drag is estimated from second-order theory correlation with experimental data at transonic and supersonic speed [12].

The skin friction drag coefficient is determined by the following expression:

$$CD_v = \frac{4}{\pi} C_F S_w \qquad \textbf{(3)}$$

where C_F is the skin friction coefficient for a smooth flat plate and S_W is the projectile wetted surface area [12].

The base drag coefficient is determined by the following expression:

$$CD_B = \frac{2d_B{}^2}{\gamma M_\infty{}^2}\left(1 - \frac{P_B}{P_\infty}\right) \qquad \textbf{(4)}$$

where $\frac{P_B}{P_\infty}$ is the base pressure obtained from a least square fit of the data, which include Mach number and boattail effects. d_B is the diameter of the base [12].

V. AEROPREDICATION CODE 2005 (AP05)

Aeropredication code is a program based on a semi-empirical technique that is used for estimating the drag of projectiles. This version of the Aeroprediction (AP) code, AP05, used in the study is the product of over 30 years of development and enhancement. It was developed in 1972 as a code to predict the aerodynamic performance of spin-stabilized projectiles and has since evolved to include technologies that meet emerging weapon requirements [14].

AP05 uses semi-empirical solutions that combine a large database of experimental and numerical results with theoretical methods to obtain the aerodynamic coefficients. The theoretical methods include second-order van Dyke, shock expansion theory, thin-wing theory and slender-body assumptions. It allows the aerodynamic coefficients to be determined in a short period of time as no grid is needed [15].

In this study, AP05 was used to compute the various drag coefficients, namely, total drag, base drag, skin friction drag and pressure drag, of the 155mm M549 projectile from M=0.8 to M=3.0.

A. GEOMETRIC PARAMETERS

The chosen projectile for the study is the M549, a modern U.S. Army artillery shell. The geometry of the shell is shown in Figure 1. It has a 3 caliber ogive nose, a 2 caliber cylindrical section, a .59 caliber with a 7.5^{o} angle boattail. There are simplifications made to this shape. An ogive cone with a flat nose replaces the ogive nose and the rotating band is eliminated [16]. The simplified model is used for numerical computations and is shown in Figure 2.

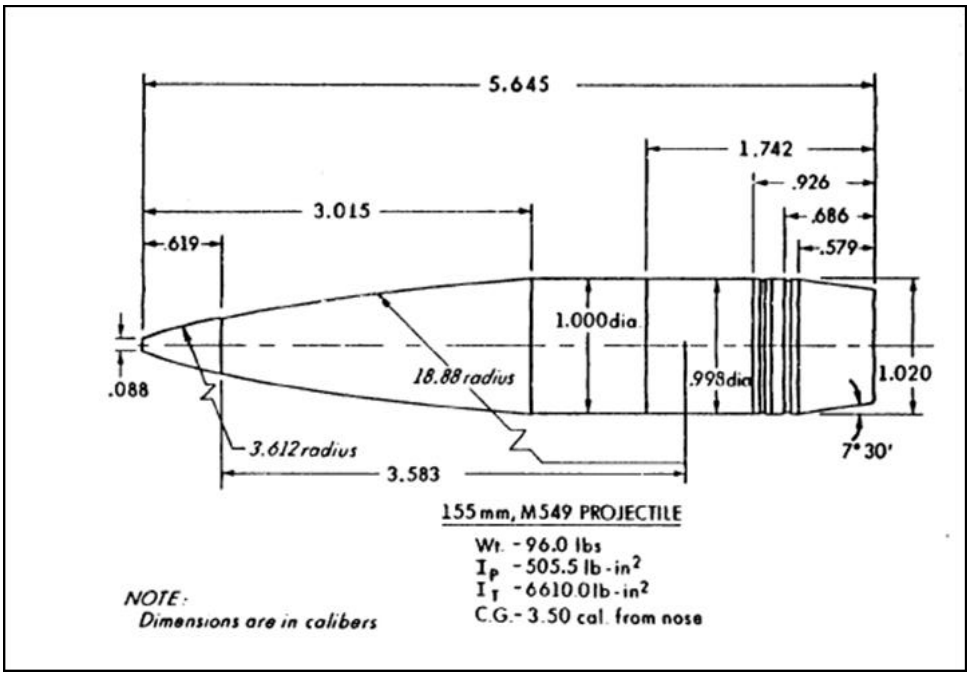

Figure 1. Geometry Profile of M549 Projectile From [16].

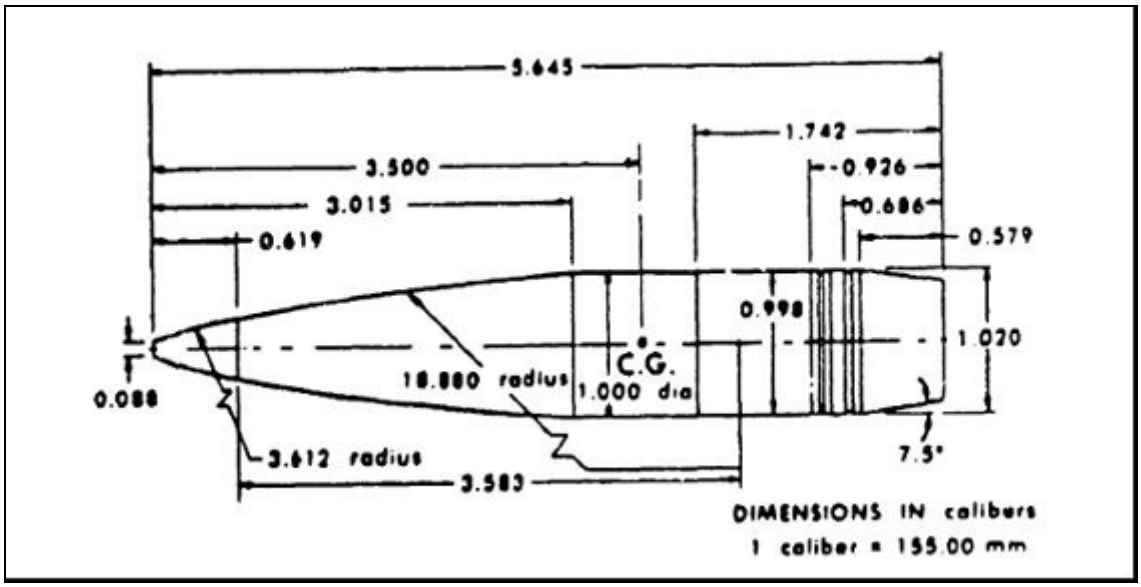

Figure 2. AP05 Computational Model of M549 Projectile From [17]

B. WORK FLOW

The AP05 consists of the following sections: pre-processor module, aerodynamic module, trim aerodynamics module, ballistic trajectory module, three-degree-of-freedom trim performance module and post-processor module [14]. The logic flow of AP05 is shown in Figure 3, and the work flow of AP05 is shown in Figure 4.

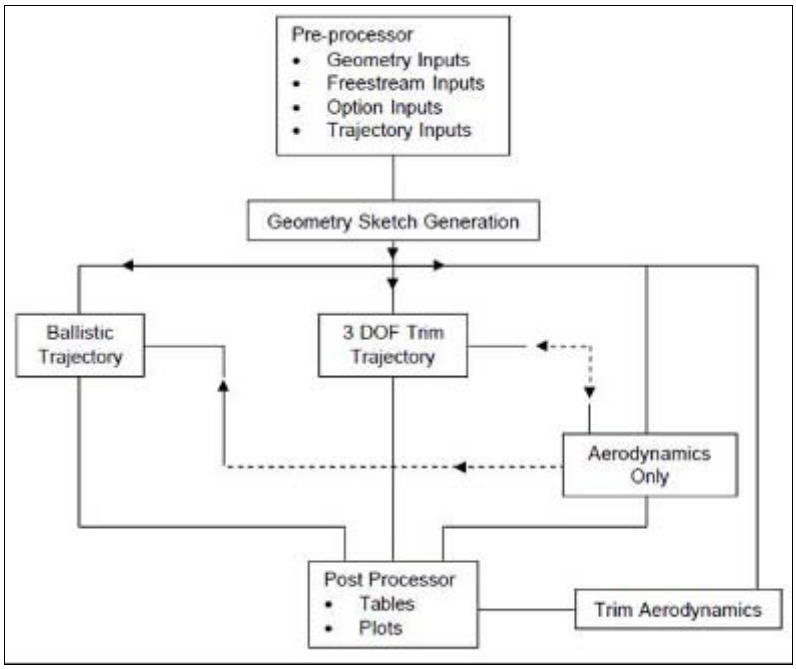

Figure 3. AP05 Logic Flow From [14].

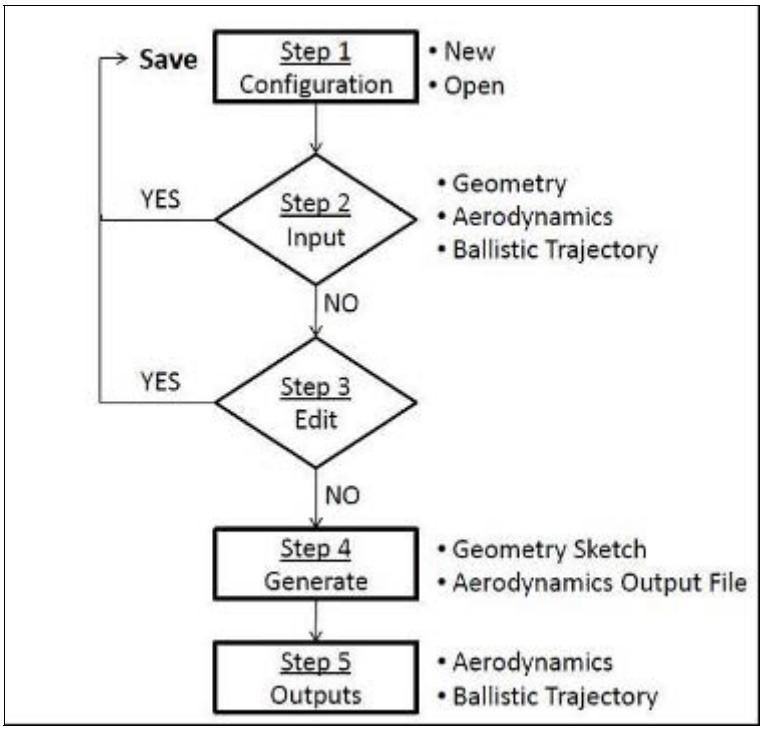

Figure 4. AP05 Work Flow.

The pre-processor module holds the geometry inputs, the aerodynamic option inputs and trajectory inputs. The geometric profile of the M549 is drawn and entered in the geometry input to generate a two-dimensional model. A sample interface geometric data entry in AP05 is shown in Figure 5. The angle of attack, Mach number range of M=0.8 to M=3.0 and other aerodynamic parameters are specified in the aerodynamic option inputs. A sample view of the aerodynamic parameter for an alpha sweep input configuration in the pre-processor module is shown in Figure 6.

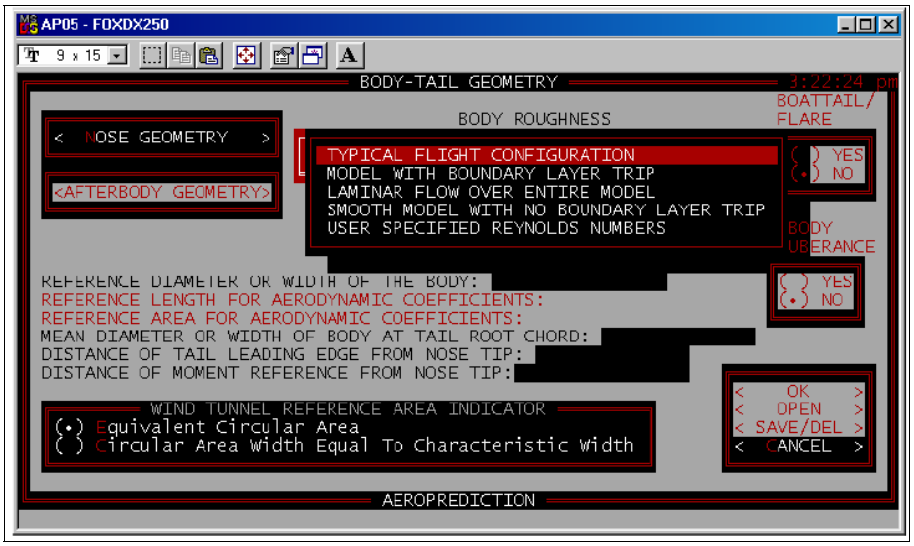

Figure 5. Geometry Data Entry in AP05 From [14].

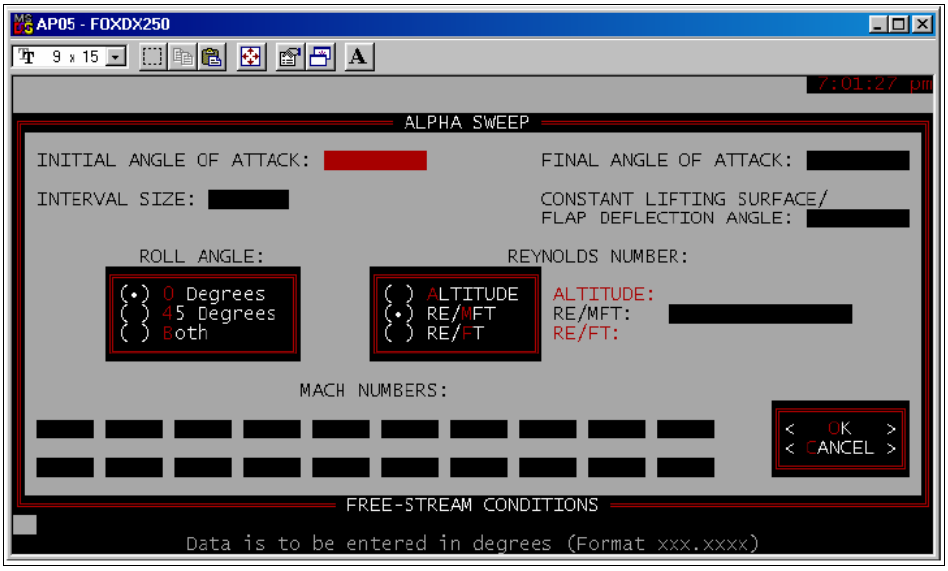

Figure 6. Free-stream Conditions Alpha Sweep Data Entry Screen From [14].

The post-processor module generates outputs in the form of tables of data, plots of aerodynamic data, and details of the trajectory information. The table of data includes the skin friction drag coefficient, base drag coefficient, and total drag coefficient required for the comparison for the specified angle of attack and Mach number range. Samples of the

output data generated by the post-processor module are shown in Figure 7, Figure 8, and Figure 9 for the table of aerodynamic data, data plot options, and data plot, respectively.

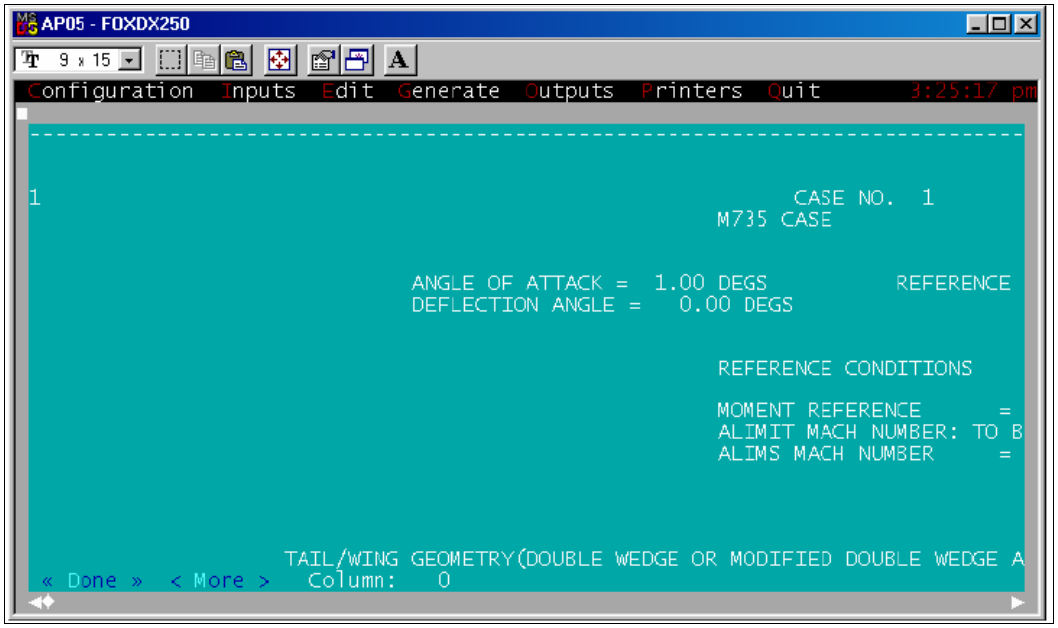

Figure 7. Aerodynamic Output File of AP05 From [14].

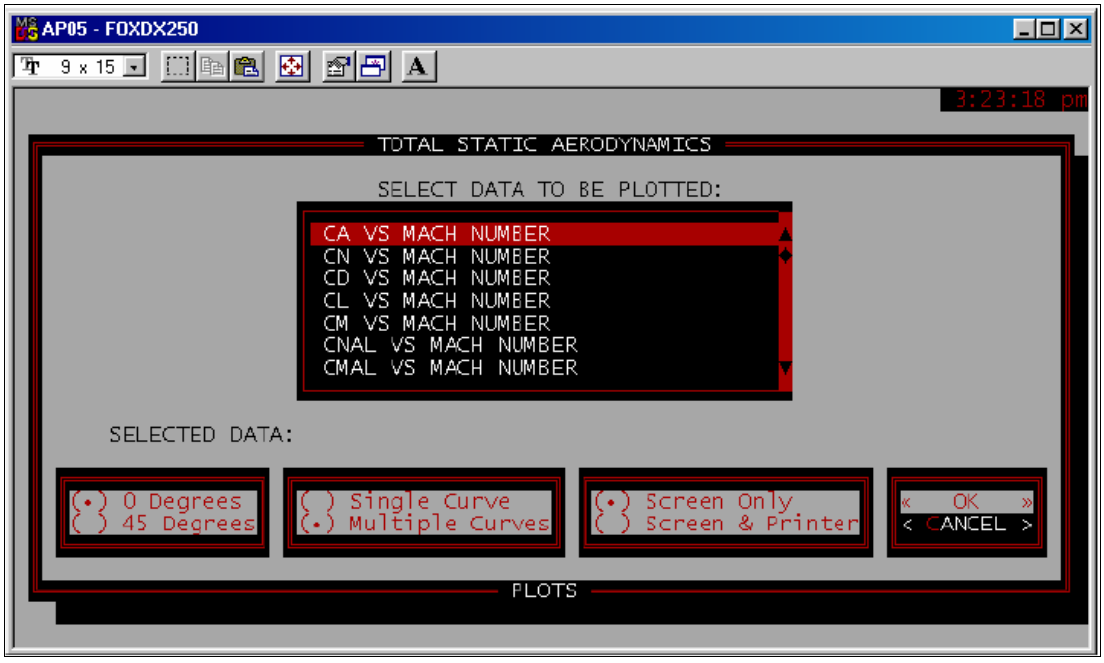

Figure 8. Data Plot Options in AP05 From [14].

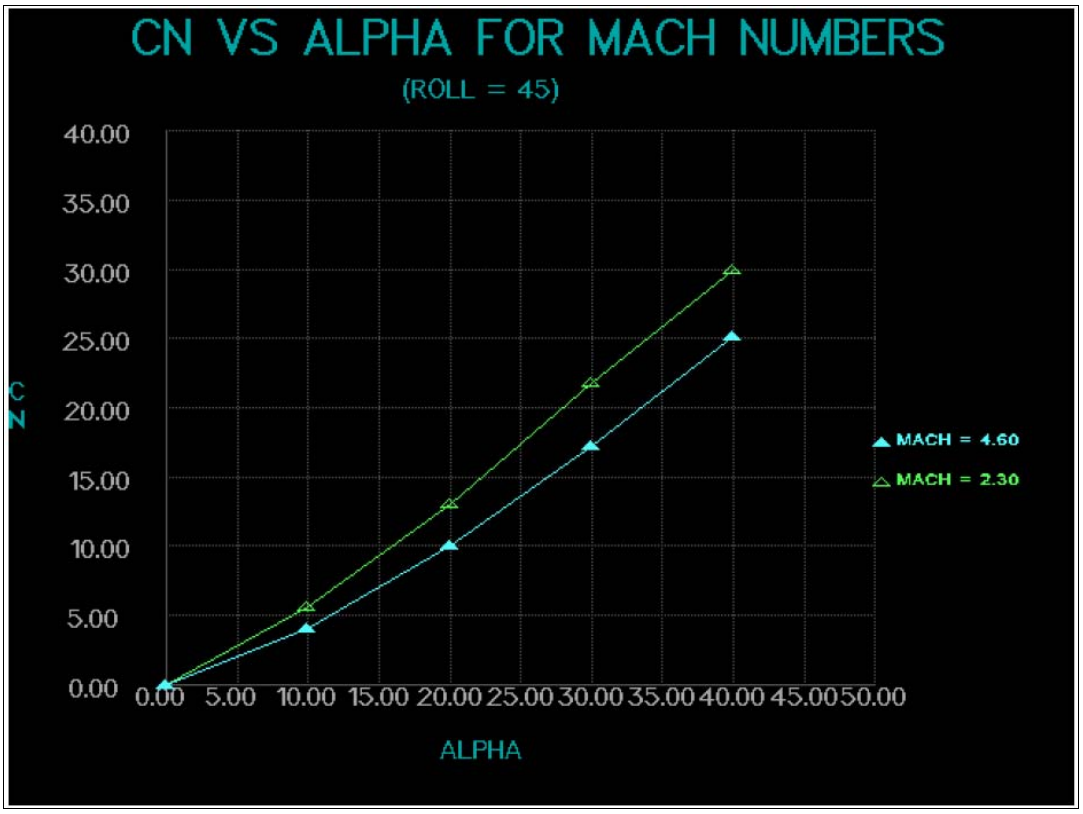

Figure 9. Data Plot of AP05 From [14].

The aerodynamics module includes the computations that are essential for the calculation of the various aerodynamic parameters. It can be used in a stand-alone mode or as an input provider for the trajectory module.

C. RESULTS

The various drag coefficients, namely, skin friction drag coefficient and base drag coefficient, as well as total drag coefficient from NSWCAP, MCDRAG and BRL-computed Sahu [16] predictions, are shown in Figure 10, Figure 11, and Figure 12, respectively. The skin friction drag coefficient, base drag coefficient and total drag coefficient from AP05 are shown in Figure 13, Figure 14, and Figure 15, respectively. The drag coefficients obtained from AP05 are compared with NSWCAP, MCDRAG and BRL Navier-Stokes predictions by Sahu [16], and are shown in Figure 16, Figure 17, and Figure 18.

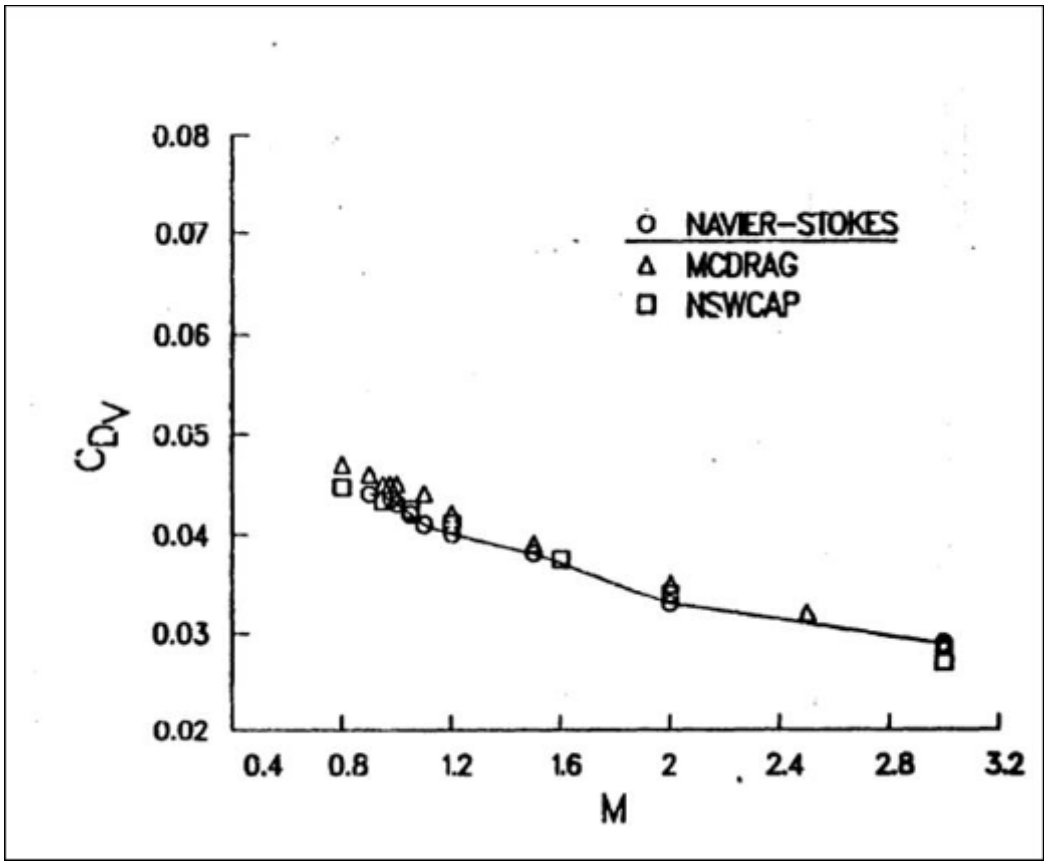

Figure 10. Skin Friction Drag Coefficient vs. Mach Number for M549 Projectile From [16].

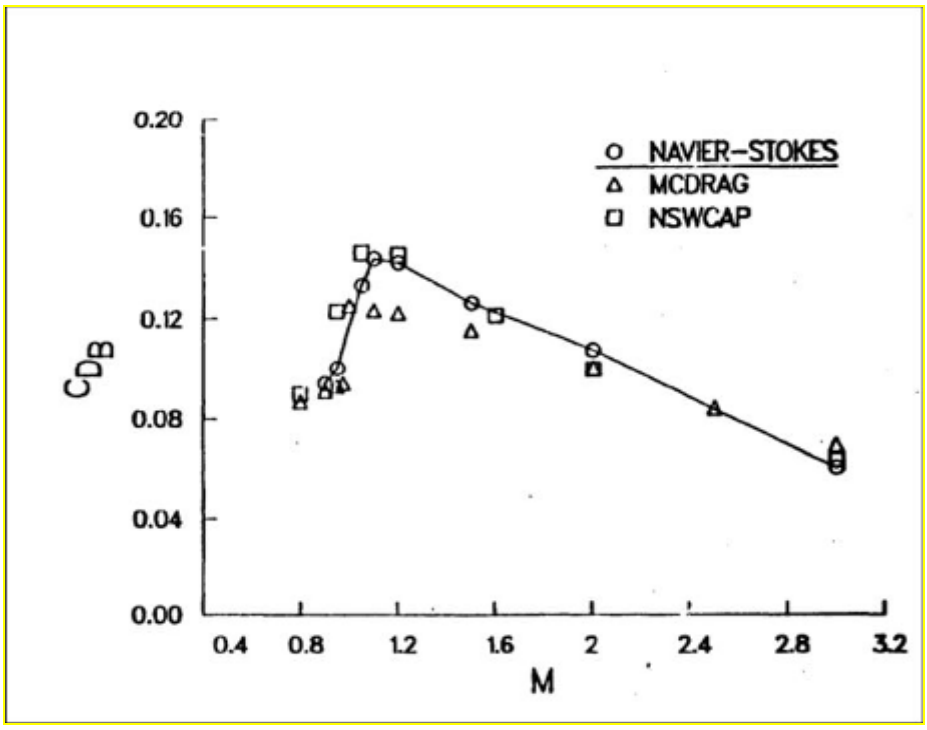

Figure 11. Base Drag Coefficient vs. Mach Number for M549 Projectile From [16].

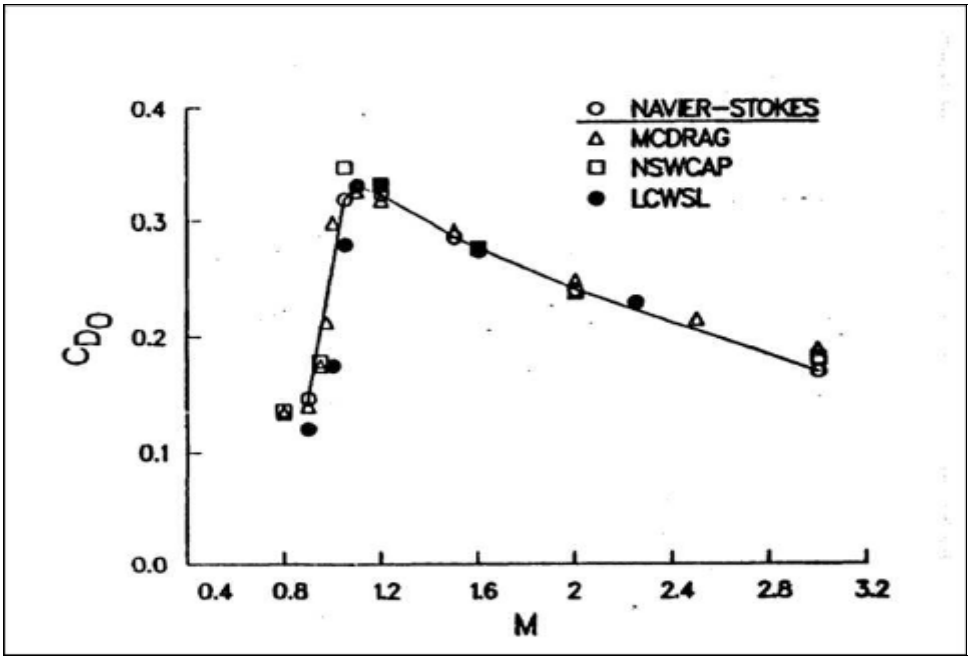

Figure 12. Total Drag Coefficient vs. Mach Number for M549 Projectile From [16].

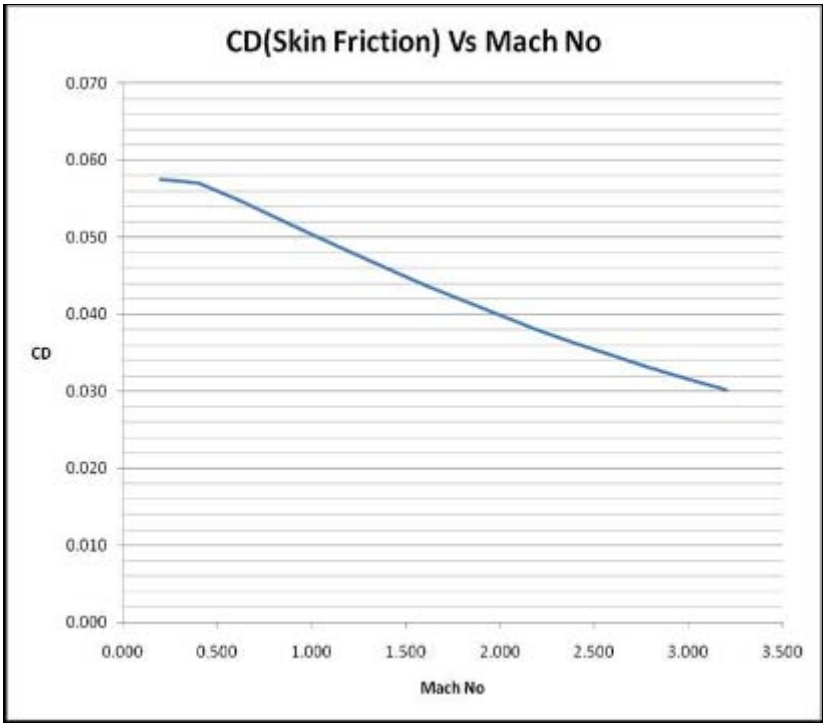

Figure 13. Skin Friction Drag Coefficient vs. Mach Number of AP05.

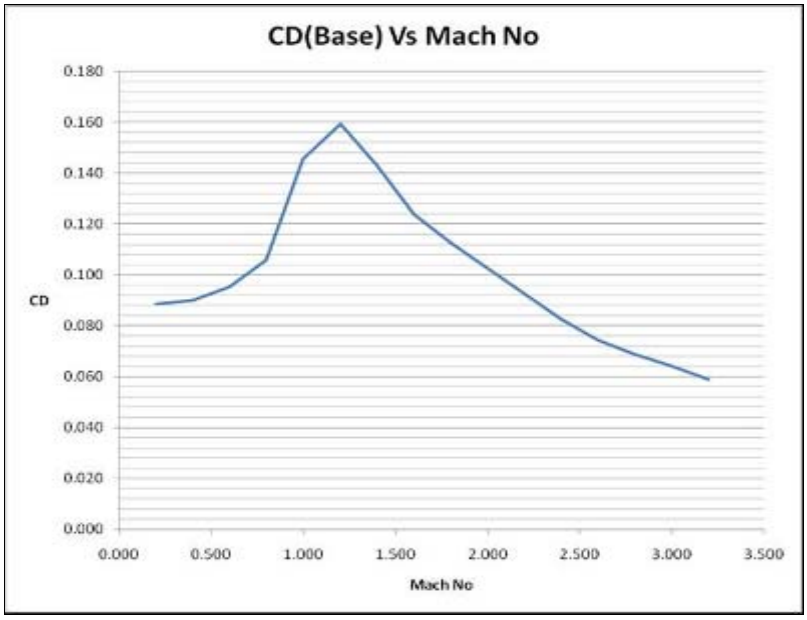

Figure 14. Base Drag Coefficient vs. Mach Number of AP05.

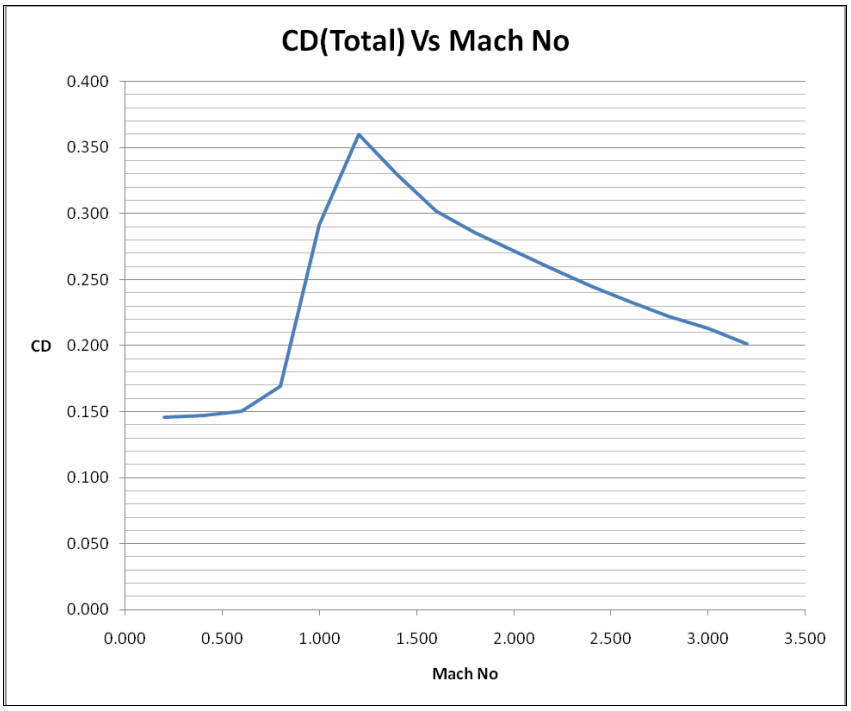

Figure 15. Total Drag Coefficient vs. Mach Number of AP05.

The skin friction drag coefficient comparison is shown in Figure 16. The skin friction drag predicted by AP05 is in agreement with the other aero-prediction codes for supersonic speeds; however, in the transonic region, it overpredicts the skin friction drag coefficient by 20–25% as compared to the other codes.

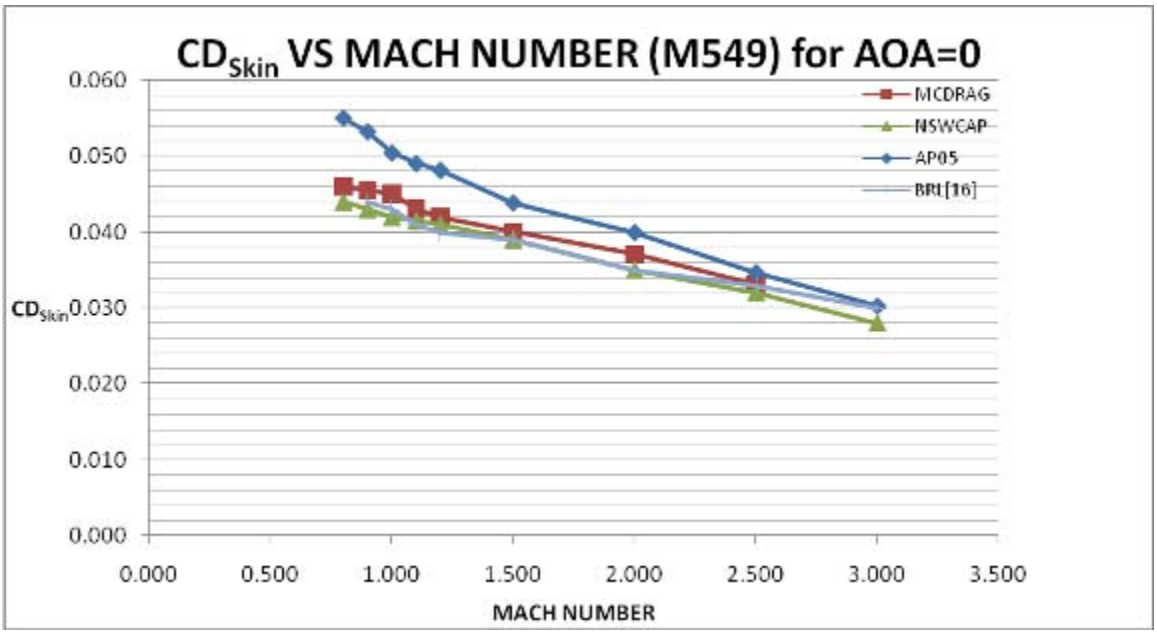

Figure 16. Skin Drag Coefficient vs. Mach Number Comparsion.

The base drag coefficient comparison is shown in Figure 17. The base drag predicted by AP05 is in good agreement with the other aero-prediction codes for subsonic and supersonic speeds; however, it overpredicts the base drag coefficient by 10–15% as compared to the other codes in the transonic region (M=1.0 to M=1.5).

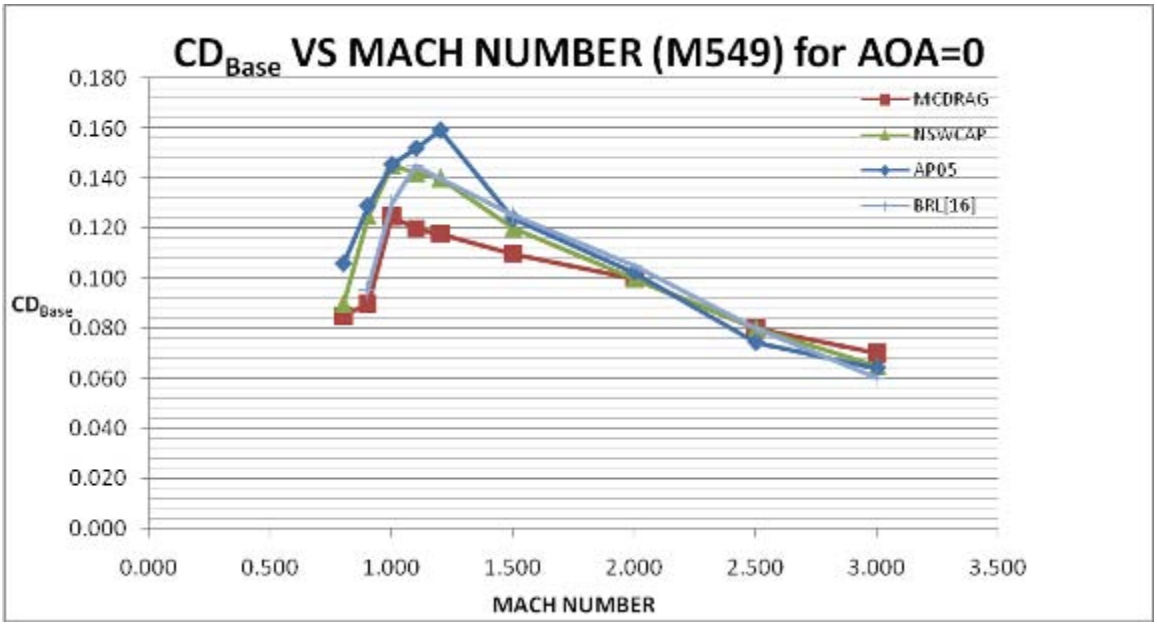

Figure 17. Base Drag Coefficient vs. Mach Number Comparsion.

The total drag coefficient comparison is shown in Figure 18. The total drag predicted by AP05 is in good agreement with the other aero-prediction codes for subsonic and supersonic speeds; however, it overpredicts the total drag coefficient by 10–15% as compared to the other codes in the transonic region (M=1.0 to M=1.5).

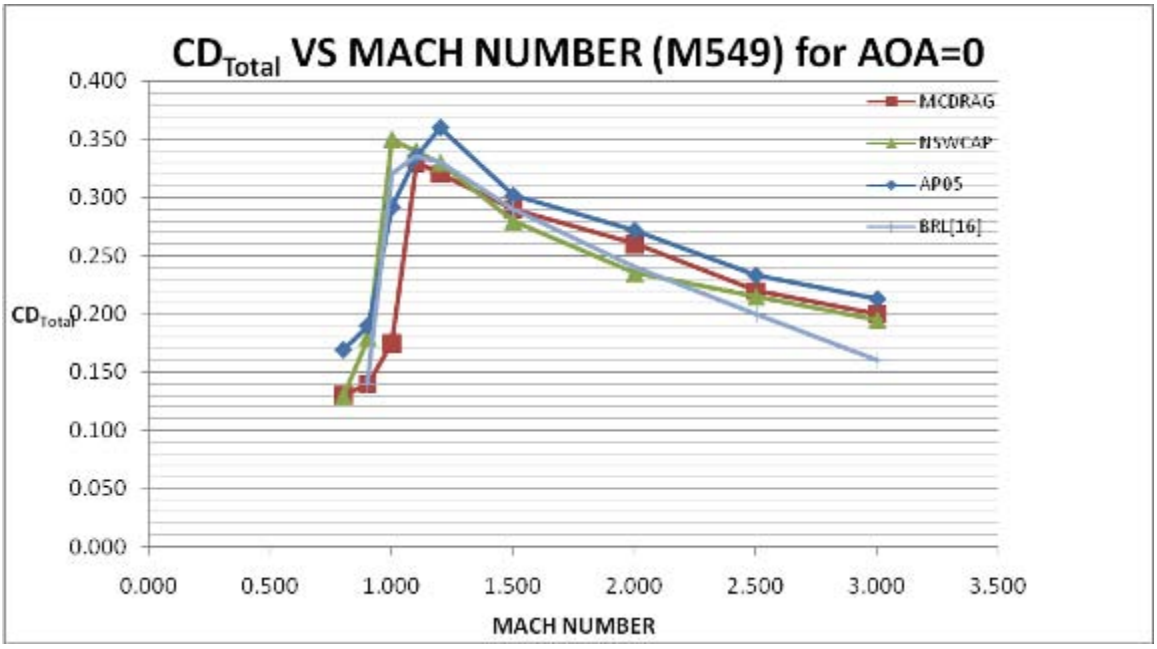

Figure 18. Total Drag Coefficient vs. Mach Number Comparsion.

VI. FLOW OVER A CONICAL FOREBODY

A. THEORETICAL METHOD FOR CIRCULAR CONE

The conical shock wave was first studied in the 1930s by various investigators [19]. They considered a circular cone at zero incidence to the free stream and derived the ordinary non-linear differential equations to be satisfied between the shock and body. These equations were numerically integrated by Kopal in 1947 [20] using the equations derived by Taylor and Macoll in 1932. Kopal made the original numerical integration of the resulting equations. In the 1960s, Sims [21] computed these zero-order solutions and presented the results in a convenient table form. This has provided an excellent opportunity for comparison of the results by ANSYS with the theoretical method computed by Sims for circular cone at zero incidence.

B. SOLUTION EQUATIONS OF THEORETICAL METHOD

The differential equations for the formulation of the conical flow problem in Figure 19 in the spherical coordinate system [21] are:

$$\frac{d^2u}{d\theta^2} + u = \frac{a^2(u + v\cot\theta)}{v^2 - a^2} \tag{5}$$

where

$$v = \frac{du}{d\theta} \tag{6}$$

And

$$a^2 = \frac{\gamma - 1}{2}(1 - u^2 - v^2) \tag{7}$$

Free-stream boundary conditions for Equations (5) to (7) are:

$$\begin{aligned} u &= u_s \\ v &= 0 \end{aligned} \tag{8}$$

at the cone surface.

The upper boundary condition is solved by requiring the results obtained from the integration of Equation (5) to satisfy the Rankine-Hugoniot equations expressed as follows:

$$\tan\theta = \left(\frac{\gamma-1}{\gamma+1}\right)\frac{u^2-1}{uv} \qquad \textbf{(9)}$$

When Equation 9 is found by integrating Equation 5, the free-stream Mach number is given as:

$$M_\infty = \sqrt{\left(\frac{2}{\gamma-1}\right)\frac{u^2}{\cos^2\theta - u^2}} \qquad \textbf{(10)}$$

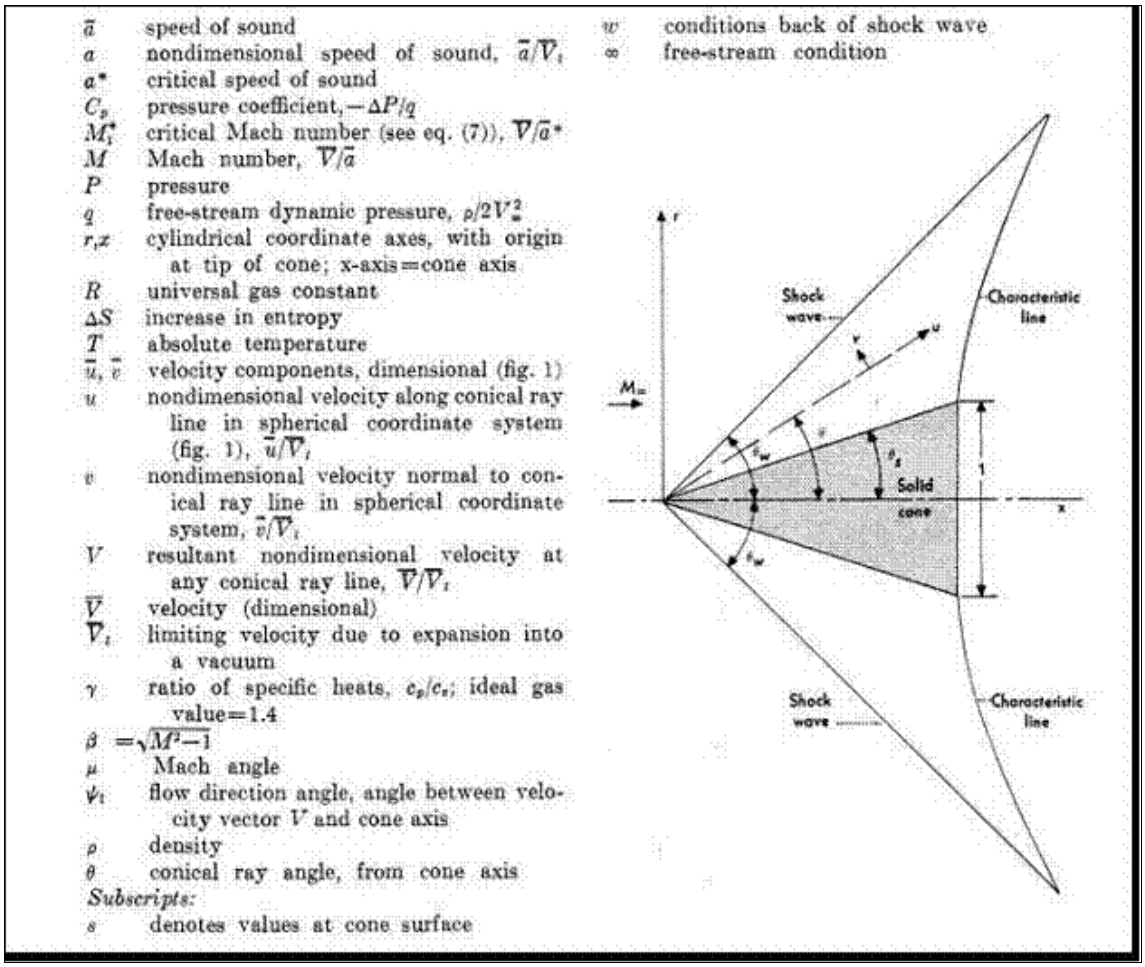

Figure 19. Coordinate System From [21].

The solution of Equation 5 was obtained using Runge-Kutta integration. Computation began at the cone surface by specifying the value of u_s and ended when the shock wave conditions were satisfied.

The solution method did not give an arbitrary free-stream Mach number without a prior specified value of u_s. The iteration on u_s was included in the procedure in order for both cone angle and free-stream Mach number to be specified.

Integration of Equation 11 gives values of u, v and a at each conical ray angle of θ. These results are transformed into forms of M_1^*, ψ_1 and u in the following form:

$$M_1^* = \frac{V}{a^*} = \sqrt{\frac{\gamma+1}{\gamma-1}(u^2+v^2)} \qquad \textbf{(11)}$$

since

$$\frac{V_t}{a^*} = \sqrt{\frac{\gamma+1}{\gamma-1}} \qquad \textbf{(12)}$$

and the flow direction angle ψ_1 is

$$\psi_1 = \theta + \tan^{-1}\frac{v}{u} \qquad \textbf{(13)}$$

and

$$u = \sin^{-1}\sqrt{\frac{a^2}{u^2+v^2}} \qquad \textbf{(14)}$$

THIS PAGE INTENTIONALLY LEFT BLANK

VII. CFX IN ANSYS WORKBENCH

Rapid technological advancements have increased computer power tremendously. With the boost of processor speed and graphic software, computers are widely used in aerodynamic prediction modeling. This led to a new field of study named computational fluid dynamics (CFD). CFD uses fundamental conservation laws, like Navier-Stokes equations, to numerically solve fluid flow over a region of interest with specific boundary conditions. It provides an excellent cost-effective tool to study fluid flows and complements empirical methods and wind tunnel testing.

In this study, the computer program ANSYS CFX was used to compute the axisymmetric flow over the M549 projectile. ANSYS CFX uses the full Navier-Stokes equations to solve. ANSYS CFX is an advanced CFD solver that has the facilitating technologies of geometry handling and meshing pre- and post-processing all housed within and integrated into the ANSYS Workbench. ANSYS Workbench has a platform's project page that can launch and track the geometry module, mesh module, setup pre-processor, solution module and results post-processor. These modules form the process of creating a CFD analysis on the M549 projectile.

A. ASSESSMENT OF CFX CIRCULAR CONE

Solidworks® was used to sketch and design a conical nose in the front of the M549 projectile with a cone angle of 9.4 degrees. The "Solidwork" file is saved as a "Parasolid" file and imported into the ANSYS Workbench geometry module as an input geometry. The mesh properties of the pointed M549 projectile and its control volume are as follows: angular resolution = 10º, body spacing = 200mm, minimum edge length in face spacing = 0.07mm, number of inflation layer = 8, minimum internal angle = 2.5º, minimum external angle = 20º, line control with point spacing length of 0.1mm, radius of influence of 5mm, expansion factor of 1.2, and a computational domain of about 4 million cells structured mesh was constructed around the model. Point control was used for a pointed nose as shown in Figure 20. The point spacing specifications were length scale of 0.1mm, radius of influence of 5mm and expansion factor of 1.2. The inflation

details set are number of inflated layers of 8, expansion factor of 1.2, number of spreading iterations of 0, minimum internal angle of 2.5, minimum external angle of 20 and first-layer thickness used in the inflation option. Figure 21 shows the pointed M549 projectile at M=2.0 in ANSYS Workbench.

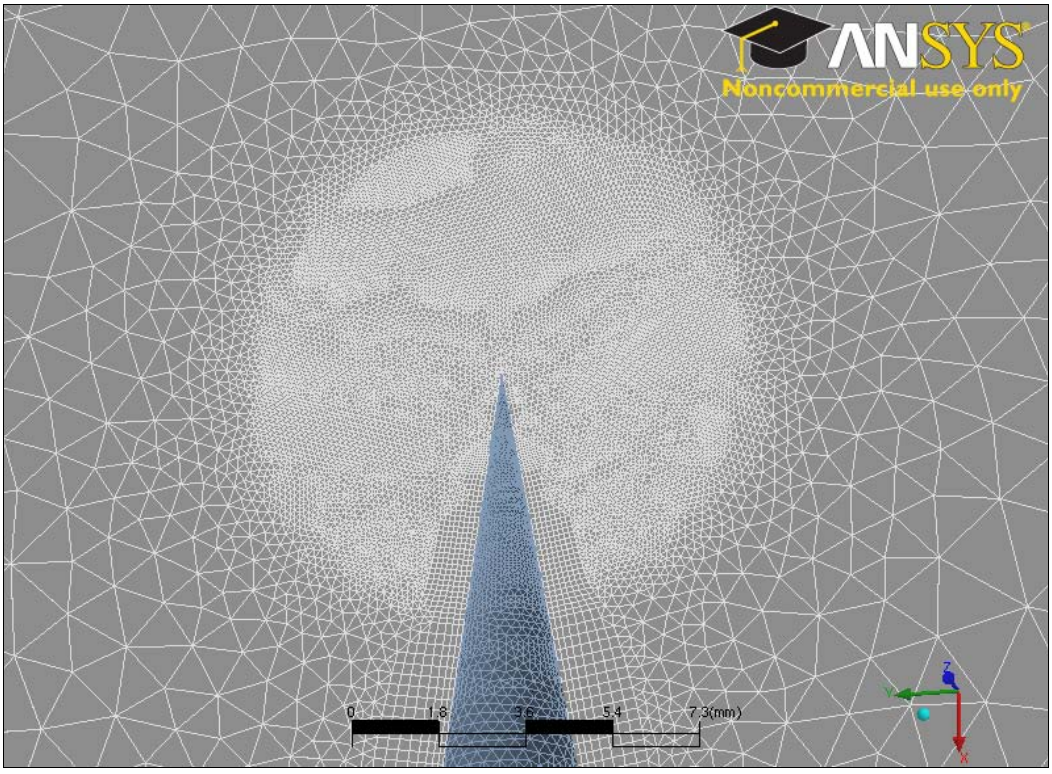

Figure 20. Point Control at a Pointed M549 Projectile Nose in ANSYS Workbench.

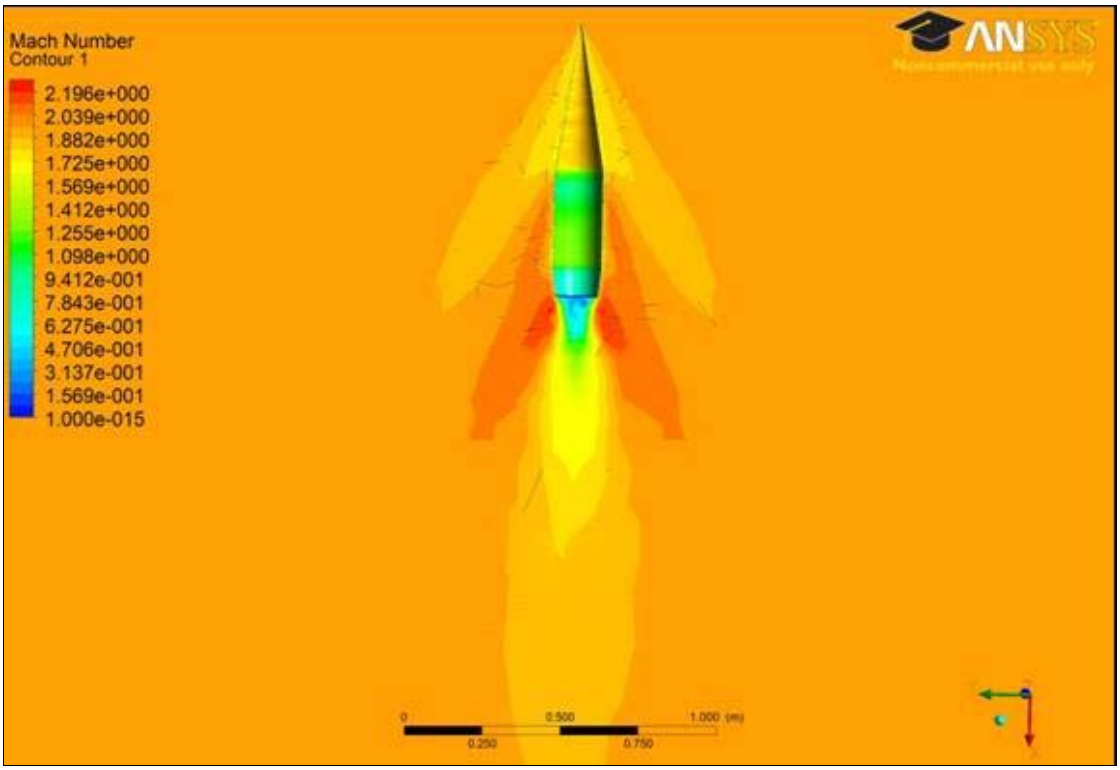

Figure 21. Pointed M549 Projectile at M=2.0 in ANSYS Workbench.

B. COMPARISON OF RESULTS

Figure 22 shows a comparison of the results of Sims [21] with ANSYS. The cone angle, θ, for the pointed M549 cone is 9.4^{o}. It is apparent that good agreement is obtained between the theoretical results from Sims with those generated by ANSYS.

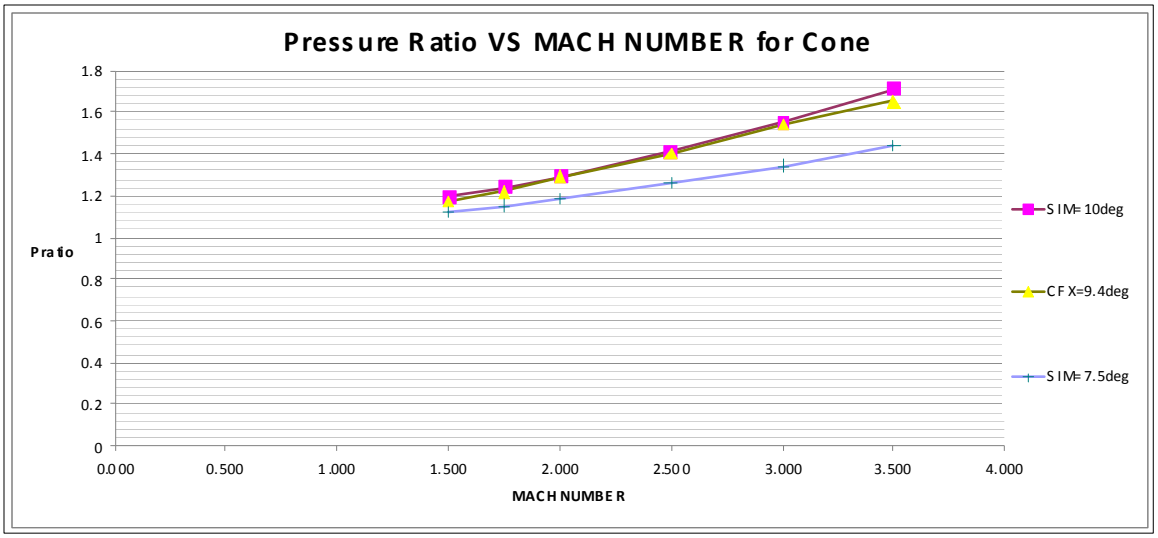

Figure 22. Pressure Ratio vs. Mach Number for Cone.

C. GEOMETRY AND MESH CREATION

The Computer-Aided Design (CAD) program Solidworks® was used to sketch and design a three-dimensional (3D) axisymmetric profile of the M549 projectile and its control volume. This was the first step of defining the geometry of the projectile. The "Solidwork" file was then saved as a "Parasolid" file. The M549 "Parasolid" file was then imported into the ANSYS Workbench geometry module as an input geometry. The geometry module used ANSYS DesignModeler™ software to create and prepare the geometry for simulation. The 3D geometry profile of the M549 projectile and its control volume are shown in Figure 23. The next step was to create regions of fluid flow, solid areas and surface boundary names. The ANSYS CFX-MESH meshing tool in Workbench Mesh module was used to specify the spacing between the mesh points. By setting the mesh properties of the following: angular resolution = 10º, body spacing = 200mm, minimum edge length in face spacing = 0.07mm, number of inflation layers = 8, minimum internal angle = 2.5º, minimum external angle = 20º, line control with point spacing length of 0.1mm, radius of influence of 5mm, expansion factor of 1.2, and a computational domain of about 4 million cells unstructured mesh was constructed around the model. The mesh is shown in Figure 24 and Figure 25. The last step in the mesh

module was the generation of the surface and volume mesh of the control volume. A total of 723610 nodes and 3931862 elements were generated. The ANSYS report generated is placed in Appendix A.

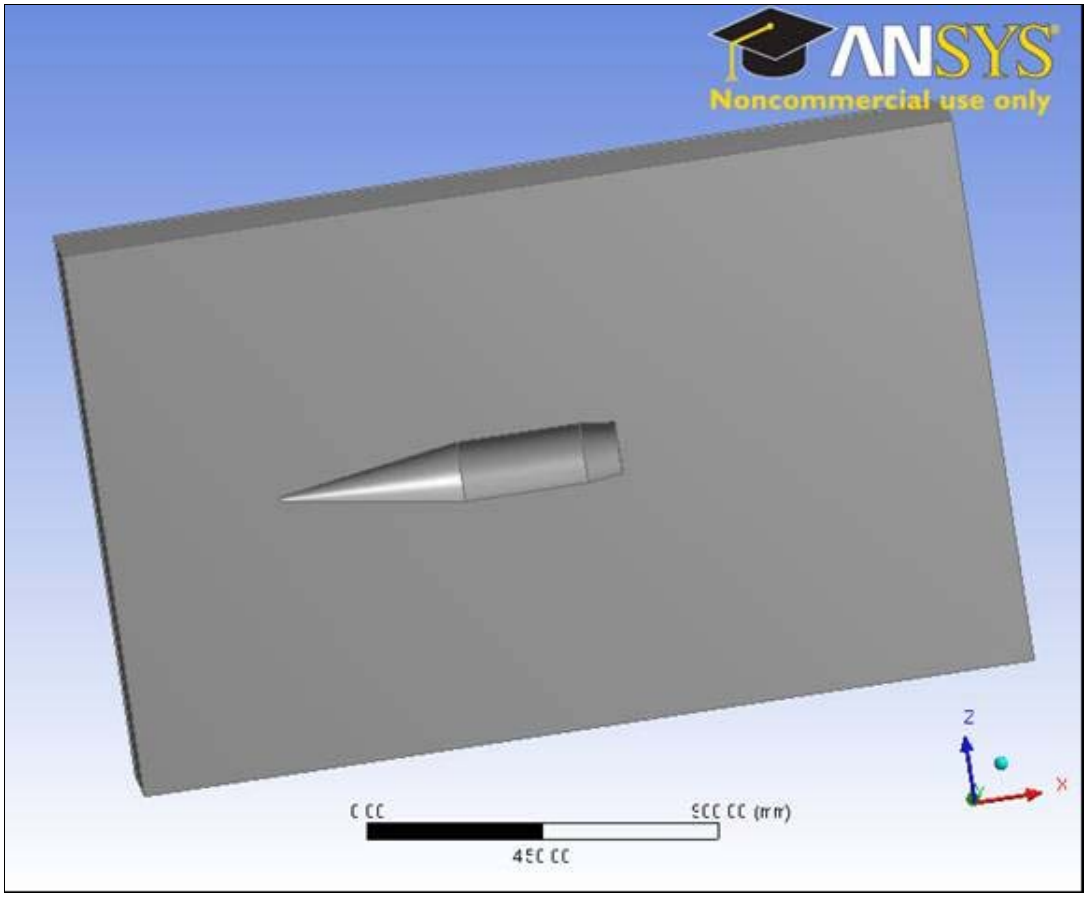

Figure 23. 3D Geometry Profile of M549 Projectile and its Control Volume in ANSYS Workbench.

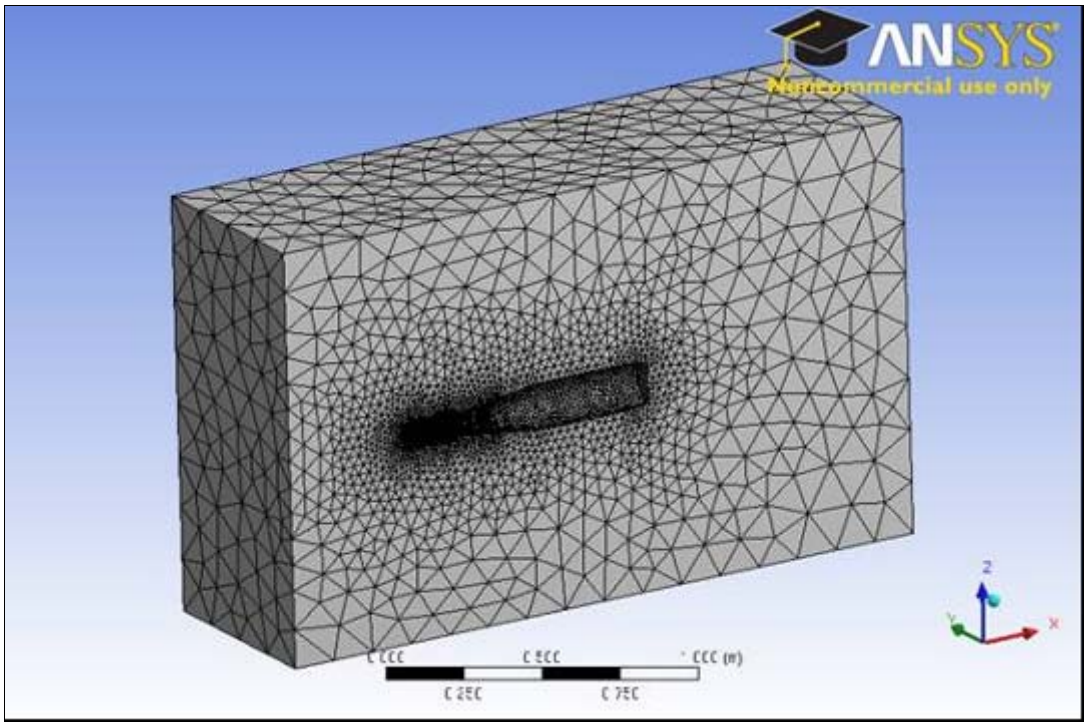

Figure 24. Meshing of M549 Projectile and its Control Volume in ANSYS Workbench.

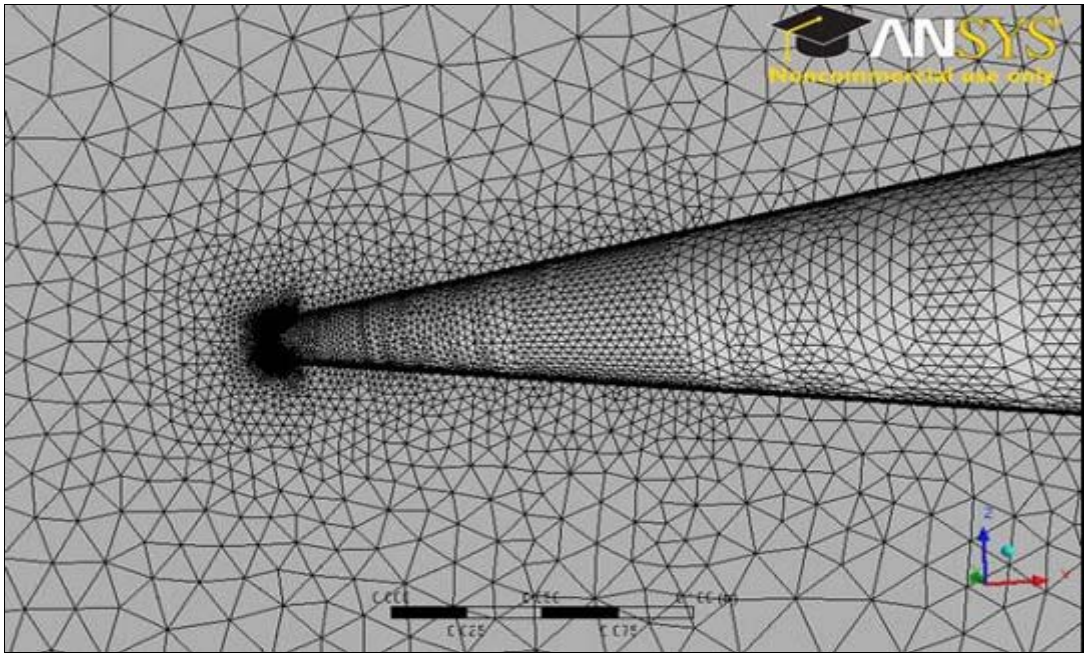

Figure 25. Mesh Refinement of M549 Projectile and its Control Volume in ANSYS Workbench.

D. SETUP OF FLUID FLOW PARAMETERS IN PRE-PROCESSOR

In the setup module of Workbench, the fluid flow simulation parameters were specified. All boundary conditions were explicitly specified. The far field and inflow boundaries were set to free-stream condition by specifying the Cartesian velocity components. The outflow boundary was set to free-stream conditions for subsonic and supersonic outflow. Free-stream pressure and temperature were set to 101325 Pa and 288.15 K, respectively. Density was calculated from the perfect gas law. For the projectile body, the boundary condition was set to be non-slip, isothermal wall (288.15 K). At the solver control, high-speed numerics were chosen. The turbulence model chosen was the SST model. The setup with inlet, M549 projectile, outlet and symmetry depicted is shown in Figure 26.

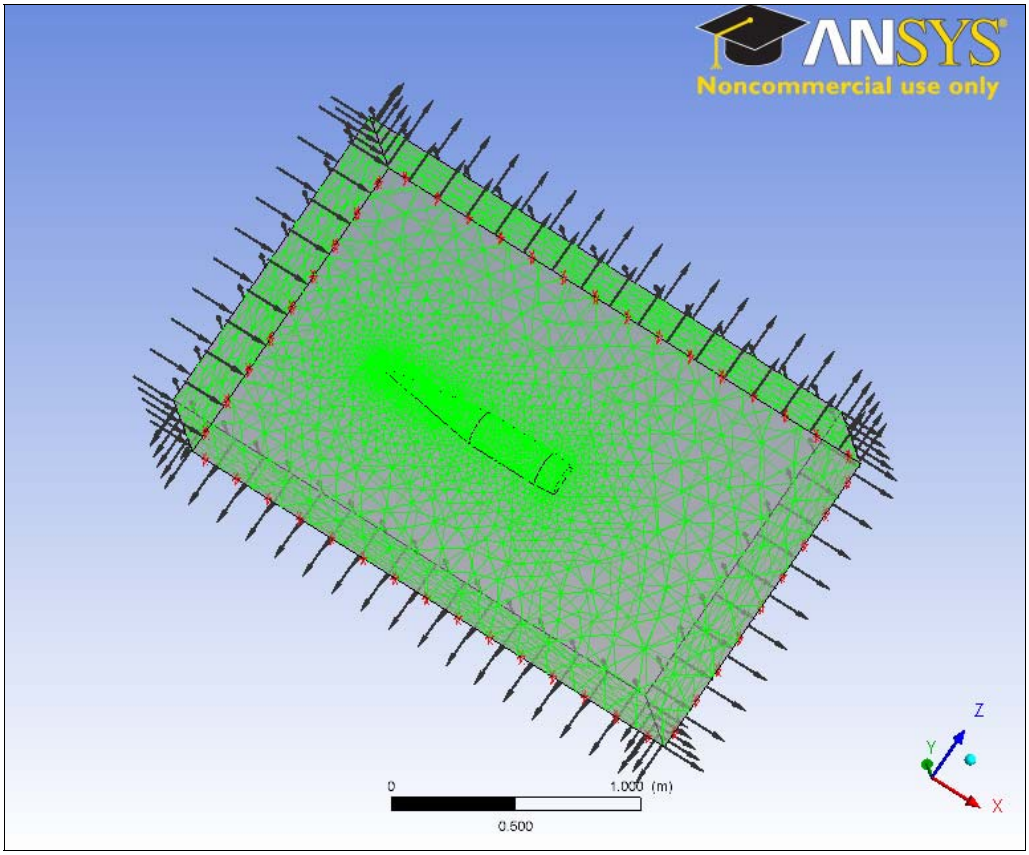

Figure 26. Setup of M549 Projectile and its Control Volume in ANSYS Workbench.

E. FLOW SOLVER IN SOLUTION MANAGER

The CFX Solver computes the Navier-Stokes equations with a finite volume and algebraic multigrid method [18]. The partial differential equations are integrated over the control volumes specified in the region of interest. It applies the conservation of mass, momentum and energy to the control volumes. These integral equations are translated to algebraic equations by generating approximations for all the terms in the integral equations. The algebraic equations are then solved iteratively. The iterations are due to the non-linear nature of the equations and convergence occurs when the residuals have been reduced by at least three orders of magnitude. This solution process usually required no user intervention and was carried out as a batch process. The results files produced were then passed to the post-processor. The sample of the SOLVER manager is shown in Figure 27.

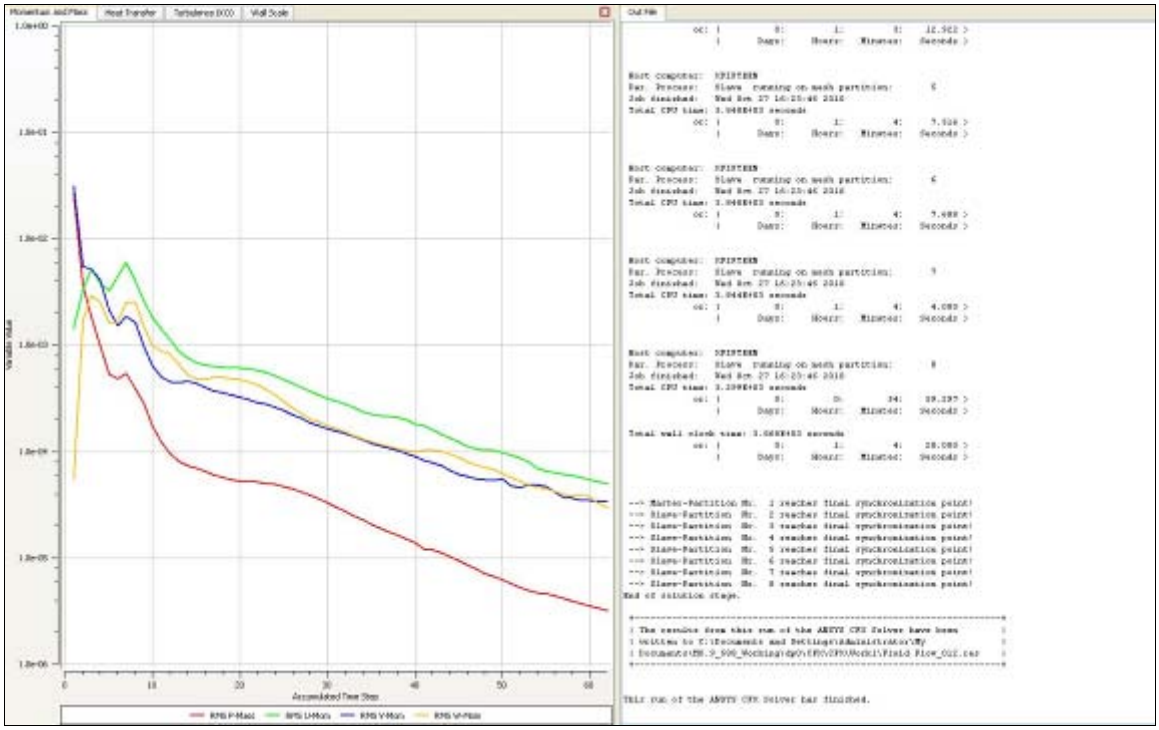

Figure 27. Sample View of Flow Manager in ANSYS Workbench.

F. RESULTS IN POST-PROCESSOR

The results module in the post-processor was used to analyze and visualize the results. It enabled the visualization of the M549 projectile's geometry and its control volume. Vector plots, like Velocity Plot, show the direction and magnitude of the fluid flow parameters. It also enabled the visualization of scalar variables, like temperature, pressure, and speed, throughout the domain. In addition, a quantitative numerical calculator is incorporated that could be used to calculate the various flow parameters on the M549 projectile or in the control volume.

Figure 28 shows a supersonic free-stream Mach number (M=2.0) flow over the M549 projectile. The computed bow shock is clearly shown in the front of the nose. In between the bow shock and nose is a subsonic region. The position of the shock is dependent on the shape of the projectile and the free-stream Mach number. The bow shock is more inclined for higher free-stream Mach numbers. The flow accelerates along the cone to supersonic speeds. The expansion flow occurs at the turning angle of the cone, resulting in a local maximum Mach number that is reached at the end of the Prandtl-Meyer expansion. A weak shock is also observed at the base of the boattail. Flow separation occurs at the base and this accounts for base drag, which constitutes a substantial part of the total drag of the M549 projectile. The computed values are $C_{D_{TOTAL}}$ = 0.34, $C_{D_{BASE}}$ = 0.14, $C_{D_{VIS}}$ = 0.045 and $C_{D_{WAVE}}$ = 0.155. The convergence took about 100 iterations.

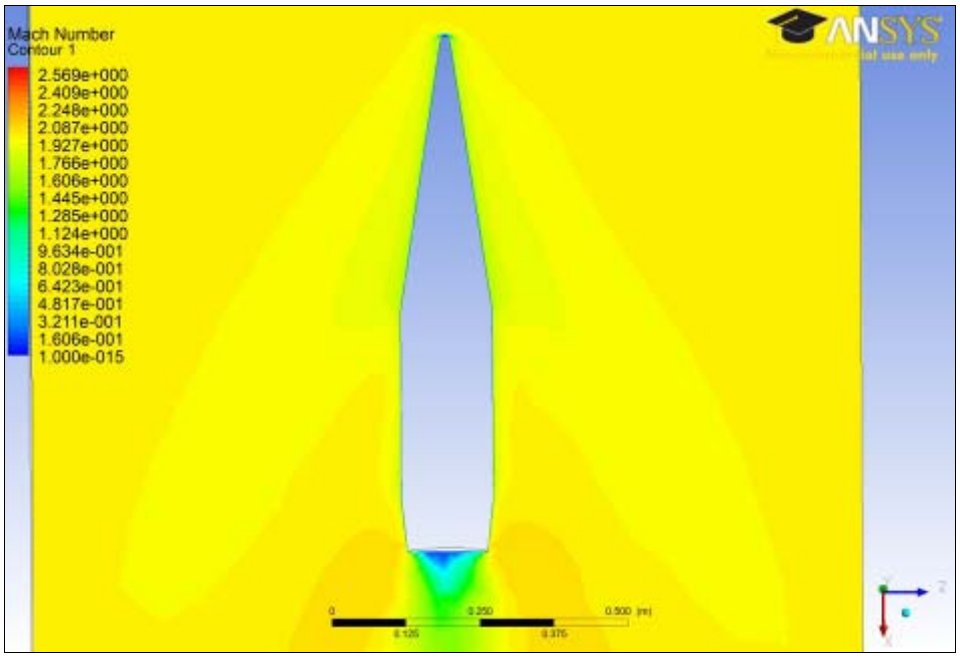

Figure 28. Blunted M549 Projectile at M=2.0 in ANSYS Workbench.

The total drag coefficient versus free-stream Mach number is plotted in Figure 29. The total drag coefficient rises sharply as the M549 projectile approaches transonic speeds and peaks at M=1.0. The total drag coefficient then decreases gradually as the free-stream Mach number increases. The total drag predicted by CFX is in agreement with the other aero-prediction codes for subsonic speeds; however, in the transonic region, it constantly underpredicted by 3–5% as compared to the BRL code. CFX also underpredicted by 10% as compared to the BRL code at M=3.

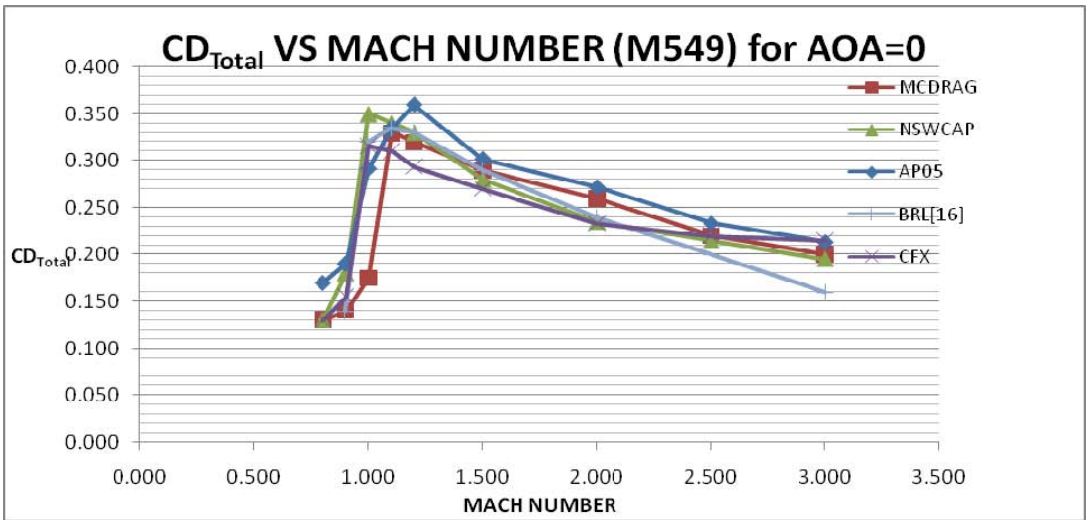

Figure 29. Total Drag Cofficient vs. Mach Number of ANSYS Workbench.

G. MESH REFINEMENT

A further investigation was conducted to enhance the meshing. However, a compromise among accuracy, computational time and resources has to be made. From experimentation, the lesson learned is that not all expanses in the simulation sphere contribute to the accuracy of the numerical solution. This leads to a targeted approach, where finer mesh is used in areas where large gradients in velocity and pressure are likely and where high resolution is crucial. The rest of the less important areas use a coarser mesh to help reduce the computational time and resources.

One of the mesh refinement options used in the study was the application of mesh control in the leading-edge region. Mesh control was used to refine the surface and volume mesh close to the body. There are three types of volumetric control, namely, point control, line control and triangle control. In the study, line control was used at the blunt nose of the M549 projectile, as shown in Figure 30. Alternatively, point control was used for a pointed nose, as shown in Figure 31. The point spacing specifications were as follows: length scale of = 0.1mm, radius of influence of 5mm and expansion factor of 1.2.

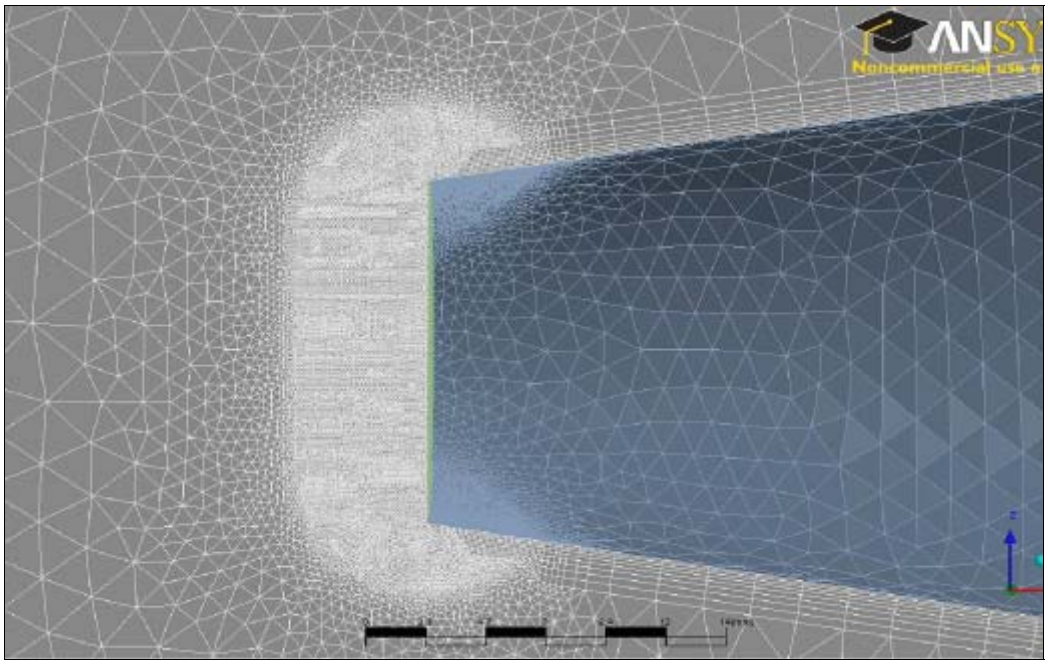

Figure 30. Line Control at a Blunt M549 Projectile Nose in ANSYS Workbench.

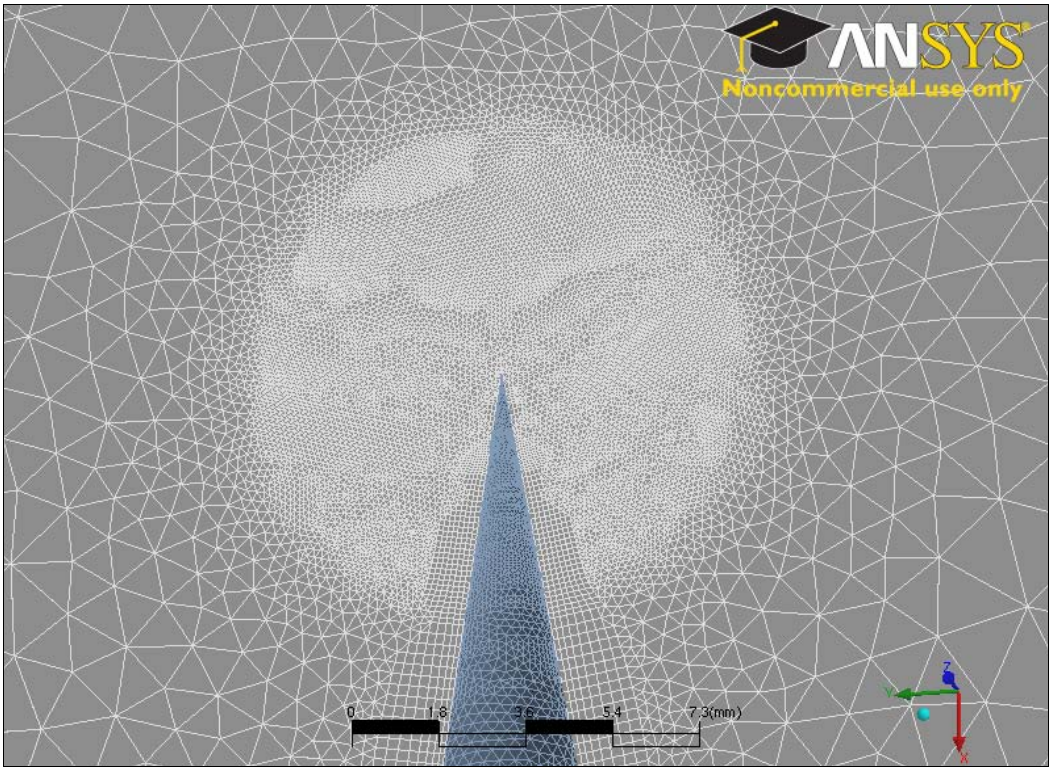

Figure 31. Point Control at a Pointed M549 Projectile Nose in ANSYS Workbench.

The velocity gradient near the projectile wall can vary significantly. The meshes at the near-wall region require the elements to have high aspect ratios. By applying inflation at these areas, the mesher used local face element normals to “inflate” 2D triangular elements into 3D prism elements. The inflation details in the study were set as follows: number of inflated layers of 8, expansion factor of 1.2, number of spreading iterations of 0, minimum internal angle of 2.5, minimum external angle of 20 and first-layer thickness used in the inflation option. The location of the inflated boundary was at the surfaces of the M549 projectile, as shown in Figure 32.

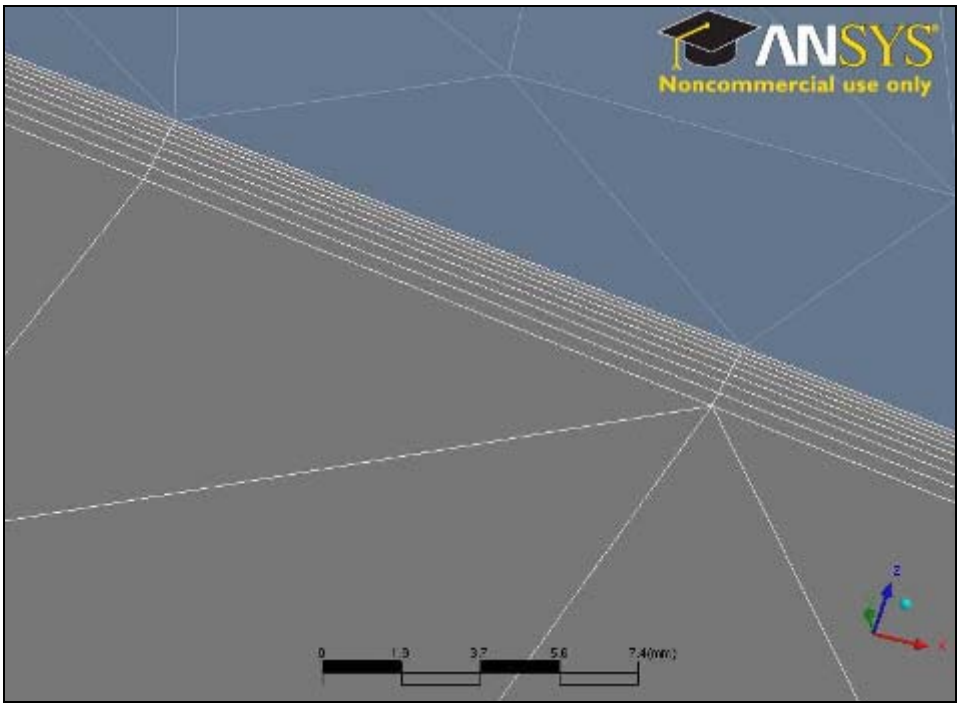

Figure 32. Inflation Layers at the Surface of the M549 Projectile.

Mesh refinement was used to increase the accuracy of the numerical solution. The important areas in this case were the surfaces of the M549 projectile, particularly the nose. Mesh refinement was applied on the projectile body. A line was drawn from the nose to determine the changes in profile from the nose to the front of the shock, as shown in Figure 33. A comparison between plots of Mach number, pressure and density profiles of the line with and without mesh adaptations is made. The plots without mesh adaptation are shown in Figure 34, Figure 35 and Figure 36, while the plots with mesh adaptation

are shown in Figure 37, Figure 38 and Figure 39. There was a significant improvement at the shock boundary for mesh adaptation. This further showed that by application of mesh adaptation at the right places, the solution outcome further improved. The values of pressure ratio, density ratio and Mach number agreed with the values from standard shock tables.

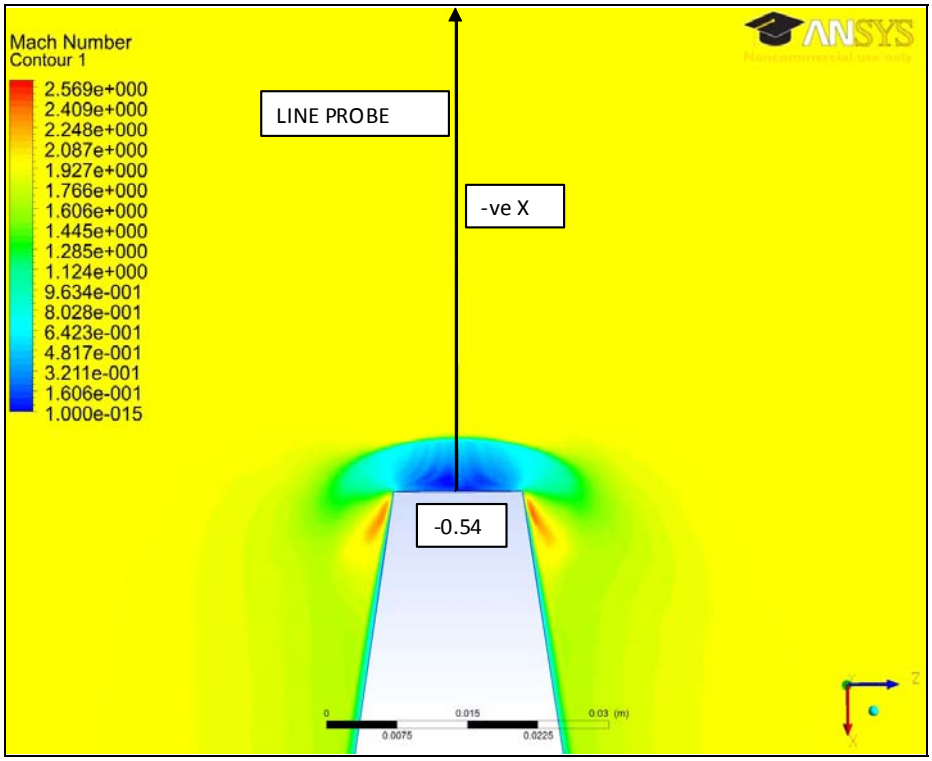

Figure 33. Probe Profile from Nose to Shock Front.

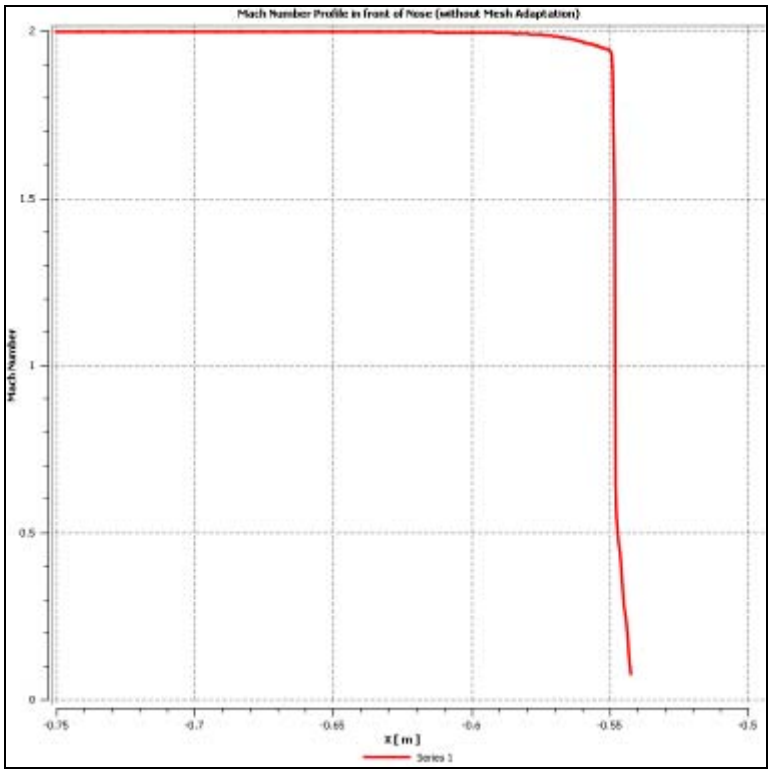

Figure 34. Mach Number Profile in front of Nose (Without Mesh Adaptation).

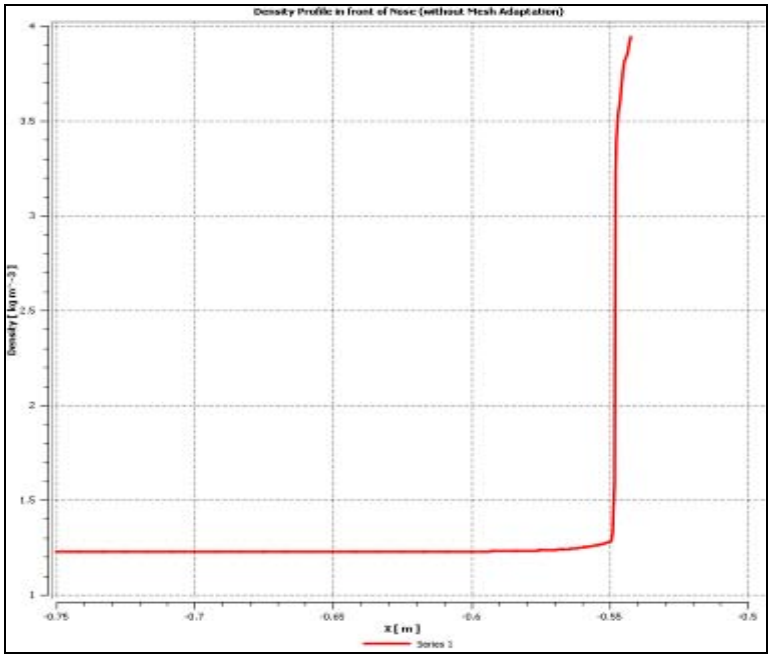

Figure 35. Density Profile in front of Nose (Without Mesh Adaptation).

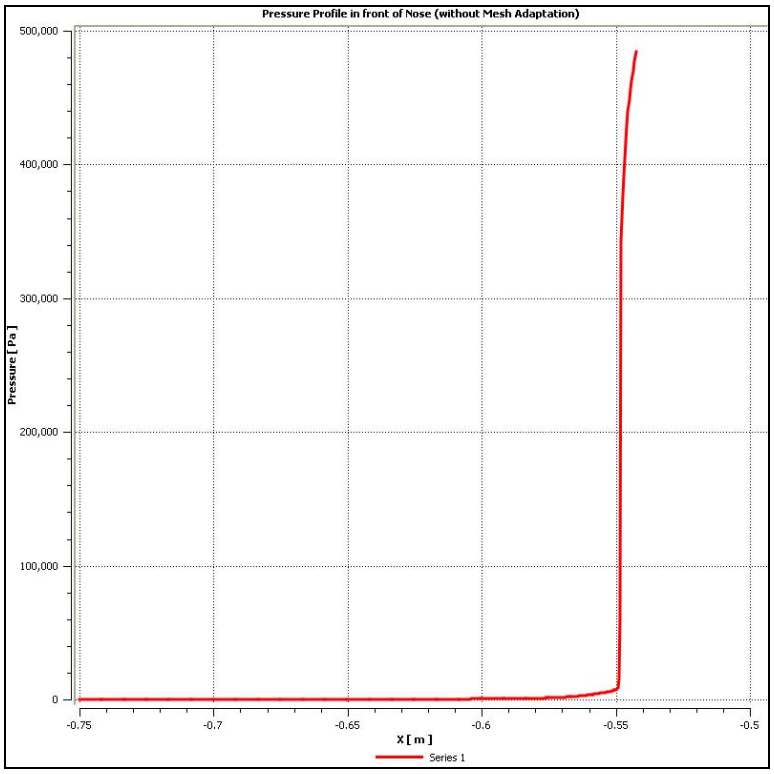

Figure 36. Pressure Profile in front of Nose (Without Mesh Adaptation).

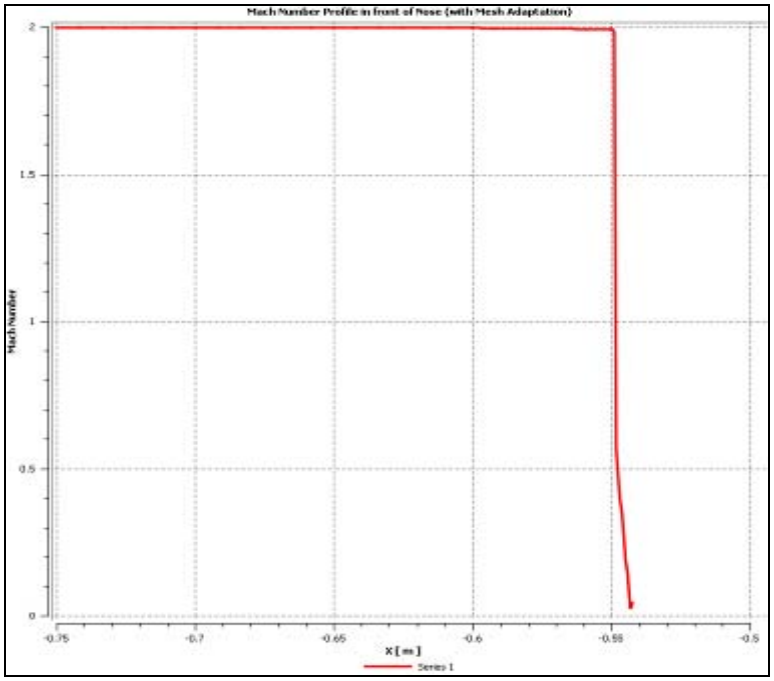

Figure 37. Mach Number Profile in front of Nose (With Mesh Adaptation).

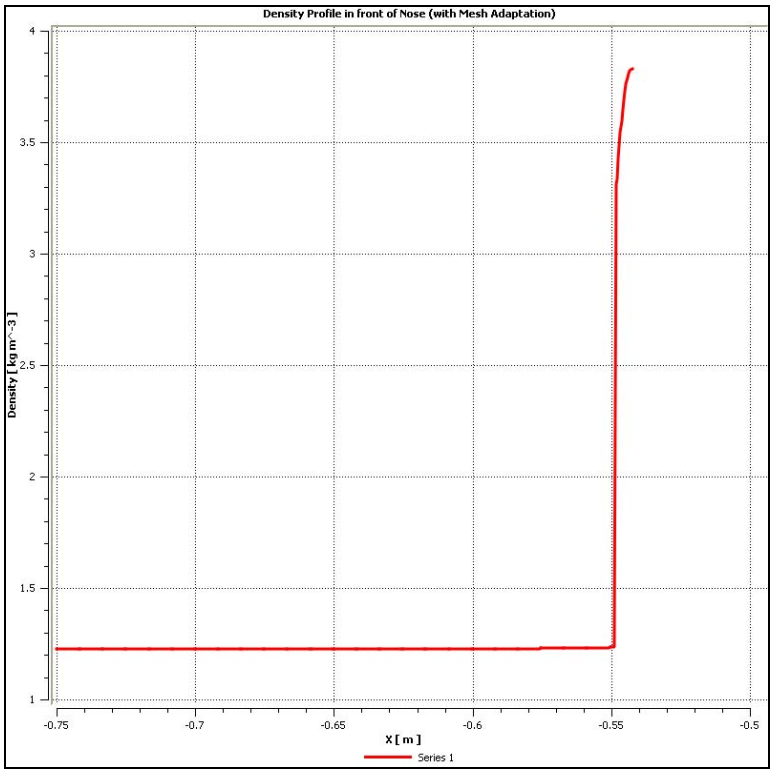

Figure 38. Density Profile in front of Nose (With Mesh Adaptation).

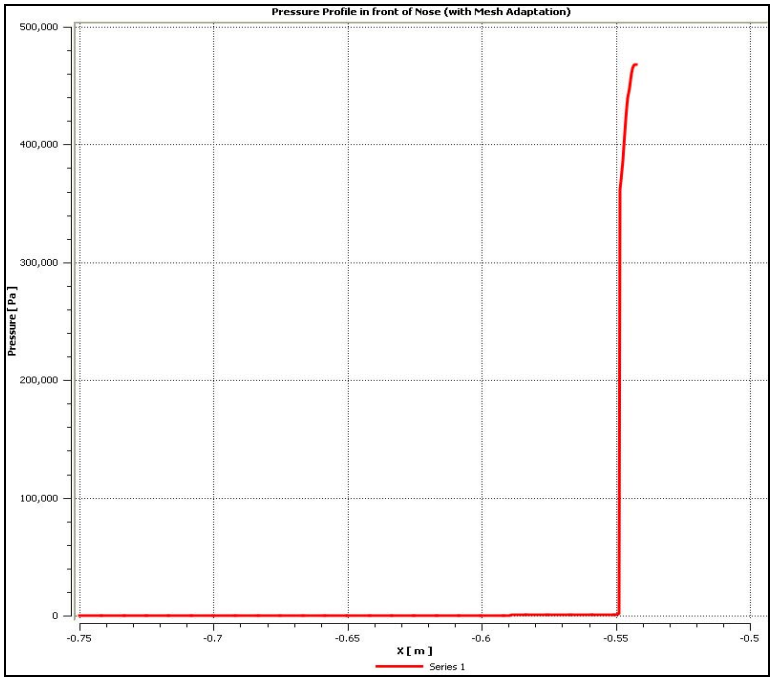

Figure 39. Pressure Profile in front of Nose (With Mesh Adaptation).

H. PROFILE CHANGES ACROSS BODY

An additional investigation was conducted to determine the Mach number, density and pressure changes across the body. Three probes were located at the nose, near cone and far cone, as shown in Figure 40. The Mach number, density and pressure profiles of the probe at the nose are shown in Figure 41, Figure 42 and Figure 43, respectively. The Mach number, density and pressure profiles of the probe at the near cone are shown in Figure 44, Figure 45 and Figure 46, respectively. The Mach number, density and pressure profiles of the probe at the far cone are shown in Figure 47, Figure 48 and Figure 49, respectively.

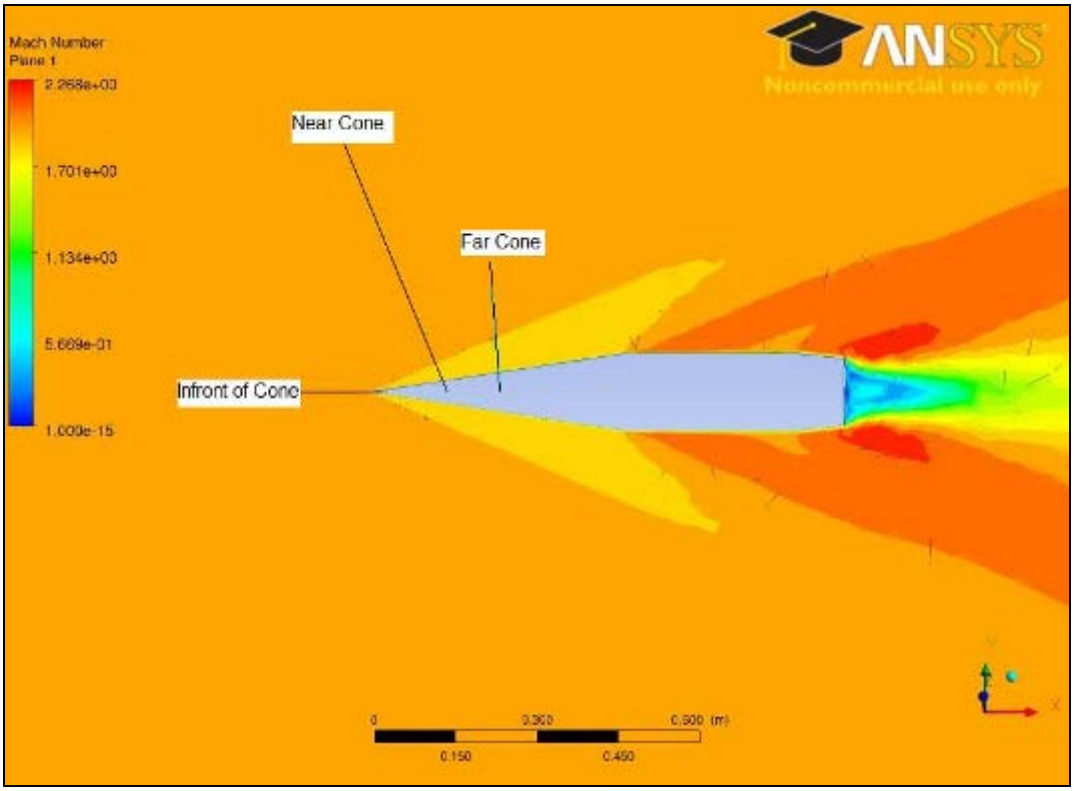

Figure 40. Locations of Probe from Nose to Cone of M549 Projectile.

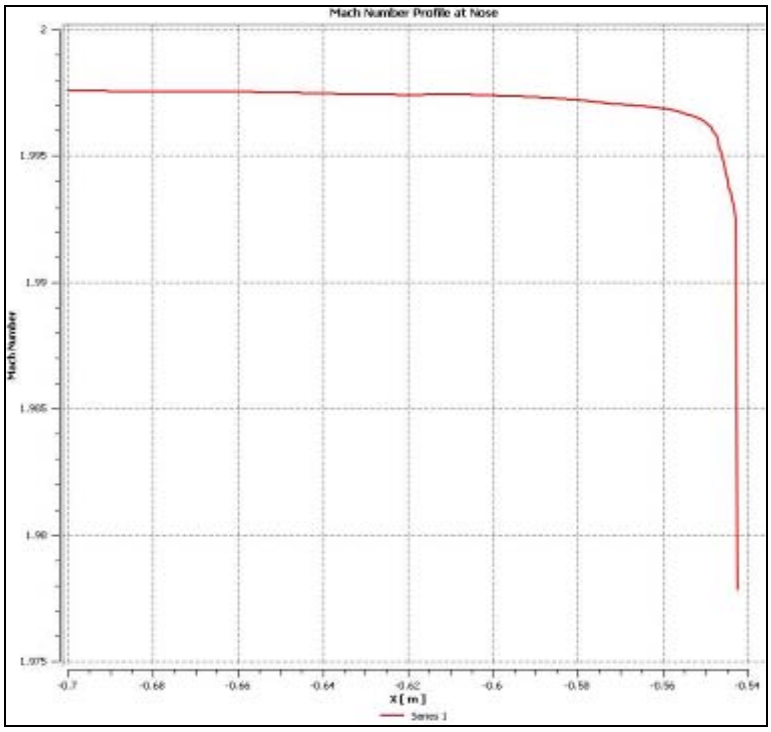

Figure 41. Mach Number Profile at Nose.

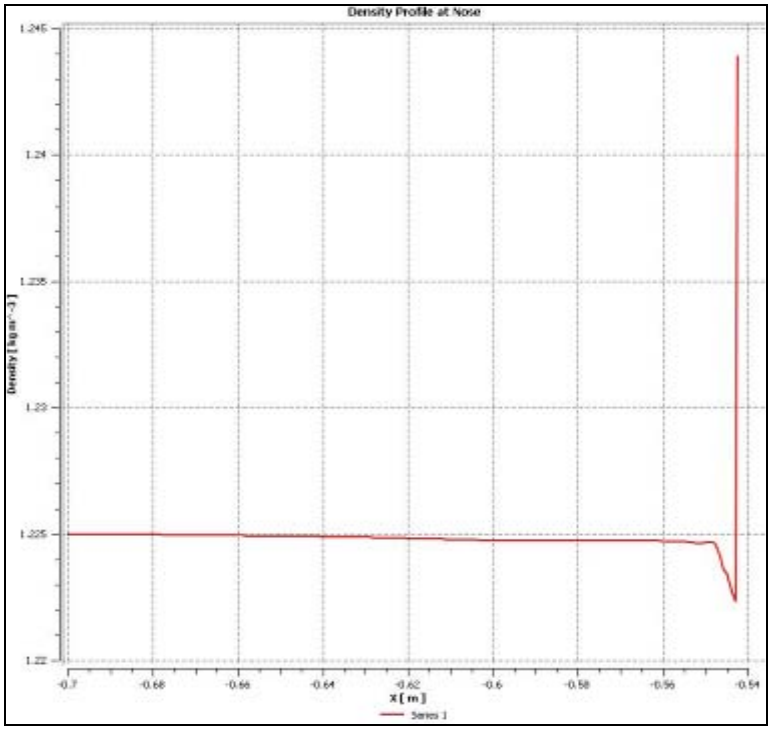

Figure 42. Density Profile at Nose.

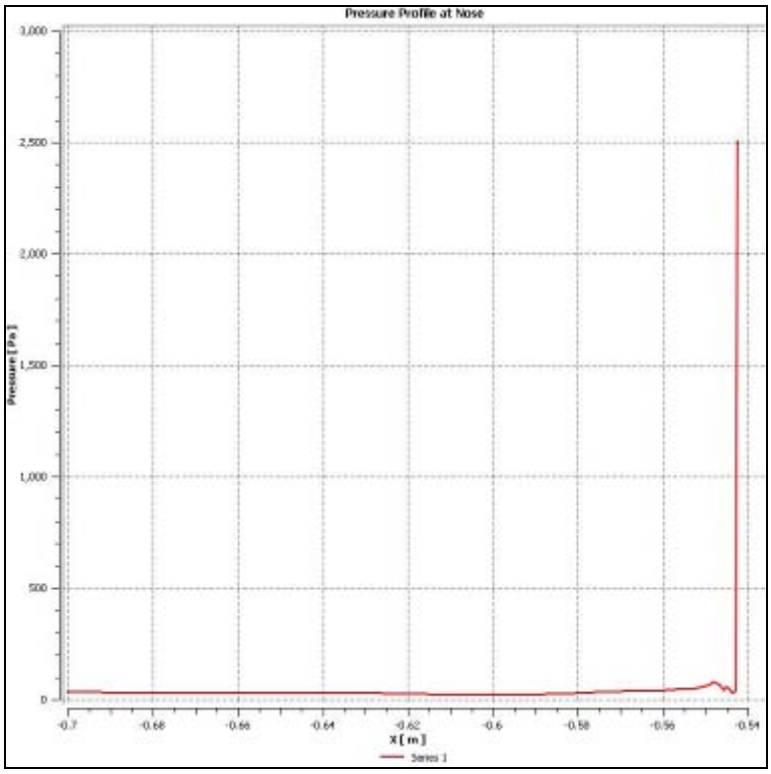

Figure 43. Pressure Profile at Nose.

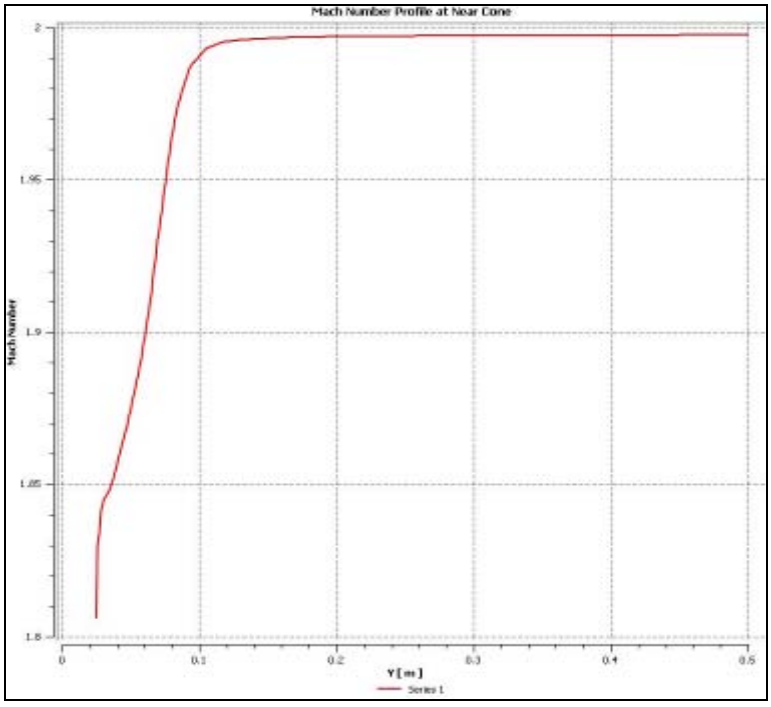

Figure 44. Mach Number Profile at Near Cone.

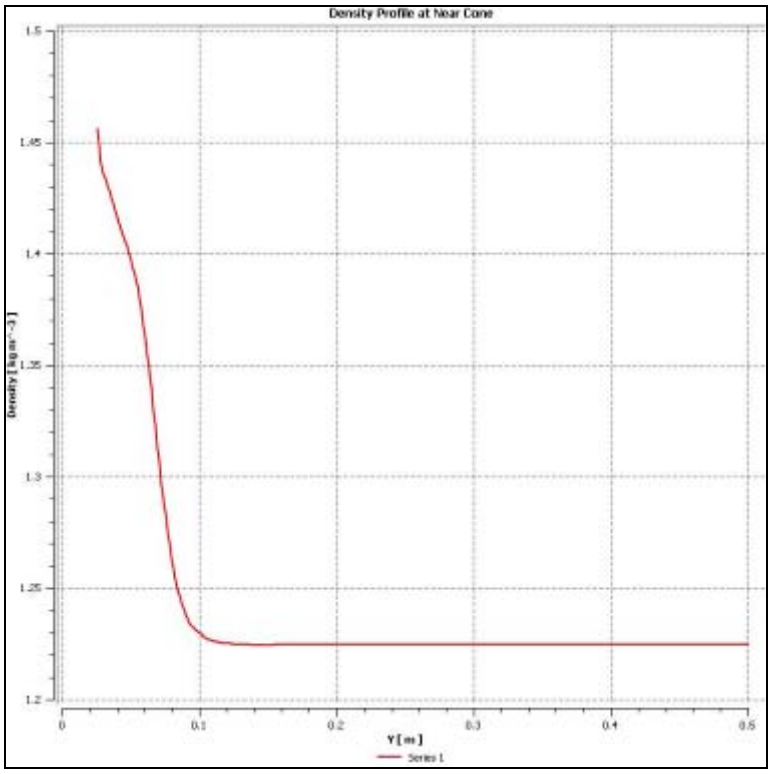

Figure 45. Density Profile at Near Cone.

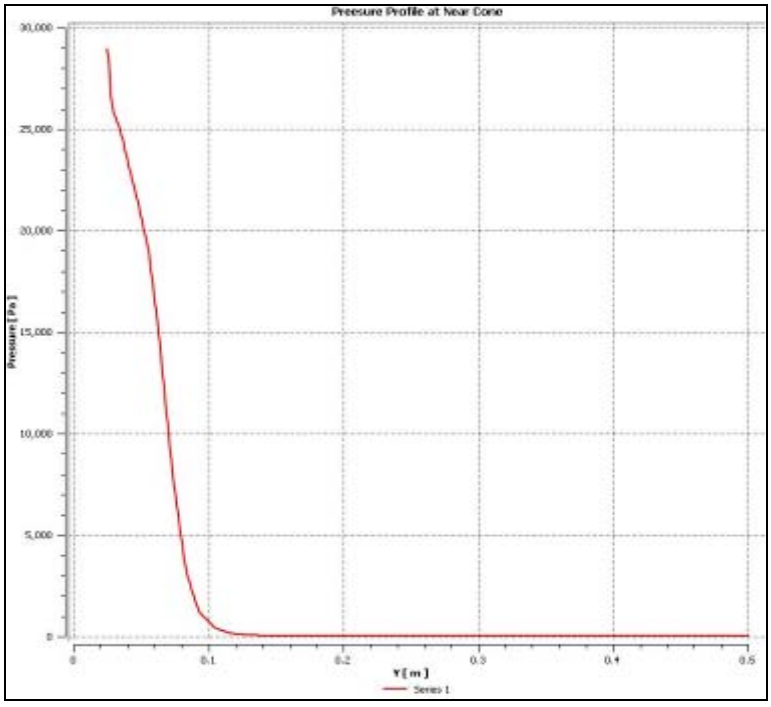

Figure 46. Pressure Profile at Near Cone.

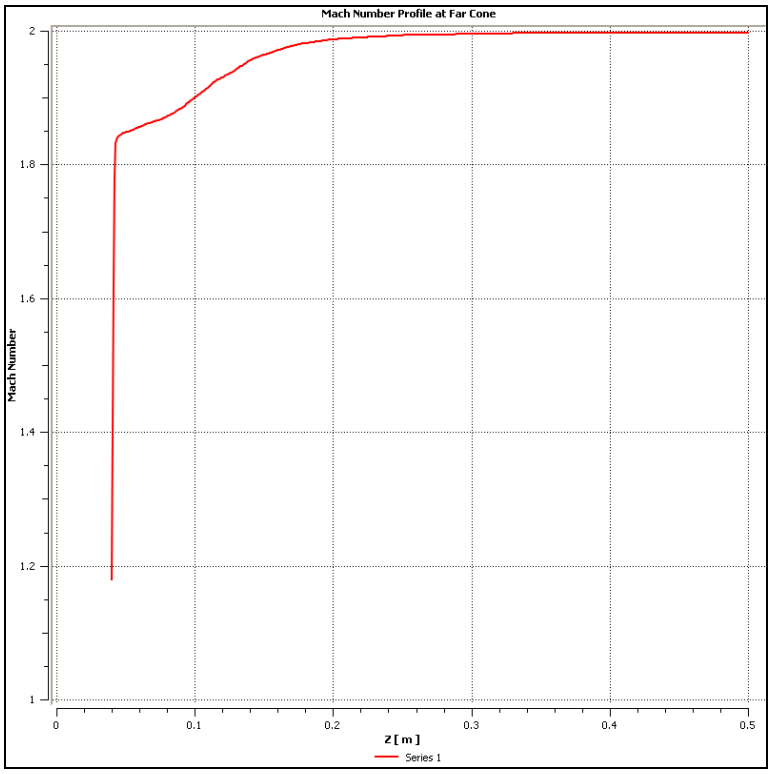

Figure 47. Mach Number Profile at Far Cone.

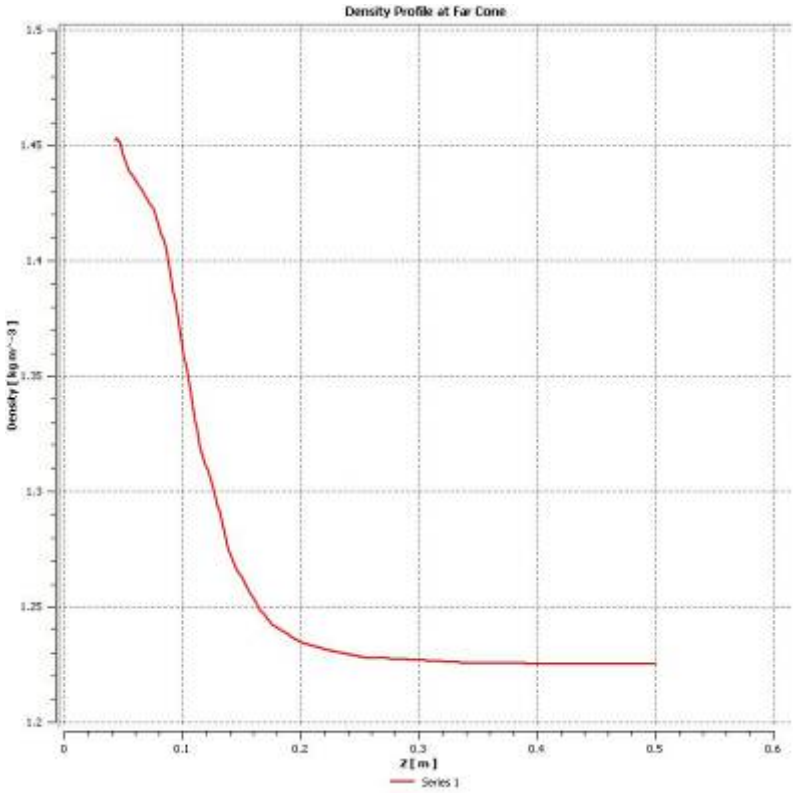

Figure 48. Density Profile at Far Cone.

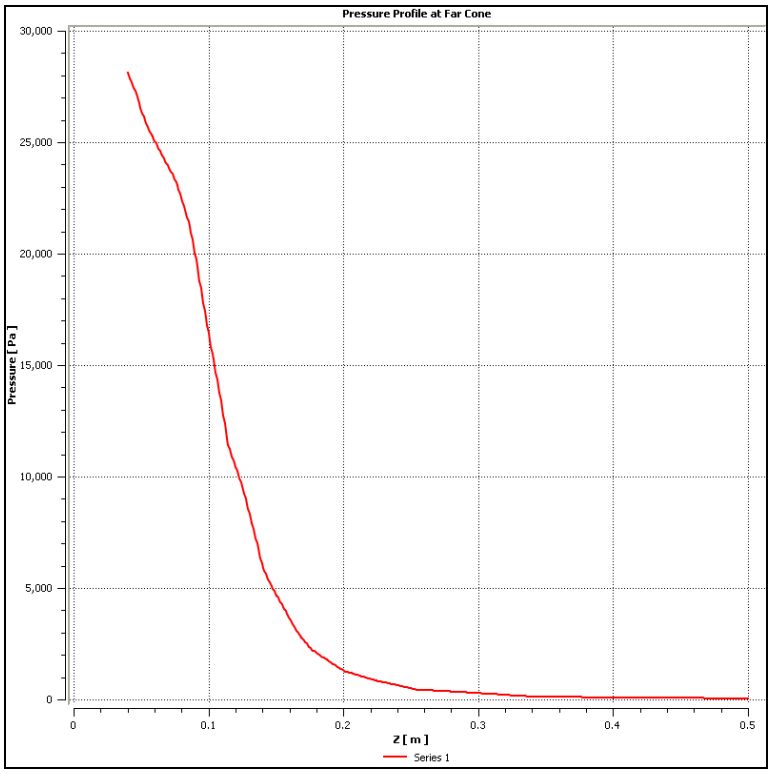

Figure 49. Pressure Profile at Far Cone.

It can be seen that there is a sharp jump observed in all the profiles at the nose of the cone. The profiles spread as the probe moves away from the nose. The following mesh refinements have been done: increasing the inflation layer from 8 to 16, decreasing the face spacing from 0.07mm to 0.06mm and decreasing the expansion factor from 1.2 to 1.1. The results obtained did not vary significantly from the original.

I. PROJECTILE ROCKET ORDNANCE DESIGN AND ANALYSIS SYSTEM (PRODAS)

One of the advanced professional ballistic softwares widely used by the military and defense industries is the Projectile Rocket Ordnance Design and Analysis System (PRODAS). PRODAS is based on six degrees of freedom (6 DOF) calculations that need detailed input, in-depth knowledge of the chosen projectile and is time-intensive. In Figure 50 a comparison of the total drag coefficient is shown for all the codes, including PRODAS. These PRODAS results were kindly provided by Colonel O. Mahmoud,

Egyptian Army [23]. In Figures 51 through 53, the AP05, CFX and the PRODAS total drag coefficients are shown individually. Finally, in Figure 54 only the AP05, CFX and the thin-layer BRL Navier-Stokes predictions are compared.

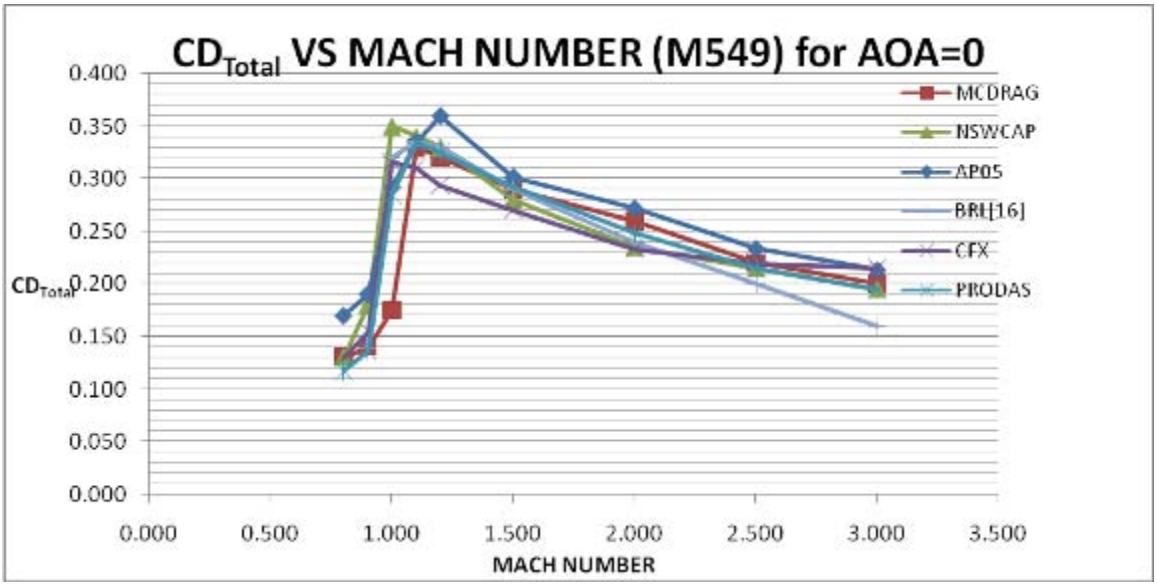

Figure 50. Total Drag Coefficient vs. Mach Number of PRODAS.

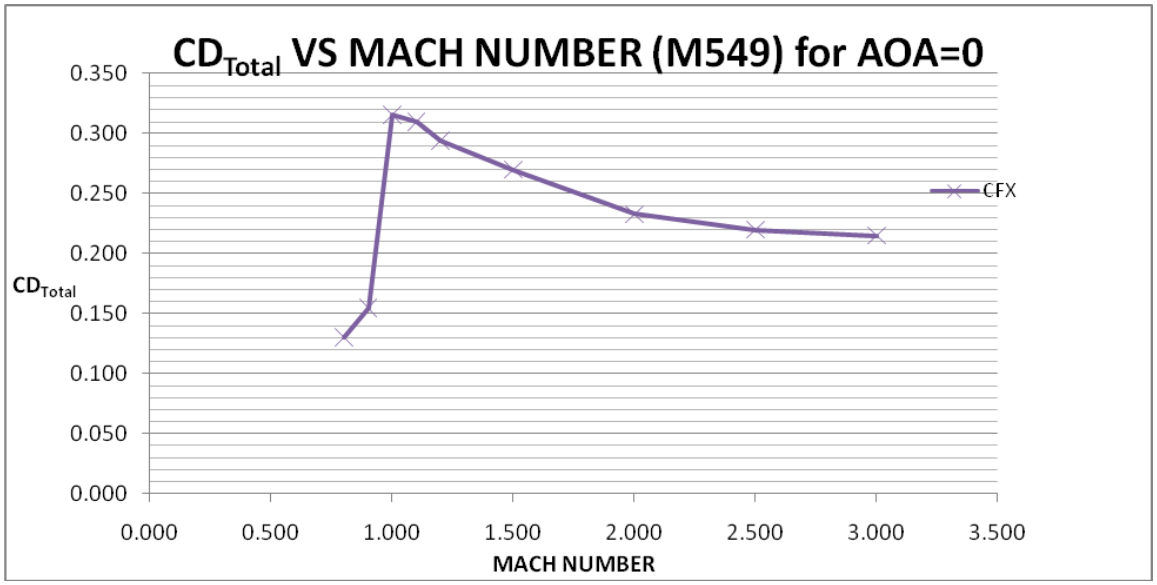

Figure 51. Total Drag Coefficient vs. Mach Number of CFX.

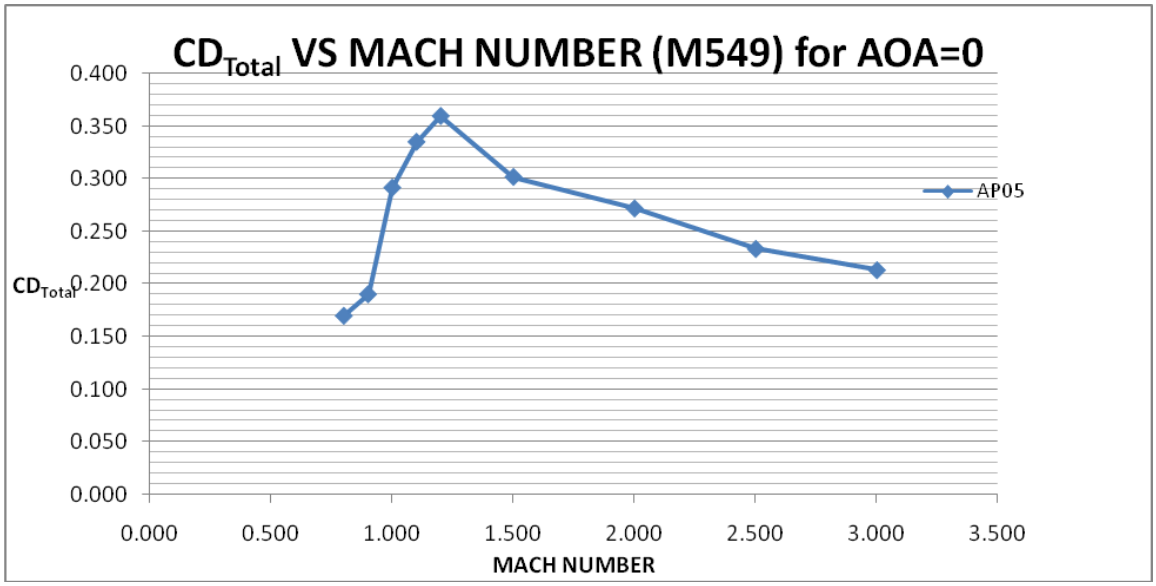

Figure 52. Total Drag Coefficient vs. Mach Number of AP05.

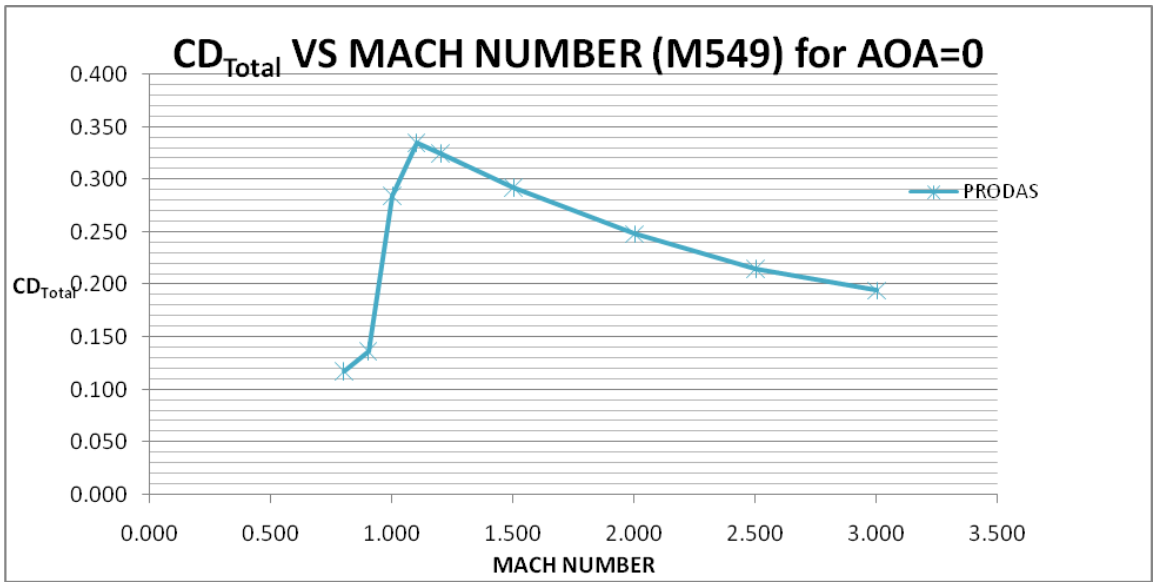

Figure 53. Total Drag Coefficient vs. Mach Number of PRODAS.

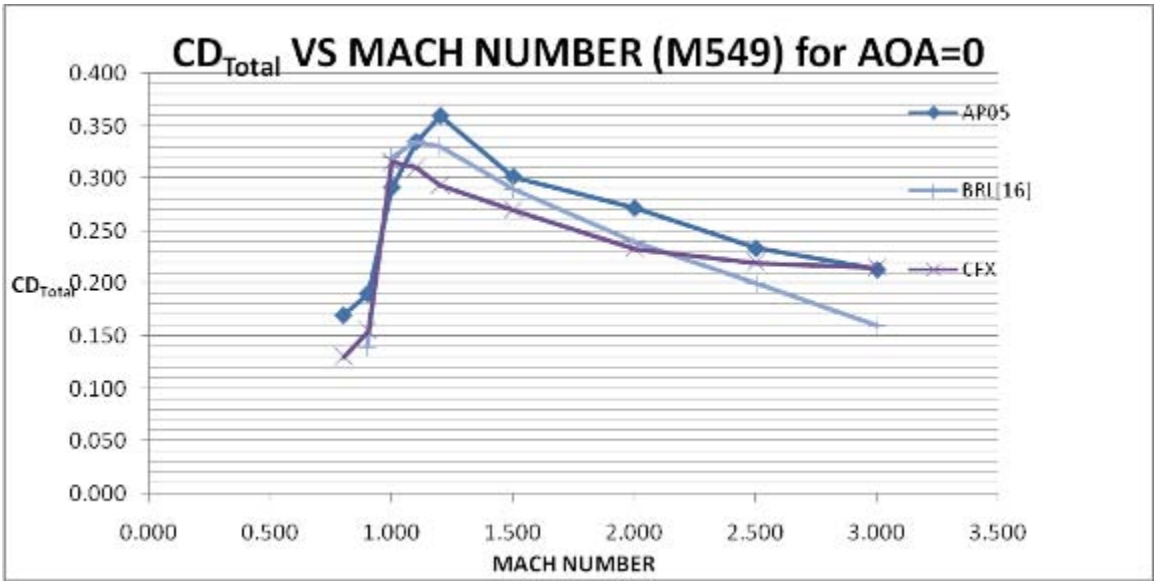

Figure 54. Total Drag Coefficient vs. Mach Number of AP05, CFX and PRODAS.

THIS PAGE INTENTIONALLY LEFT BLANK

VIII. CONCLUSION AND RECOMMENDATIONS

The semi-empirical AP05 code has provided a very fast way to obtain results. The CFX code, based on the numerical solution of the full Navier-Stokes equations, took about four hours for one data point. The comparison between the AP05 and CFX computed total drag coefficient shows a difference of about 30 percent in the high subsonic range, good agreement in the transonic region, but a difference of 22 percent at M=1.2, decreasing to zero at M=3. The BRL design codes are generally in better agreement with CFX and AP05, but the BRL thin-layer Navier-Stokes prediction deviates significantly at the high supersonic Mach numbers.

The use of mesh refinement in the critical regions produced better simulation results than without mesh refinement. In particular, the application of line control at the projectile's nose and inflation layer at the projectile's surfaces produced the correct bow shock characteristics at supersonic speeds.

In conclusion, this study serves as a foundation for using CFD to predict the aerodynamic performance of projectiles and missiles over the whole angle of attack range. The effect of better mesh refinement and different turbulent modeling can be explored.

THIS PAGE INTENTIONALLY LEFT BLANK

LIST OF REFERENCES

[1] C. J. Nietubicz, J. Sahu *et al.*, "Aerodynamic Coefficient Predictions for a Projectile Configuration at Transonic Speeds," US Army Ballistic Research Laboratory, Aberdeen Proving Ground, MD, BRL-MR-3639, December 1987.

[2] J. Sahu, "Numerical Computations of Transonic Critical Aerodynamic Behaviour," AIAA Journal, vol. 28, no. 5, May 1990.

[3] J. D. Anderson, Jr., "*Introduction to Flight,*" Fourth Edition, McGraw-Hill Higher Education, Boston, MA, 2000.

[4] U.S. Centennial of Flight Commission Website. Available: http://www.centennialofflight.gov/index.cfm.

[5] J. Sahu, and R. H. Karen, "Numerical Investigation of Supersonic Base Flow with Base Bleed," Army Research Laboratory, ARL-TR-955, December 1995.

[6] J. Sahu, and R. H. Karen, "Computational Modeling of a Segmented Projectile," Army Research Laboratory, ARL-TR-1988, June 1999.

[7] F. R. Menter, "Zonal Two Equation k-ω Turbulence Models for Aerodynamic Flows," AIAA Paper 93-2906, 1993.

[8] F. G. Moore, and R. C. Swanson, "Aerodynamics of Tactical Weapons Mach 3 and Angle-of-Attack 15^{o}, Part I-Theory Application," NSWC/DL TR-3584, February 1977.

[9] F. G. Moore, and R. C. Swanson, "Aerodynamics of Tactical Weapons Mach 3 and Angle-of-Attack 15^{o}, Part II-Computer Application and Usage," NSWC/DL TR-3600, February 1977.

[10] M. J. Van Dyke, "The Similarity Rules for Second Order Subsonic and Supersonic Flow," NACA Tech Notes 3875, October 1956.

[11] E.R. Van Driest, "Turbulent Boundary Layers in Compressible Fluids" Journal of the Aeronautical Science, vol. 18, no. 3, pp. 145–160, 1951.

[12] R. L. McCoy, "MCDrag – A Computer Program for Estimating the Drag Coefficient of Projectiles," US Army Ballistics Research Laboratory, Aberdeen Proving Ground, MD, ARBRL-PR-02293, February 1981.

[13] K. A. Hoffman, "Computational Fluid Dynamics for Engineers, Engineering Education System," Austin, TX, 1989.

[14] F. G. Moore, T. C. Hymer *et al.*, "The 2005 Version of the Aeroprediction Code: Part II- Users Guide," API Report no. 2, June 2004.

[15] S. I. Silton, "Navier Stokes Computations for Spinning Projectile from Subsonic to Supersonic Speeds," Army Research Laboratory, ARL-TR-2850, September 2002.

[16] J. Sahu, "Drag Predictions for Projectiles at Transonic and Supersonic Speeds," US Army Ballistics Research Laboratory, Aberdeen Proving Ground, MD, BRL-MR-3523, June 1986.

[17] J. Sahu, W. Sturek *et al.*, "Recent Application of CFD to the Aerodynamics of Army Projectiles," Army Research Laboratory, ARL-TR-22, December 1992.

[18] ANSYS, Inc. website. Available: http://www.ansys.com.

[19] D. Jones, "Numerical Solutions of the Flow Field for Conical Bodies in a Supersonic Stream," AD686646.

[20] Z. Kopal, "Table of Supersonic Flow Around Cones," Massachusetts Institute of Technology, Dept. of Electrical Engineering Tech. Report No. 1, Cambridge, MA, 1947.

[21] J. L. Sims, "Tables for Supersonic Flow Around Right Circular Cones at Zero Angle of Attack," NASA SP-3004, National Aeronautics and Space Administration, Washington, DC, 1964.

[22] J. L. Sims, "Tables for Supersonic Flow Around Right Circular Cones at Small Angle of Attack," NASA SP-3007, National Aeronautics and Space Administration, Washington, DC, 1964.

[23] O. Mahmoud (Private Communication), 2010.

APPENDIX A. AP05 RESULTS

CASE NO. 1

EXAMPLE CASE NO 1

ANGLE OF ATTACK = 0.00 DEGS
REFERENCE DIAMETER = 0.517 FT

REFERENCE CONDITIONS

MOMENT REFERENCE = 3.50 CALIBERS FROM NOSE TIP

ALIMIT MACH NUMBER = 2.00

ALIMS MACH NUMBER = 4.20

********** BODY GEOMETRY SAME AS PREVIOUS CASE **********

1

SUMMARY OF AERODYNAMIC COEFFICIENTS FOR CASE NO. 2

EXAMPLE CASE NO 1

ROLL = 0

BODY AXIAL FORCE CONTRIBUTIONS

MACH NO.	REYS. NO./MACH NO./FT.	SKIN FRICTION	BASE PRESSURE	PRESSURE	PROTRUSIONS	TOTAL
3.200	0.6929E+07	0.0302	0.0588	0.1141	0.0000	0.2031
3.000	0.6929E+07	0.0316	0.0642	0.1171	0.0000	0.2129

```
    2.500                   0.6929E+07                              0.0354
0.0779                           0.1259                             0.0000
0.2392
    2.400                   0.6929E+07                              0.0363
0.0825                           0.1265                             0.0000
0.2452
    2.200                   0.6929E+07                              0.0380
0.0926                           0.1278                             0.0000
0.2584
    2.000                   0.6929E+07                              0.0399
0.1025                           0.1293                             0.0000
0.2717
    1.800                   0.6929E+07                              0.0418
0.1125                           0.1311                             0.0000
0.2855
    1.600                   0.6929E+07                              0.0438
0.1238                           0.1341                             0.0000
0.3017
    1.400                   0.6929E+07                              0.0460
0.1429                           0.1403                             0.0000
0.3292
    1.200                   0.6929E+07                              0.0481
0.1592                           0.1524                             0.0000
0.3597
    1.100                   0.6929E+07                              0.0492
0.1551                           0.1468                             0.0000
0.3511
    1.000                   0.6929E+07                              0.0504
0.1455                           0.0956                             0.0000
0.2915
    0.900                   0.6929E+07                              0.0515
0.1312                           0.0176                             0.0000
0.2003
    0.800                   0.6929E+07                              0.0527
0.1059                           0.0109                             0.0000
0.1695


                                                          TOTAL         STATIC
AERODYNAMICS(FORCE/ALPHA)

          MACH NO.            CA            CN            CD            CL
CM          CNAL            CMAL        XCP/DREF        XCP/L

            3.200           0.203           0.000       0.203         0.000
0.000        2.457          4.147         -1.688         -0.297
            3.000           0.213           0.000       0.213         0.000
0.000        2.493          4.185         -1.679         -0.295
            2.500           0.239           0.000       0.239         0.000
0.000        2.616          4.356         -1.665         -0.293
            2.400           0.245           0.000       0.245         0.000
0.000        2.638          4.478         -1.697         -0.298
            2.200           0.258           0.000       0.258         0.000
0.000        2.671          4.711         -1.764         -0.310
```

```
            2.000          0.272          0.000       0.272        0.000
0.000        2.686         4.931         -1.836        -0.323
            1.800          0.285          0.000       0.285        0.000
0.000        2.498         5.155         -2.064        -0.363
            1.600          0.302          0.000       0.302        0.000
0.000        2.294         5.323         -2.320        -0.408
            1.400          0.329          0.000       0.329        0.000
0.000        2.081         5.332         -2.563        -0.450
            1.200          0.360          0.000       0.360        0.000
0.000        1.848         5.166         -2.796        -0.491
            1.100          0.351          0.000       0.351        0.000
0.000        1.910         5.395         -2.824        -0.496
            1.000          0.291          0.000       0.291        0.000
0.000        1.969         5.546         -2.817        -0.495
            0.900          0.200          0.000       0.200        0.000
0.000        2.013         5.496         -2.730        -0.480
            0.800          0.169          0.000       0.169        0.000
0.000        1.776         4.772         -2.687        -0.472
          NOTE: THE ABOVE CM, CMAL, AND XCP/DREF ARE REFERENCED TO THE
POINT AT    3.5000 CALIBERS FROM NOSE TIP
```

THIS PAGE INTENTIONALLY LEFT BLANK

APPENDIX B. BLUNT NOSE SIMULATION SOLVER SETTING

FLOW: Flow Analysis 1
&replace DOMAIN: Default Domain
Coord Frame = Coord 0
Domain Type = Fluid
Location = B28
BOUNDARY: Default Domain Default
Boundary Type = WALL
Create Other Side = Off
Interface Boundary = Off
Location = F39.28
BOUNDARY CONDITIONS:
HEAT TRANSFER:
Option = Adiabatic
END
MASS AND MOMENTUM:
Option = No Slip Wall
END
WALL ROUGHNESS:
Option = Smooth Wall
END
END
END
BOUNDARY: Inlet
Boundary Type = INLET
Interface Boundary = Off
Location = F30.28
BOUNDARY CONDITIONS:
FLOW REGIME:
Option = Supersonic
END
HEAT TRANSFER:
Option = Static Temperature
Static Temperature = 288.15 [K]
END
MASS AND MOMENTUM:
Normal Speed = 680 [m s^-1]
Option = Normal Speed and Pressure
Relative Static Pressure = 0 [Pa]
END
TURBULENCE:
Option = Medium Intensity and Eddy Viscosity Ratio
END

END
END
BOUNDARY: Missile
Boundary Type = WALL
Create Other Side = Off
Interface Boundary = Off
Location = F38.28,F37.28,F32.28,F31.28
BOUNDARY CONDITIONS:
HEAT TRANSFER:
Option = Adiabatic
END
MASS AND MOMENTUM:
Option = No Slip Wall
END
WALL ROUGHNESS:
Option = Smooth Wall
END
END
END
BOUNDARY: Outlet
Boundary Type = OUTLET
Interface Boundary = Off
Location = F36.28,F35.28,F33.28,F34.28
BOUNDARY CONDITIONS:
FLOW REGIME:
Option = Subsonic
END
MASS AND MOMENTUM:
Option = Average Static Pressure
Pressure Profile Blend = 0.05
Relative Pressure = 0 [Pa]
END
PRESSURE AVERAGING:
Option = Average Over Whole Outlet
END
END
END
BOUNDARY: sym
Boundary Type = SYMMETRY
Interface Boundary = Off
Location = F29.28
END
DOMAIN MODELS:
BUOYANCY MODEL:
Option = Non Buoyant

END
DOMAIN MOTION:
Option = Stationary
END
MESH DEFORMATION:
Option = None
END
REFERENCE PRESSURE:
Reference Pressure = 1 [atm]
END
END
FLUID DEFINITION: Fluid 1
Material = Air Ideal Gas
Option = Material Library
MORPHOLOGY:
Option = Continuous Fluid
END
END
FLUID MODELS:
COMBUSTION MODEL:
Option = None
END
HEAT TRANSFER MODEL:
Option = Total Energy
END
THERMAL RADIATION MODEL:
Option = None
END
TURBULENCE MODEL:
Option = SST
END
TURBULENT WALL FUNCTIONS:
Option = Automatic
END
END
END
END
FLOW: Flow Analysis 1
&replace SOLUTION UNITS:
Angle Units = [rad]
Length Units = [m]
Mass Units = [kg]
Solid Angle Units = [sr]
Temperature Units = [K]
Time Units = [s]

```
END
END
FLOW: Flow Analysis 1
&replace SOLVER CONTROL:
Turbulence Numerics = First Order
ADVECTION SCHEME:
Option = High Resolution
END
COMPRESSIBILITY CONTROL:
High Speed Numerics = On
END
CONVERGENCE CONTROL:
Length Scale Option = Conservative
Maximum Number of Iterations = 100
Minimum Number of Iterations = 1
Timescale Control = Auto Timescale
Timescale Factor = 1.0
END
CONVERGENCE CRITERIA:
Residual Target = 1.E-4
Residual Type = RMS
END
DYNAMIC MODEL CONTROL:
Global Dynamic Model Control = On
END
END
END
FLOW: Flow Analysis 1
&replace OUTPUT CONTROL:
RESULTS:
File Compression Level = Default
Option = Standard
END
END
END
```

APPENDIX C. AP05 GUIDE

A. THE 2005 VERSION OF THE AEROPREDICTION CODE (AP05)

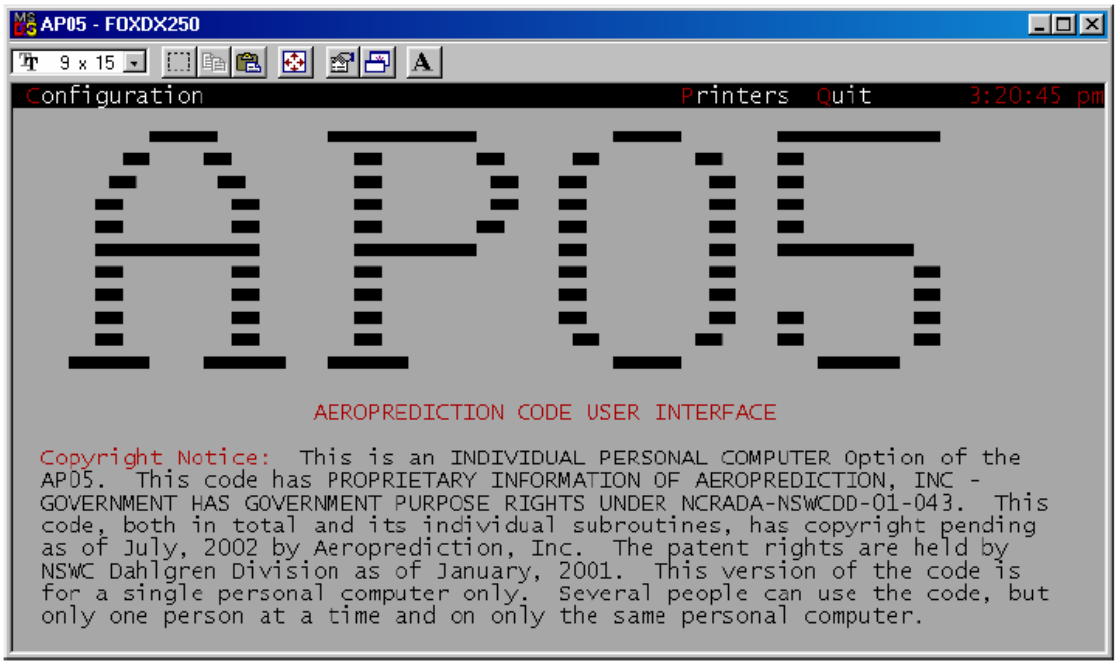

Figure 55. AP05 Welcome Screen.

B. INTRODUCTION

The current version of the Aeroprediction (AP) code is the product of over 30 years of continuing improvement and refinement. Originally developed in 1972 as a code to predict the aerodynamic performance of spin-stabilized projectiles, it was limited in its capabilities to body alone configurations at angles of attack of 10 deg or less and Mach numbers below 3. At the time, it was the only total force and moment aerodynamic prediction code oriented toward weapons technology applications. Previously, the resources available for preliminary design work in this area consisted of wind tunnel data bases, handbooks, or individually applied theoretical methods. The ability of the original AP code to integrate and automate the aerodynamic prediction process into a reliable, accurate, and more convenient form proved to be a popular innovation and several

requests for the code were received. In addition, considerable community interest was shown in expanding the capabilities of the AP code to include configurations with lifting surfaces. Sponsor approval for further improvements was forthcoming and the original code was extended to include two sets of lifting surfaces in 1974, dynamic derivatives in 1977, and Mach numbers up to 8 at higher angles of attack in 1981. This latter version of the AP code will be referred to as AP81. AP81 proved to be a very useful tool, but it still suffered from a number of shortcomings [14].

In 1993, a new version of the code was released (AP93) that addressed many of these limitations. AP93 included nonlinear wing alone methodology as well as nonlinear wing-body and body-wing interference factors. Together with improved base drag predictions for wings at angle of attack, these additions increased the useful angle of attack range up to 30 deg. The upper limit on Mach number was increased to 20 by including an option to use real gas relations. To make AP93 even more useful in the high Mach number range, methodology to compute surface heat transfer coefficients and adiabatic wall temperatures was also added. While AP93 provided an expanded high angle of attack capability, it still fell short of the full range of coverage needed to model modern weapon systems. Angles of attack close to 90 deg may be experienced at subsonic Mach numbers if significant winds are present at launch or if launch occurs from a maneuvering aircraft. At higher supersonic Mach numbers, angles of attack up to 40 deg are possible during the terminal homing phase as missiles may be forced to react quickly to intercept their targets. In order to develop a model for this extended flight envelope, experimental information from several wind tunnel data bases was used to develop a semi empirical model which could predict nonlinear aerodynamics up to angles of attack of 90 deg. This updated version of the code became AP95 and was the first release to be available in a personal computer (PC) format [14].

The AP98 added significant new capability to the AP95. This new capability includes the capability to model missile configurations in the cross or M = 45 deg roll orientation as well as the plus or M = 0 deg roll position. The AP98 also includes: the nonlinear force distribution over the body and lifting surfaces for use by the structural

analyst; an improvement in axial force computations at angle of attack; the capability to model noncircular bodies including ellipses, squares, diamonds, triangles, and inverted triangles [14].

The AP02 focused on technology needs derived from emerging projectile concepts. The AP02 was the first version in 25 years to focus on projectile, versus missile aerodynamic requirements. Technology needs addressed by the AP02 included: 6 and 8 fin aerodynamics in addition to the 2 or 4 capability; refinement of the nonlinear aerodynamic terms; improved dynamic derivatives; improved power-on base drag; incorporation of a base-bleed capability; improved zero- lift axial force for non axis symmetric bodies; trailing-edge flap aerodynamics; an aerodynamic smoother; and finally, integration of both a particle ballistic trajectory model and a trim three-degree-of-freedom trajectory model with the AP02 [14].

The AP05 continued the AP02 approach of meeting emerging weapon needs, along with refining some of the existing methods where inaccuracy has existed from the early days of the aeroprediction code development. AP05 also continues the trend started with the AP95 in making the code more user friendly, productive and cost effective from the engineer's standpoint. The technologies incorporated to meet emerging weapon requirements include trailing-edge bluntness on low angle of attack normal force coefficient slope, three- fin aerodynamics, and truncated leading and trailing edge wing axial force coefficient. Improvements made to correct existing accuracy problems were for truncated nose shapes at transonic and subsonic speeds, for small caliber weapons, and various other errors found in the AP02. As far as improved productivity for the engineer, trim aerodynamics are now available along with protuberance aerodynamic inputs and a user defined boundary layer transition for the body and wing [14].

C. AP05 MODULES

The AP05 actually contains much more than the new aerodynamics technology added to the previous version of the code, the AP02. The AP05 contains the pre-processor, the postprocessor, the aerodynamic module, trim aerodynamics module, a ballistic trajectory module and a three-degree-of-freedom trim performance module. The

pre-processor contains geometry inputs, aerodynamic option inputs, trajectory inputs, and various optional computations available in the aerodynamics module. The post-processor contains outputs that can be in the form of tables of data or plots of aerodynamic data or trajectory information. The aerodynamics module contains all aerodynamic computations and is used in a standalone mode or to provide inputs to the trajectory modules. Common to the trajectory modules and the aerodynamic modules is the geometry inputs. The geometry inputs are required for all aerodynamic computations [14].

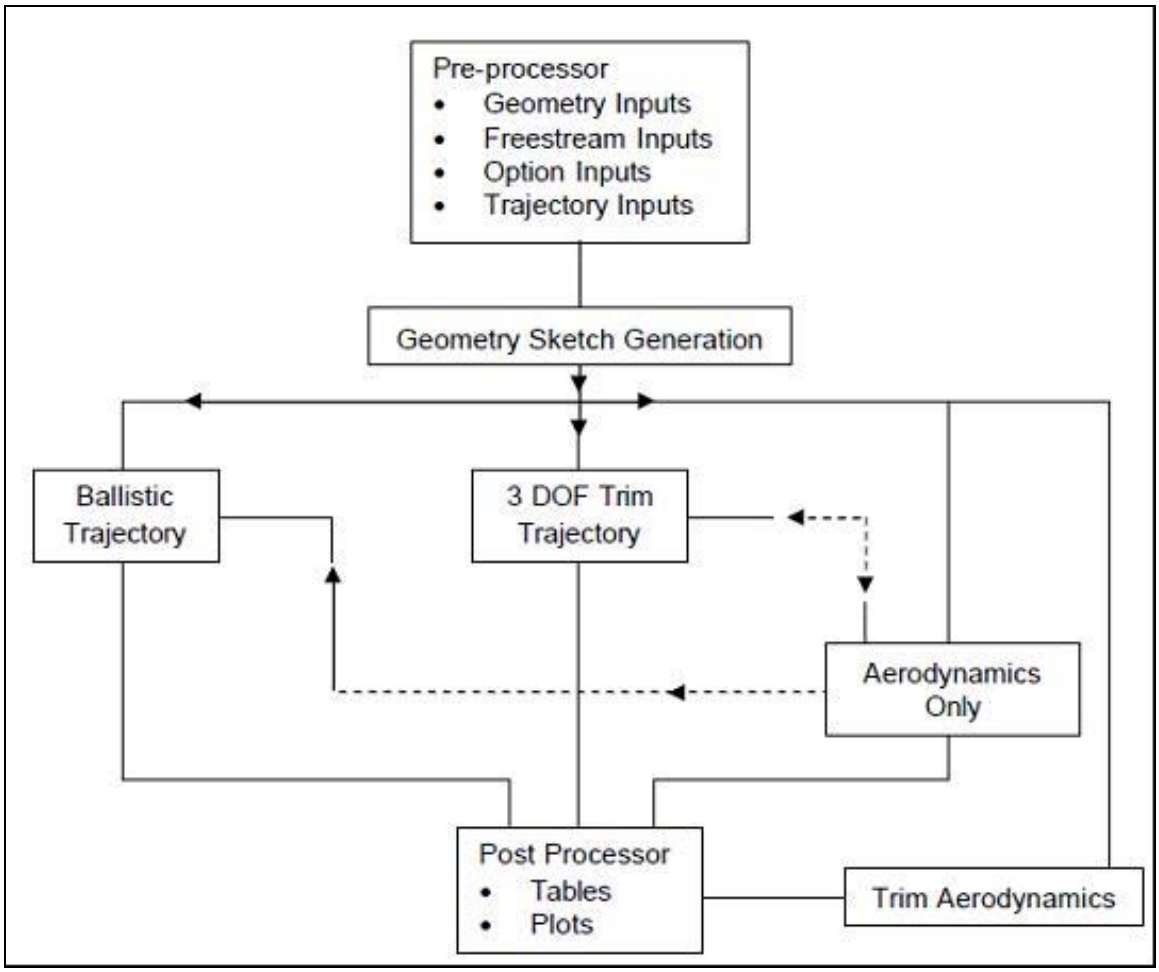

Figure 56. AP05 Logic Flow.

D. INTERFACE BASICS

The AP05 Interface consists of the menus, data entry screens, and other features that make it easy for the user to communicate with the AP05. The AP05 Interface is designed for use with a mouse or a standard keyboard. With a keyboard, the arrow keys and keystroke combinations are used to enter data or to choose objects and controls in the interface [14].

E. KEYBOARD TECHNIQUES

1. Using Menus with the Keyboard

The AP05 Interface menu system consists of the following parts: menu bar, menu pads, menu popups and menu options [14].

2. Menu Bar

The menu bar is located along the top of the AP05 Interface title screen. The *menu bar* displays names for menu popups. These names on the menu bar are called *menu pads*. The content of the menu bar changes as the user accesses different parts of the interface. Different actions cause menu pads to be added to and removed from the menu bar [14].

3. Menu Pads

Menu pads appear on the menu bar and display either the name of a menu popup, a data entry screen, or an action to be taken. The keyboard can be used to display the menu popup or data entry screen, or cause the action associated with each menu pad. Certain menu pads may be invisible and cannot be chosen. These menu pads are *disabled*. To access the menu bar, press the Alt key. The **Configuration** menu pad appears highlighted because it is selected. Press the Right and Left Arrow keys to move from menu pad to menu pad. To choose a menu pad selection, press the Enter key. An alternate method of choosing a menu pad selection is to press the hot key in the menu pad name. The *hot key* is highlighted and is usually the first letter in the menu pad name [14].

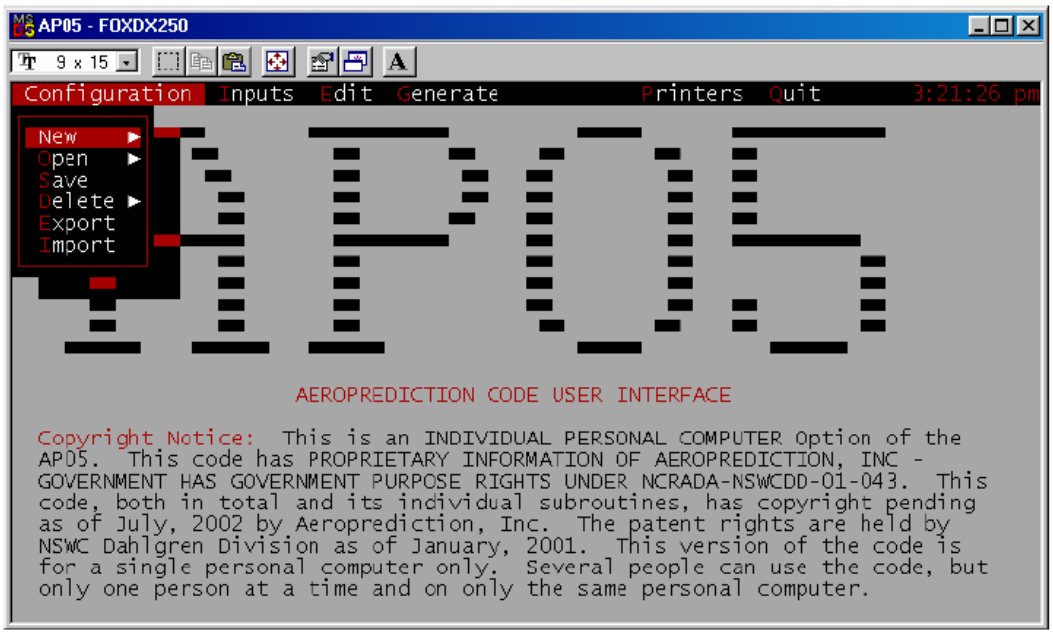

Figure 57. AP05 Interface Menu System.

4. Menu Popups

Some menu pads control menu popups. *Menu popups* are lists of related options. When you choose an option from a menu popup, you are telling the AP05 Interface what action to take. *Choose* means to activate a *selection* (highlighted option) by pressing the Enter key. Once a menu popup is displayed, you will usually choose an available option, as described in the next section. If you wish to deactivate a menu popup without choosing an option, press the Alt key [14].

5. Menu Options

Menu popups contain *options*. The options on each menu popup are logically related to the controlling menu pad. On a single menu popup, options may be further grouped to indicate that they produce similar outcomes. These groups are separated by divider lines. Certain menu options are followed by an arrow pointing to the right. When you choose this type of option, another menu popup appears with a different set of options. Sometimes a menu option will be invisible and cannot be chosen. This menu option is disabled [14].

Once a menu popup appears, an option can be chosen in one of the following ways:

- Press the hot key for the option.
- Use the Up and Down Arrow keys to select the desired option, then press the Enter key.

6. Using Data Entry Screens with the Keyboard

When you choose certain menu pads or menu popup options, a data entry screen will appear. Data entry screens contain fields to enter data and a variety of controls that are used to designate, confirm, or cancel actions. The fields and controls are explained in the next few paragraphs. In addition, methods of moving in data entry screens will also be explained [14].

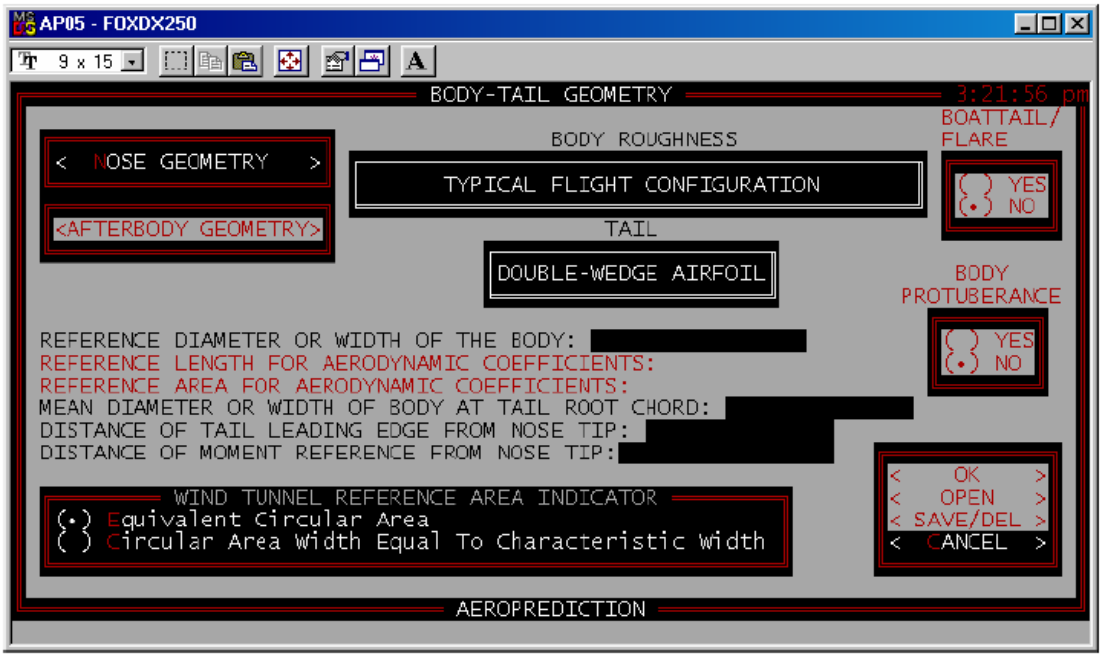

Figure 58. Example AP05 Interface Data Entry Screen.

7. Data Fields

In the data entry screen, data item descriptions consist of descriptive text followed by a colon. In most cases, the data item description is immediately followed by an associated data field. The *data field* is a rectangular area designated for the display of

specific related data from the AP05 Interface or the entry of corresponding data by the user. The AP05Interface interprets a blank numeric data field as zero, and a blank character data field as null. To select a data field, press the Tab key until the desired data field is highlighted. To enter data, type in a response and press the Enter key. In the cases where the data field requires numeric data, a message is displayed at the bottom of the data entry screen informing the user of the required units and the data entry format [14].

8. Pushbutton

A *pushbutton* is enclosed in angle brackets and contains key words that describe the action it triggers. The action associated with a pushbutton occurs immediately. The action specified may result in the completion or cancellation of the data entry process, or it may cause another data entry screen to be displayed. To select a pushbutton, press the Tab key until the desired pushbutton is highlighted. To choose a selected pushbutton, press the Enter key. 3.1.2.3 Radio Button. A *radio button* is a set of parentheses followed by text. Radio buttons are situated as groups of related items. Only one radio button in a group can be chosen at any given time. To select a radio button, press the Tab key until the desired radio button is highlighted. To choose a selected radio button, press the Enter key. When a radio button is chosen, a bullet appears in the parentheses and any previously chosen radio button in the group becomes deselected. In the AP05 Interface data entry screens, all radio button groups have a radio button that is chosen as a default [14].

9. Popup Control

The rectangle with double lines on the right and bottom edges (Figure 59) is a *popup control* that you can choose to display the associated popup. To select a popup control, press the Tab key until the desired popup control is highlighted. To choose a selected popup control and display the associated popup, press the Enter key. When the popup is displayed, use the PgDn and PgUp keys to scroll the list one full window at a time. Use the Home and End keys to move to the first or last option on the popup. To choose a popup option, press the Up and Down Arrow keys to select the option, then press the Enter key. In some popups, the popup options are listed in alphabetical order.

To move directly to an option on an alphabetized popup, type enough letters to uniquely identify the option. The letters you type don't appear on the screen. When the appropriate option is selected, press the Enter key [14].

The action associated with a popup option may cause another data entry screen to be displayed or may result in unseen internal data processing. In either case, the user's most recent selection will be displayed in the popup control rectangle. In AP05 Interface data entry screens, the first popup option is chosen as a default. Figure 59 shows the AP05 Interface data entry screen depicted in Figure 59 with a popup control chosen and its associated popup options displayed [14].

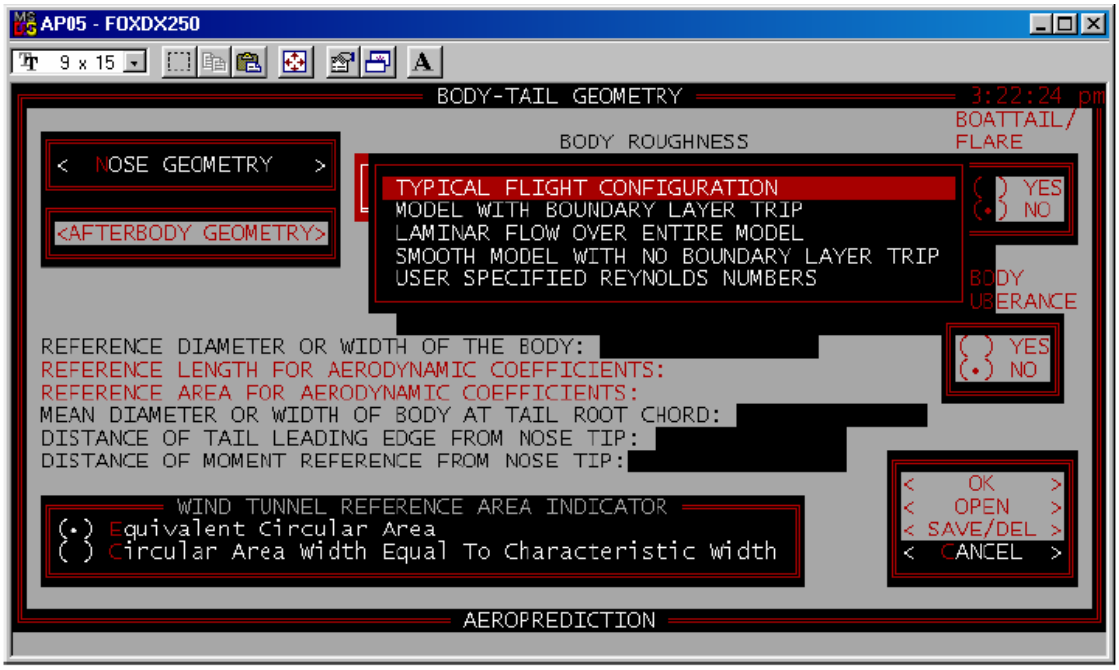

Figure 59. Example AP05 Interface Data Entry Screen with Popup Control Activated.

10. List

A *list* is simply a box containing a list of items. When using the keyboard, a list is similar to the popup options, except that a list is always displayed. Figure 60 is an example of an AP05 Interface data entry screen that contains a list [14].

11. Movement in Data Entry Screens with the Keyboard

In a data entry screen, movement flows from top to bottom and left to right. The following keys allow you to maneuver in data entry screens with the keyboard [14]:

Tab—Selects the next data field or data entry screen control.

Shift+Tab—Selects the previous data field or data entry screen control.

Up/Down Arrows—Within a list or popup control, the Up/Down Arrows move up and down through the list or popup options, item-by-item.

Home and **End**—Within a list or popup control, Home and End select the first and last item in the list or popup option.

PgUp and **PgDn**—Within a list or popup control, PgUp and PgDn display the previous or next window in the list or popup control.

Enter—When in a data field, pushbutton, radio button, popup control, or list, Enter selects the next data field or data entry screen control once all associated processing for the current data field or data entry screen control has been completed.

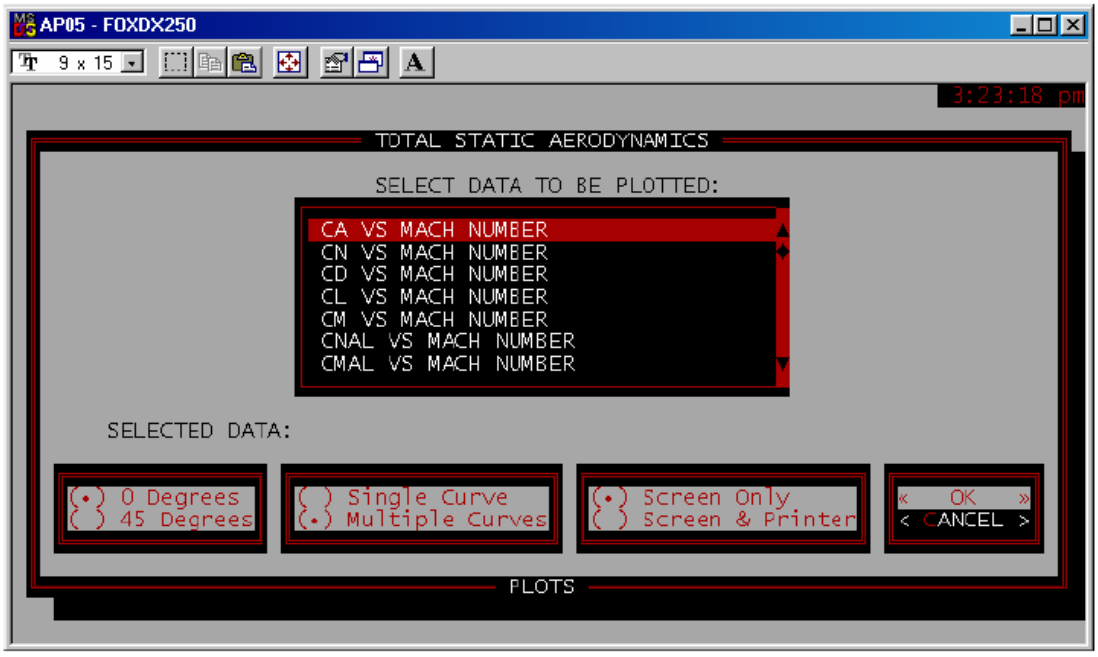

Figure 60. Example AP05 Interface Data Entry Screen Containing a List.

F. COMMON FUNCTIONS

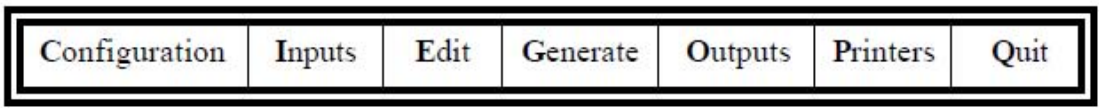

Figure 61. Menu Options.

1. Configuration/New

The New menu option is always enabled. By choosing the New me nu option, the user can begin the process of defining an aeroprediction configuration that can be processed by the AP05 code [14].

Figure 62. Configuration Sub-menu Options.

2. Configuration/Open

By choosing the Open menu option, the user can gain access to aeroprediction configuration files that have already been completed. The Open menu option will be enabled only when there are aeroprediction configuration files that have been previously saved by the user [14].

3. Configuration/Save

By choosing the Save menu option, the user can save a completed aeroprediction configuration file for future use. The Save menu option will be enabled only when the input of aeroprediction configuration data has been completed [14].

4. Configuration/Delete

The Delete menu option is useful when the user wants to get rid of any unwanted aeroprediction configuration files that are currently saved. The Delete menu option will be enabled only when there are aeroprediction configuration files that have been previously saved by the user [14].

5. Configuration/Export

By choosing the Export menu option, the user can make an aeroprediction configuration file available to other users for use on their computers [14].

6. Configuration/Import

By choosing the Import menu option, the user can gain access to aeroprediction configuration files that have been generated by another user on another computer [14].

7. Inputs

The Inputs menu pad is the controlling menu pad for the Inputs menu popup. The Inputs menu popup contains the menu options for creating a complete aeroprediction configuration file. When you choose the Inputs menu pad, the Inputs menu popup is displayed. The Inputs menu popup contains the following menu options [14]:

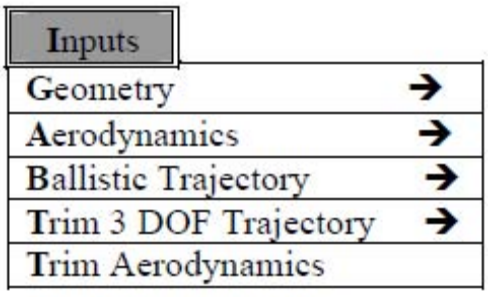

Figure 63. Input Sub-menu Options.

8. Edit

The Edit menu popup contains the menu options for editing selected portions of an aeroprediction configuration. When you choose the Edit menu pad, the Edit menu popup is displayed. The Edit menu popup contains the following menu options [14]:

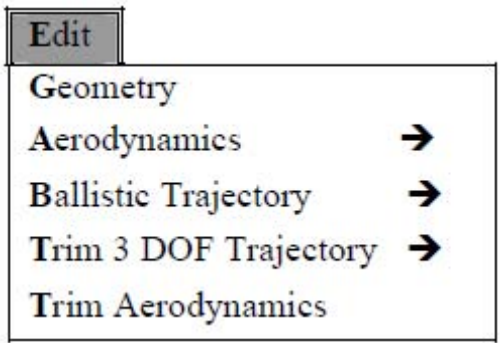

Figure 64. Edit Sub-menu Options.

9. Generate

The Generate menu pad is the controlling menu pad for the Generate menu popup. The Generate menu popup contains the menu options for creating a sketch of the input geometry, for generating aerodynamic coefficients, for generating trim aerodynamics, and for generating ballistic and trim 3 DOF trajectories. When you choose the Generate menu pad, the Generate menu popup is displayed. The Generate menu popup contains the following menu options [14]:

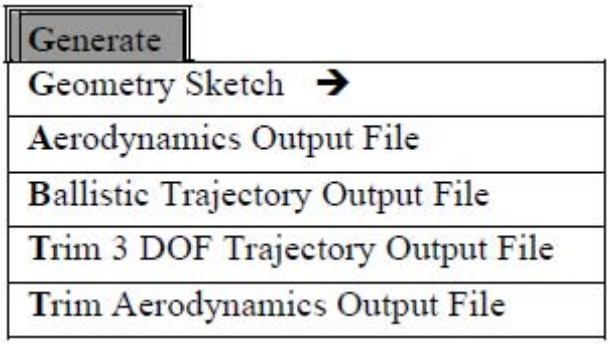

Figure 65. Generate Sub-menu Options.

10 Outputs/Aerodynamics

By choosing the Aerodynamics menu option, the user can begin the process of obtaining aerodynamic output. Upon choosing the Aerodynamics menu option, a second-tier menu popup is displayed containing the following options [14]:

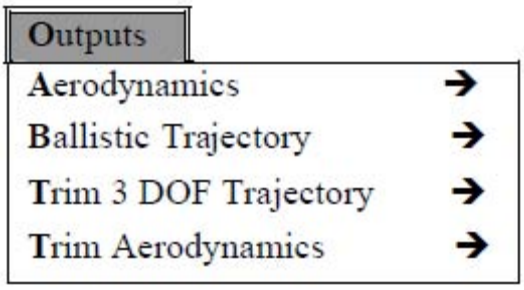

Figure 66. Output Sub-menu Options.

11. Printers

When you choose the Printers menu pad, the Printers menu popup is displayed. The Printers menu popup contains the following menu options [14]:

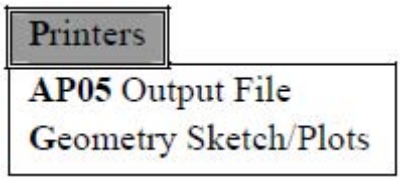

Figure 67. Printers Sub-menu Options.

12. Printers/AP05 Output File

The AP05 Output File menu option is always enabled. By choosing the AP05 Output File menu option, the user can specify the type of printer that aeroprediction output will be routed to. Upon choosing the AP05 Output File menu option, the Aeroprediction-AP05 Output File Printer Selection data entry screen will be displayed. See Section 4.2.10.1 for a discussion on the Aeroprediction-AP05 Output File Printer Selection data entry screen [14].

13. Printers/Geometry Sketch/Plots

The Geometry Sketch/Plots menu option is always enabled. By choosing the Geometry Sketch/Plots menu option, the user can specify the type of printer to which geometry sketches and plots will be routed. Upon choosing the Geometry Sketch/Plots menu option, the Aeroprediction-Geometry Sketch/Plots Printer Selection data entry screen will be displayed. See Section 4.2.10.2 for a discussion on the Aeroprediction-Geometry Sketch/Plots Printer Selection data entry screen [14].

G. EXAMPLE – CREATION OF A M549, 155MM PROJECTILE PROFILE

1. Creation of New Geometry Template

To begin, click on the ”AP05” icon on the desktop to start AP05. Create a new working template by selecting <Configuration> <New> <Body-Alone>. This generates a new geometry profile for the projectile to be designed and built upon.

2. Input Projectile Geometrical Parameters

Inputs/Geometry. Select the appropriate unit for the geometry parameters to be measured and based upon. In this example, the unit selected is millimetres.

Figure 68. Input/Geometry.

Body-Alone Geometry. This menu option allows the parameters of the nose, afterbody and boattail to be specified and input.

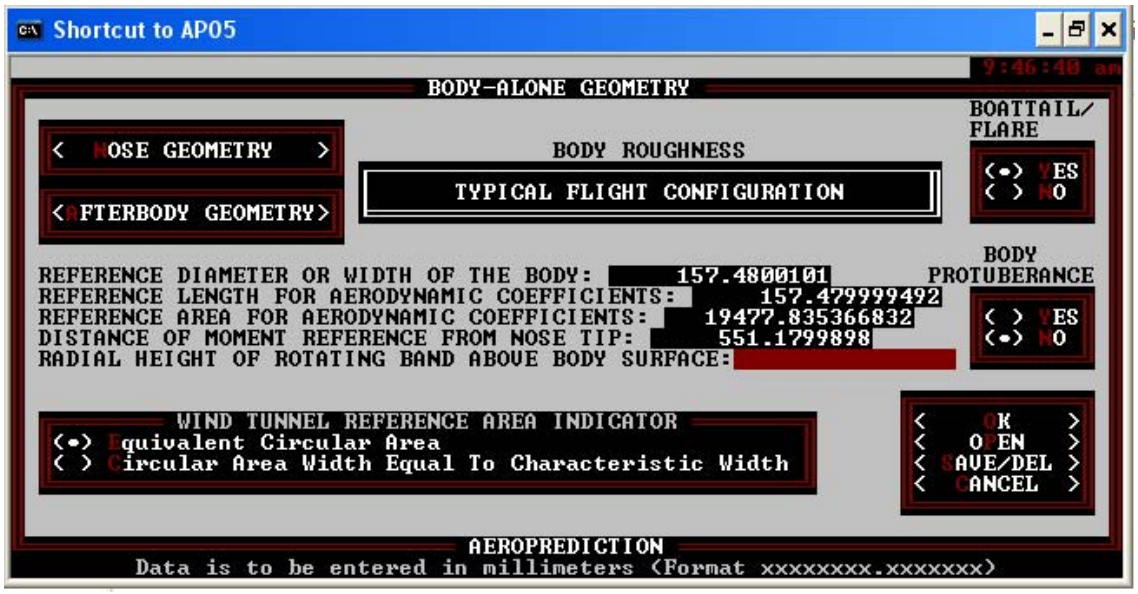

Figure 69. Body-Alone Geometry.

Body-Alone Geometry/Nose Geometry. This menu showcases the different type of nose profiles that are available and allows the user to choose the desired nose profile. In this case, the nose profile is TANGENT OGIVE TRUNCATED and the circular radius at the end of the nose is 3.1mm.

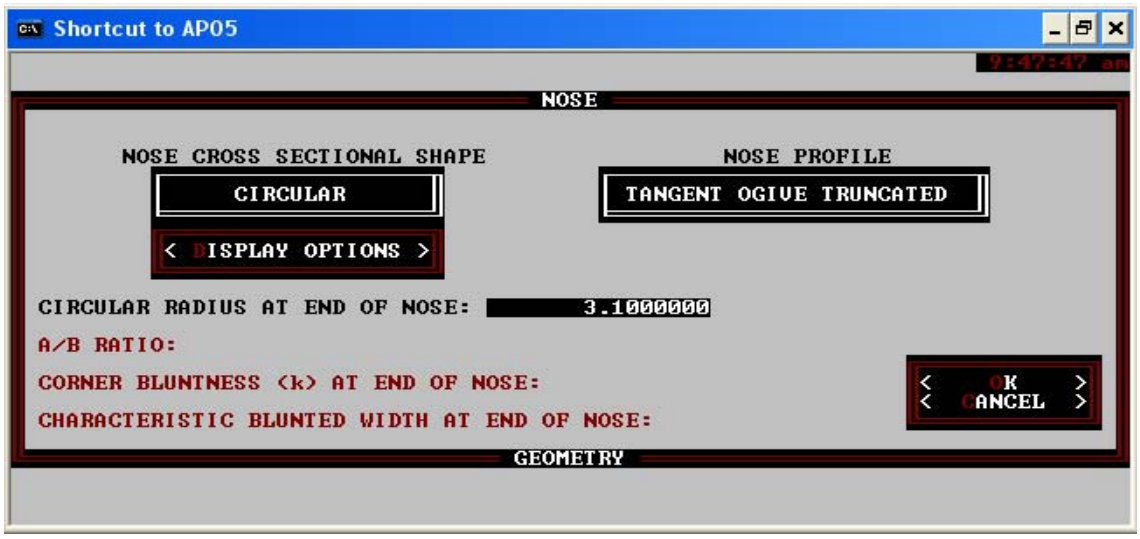

Figure 70. Body-Alone Geometry/Nose.

Body-Alone Geometry/Afterbody. This menu allows the afterbody profile to be specified. In this example, the afterbody profile selected is STANDARD, i.e., there is only one segment of afterbody. If more than one afterbody segments were required, the afterbody profile OTHER can be selected.

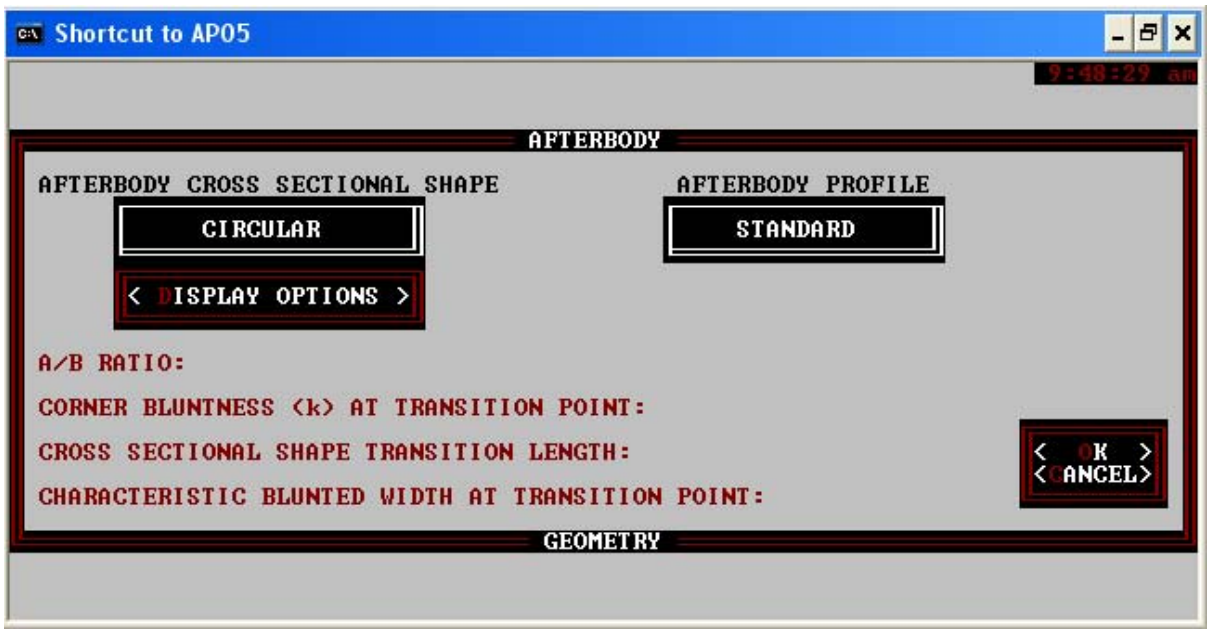

Figure 71. Body-Alone Geometry/Afterbody.

Body-Alone Geometry/Boattail/Flare. This menu allows the dimensions of the boattail to be specified. If there were no boattail requirement, this menu is disabled. In this example, the longitudinal boattail/flare coordinate from nose tip is 888.97458mm and the corresponding boattail/flare characteristic half width is 68.30696mm.

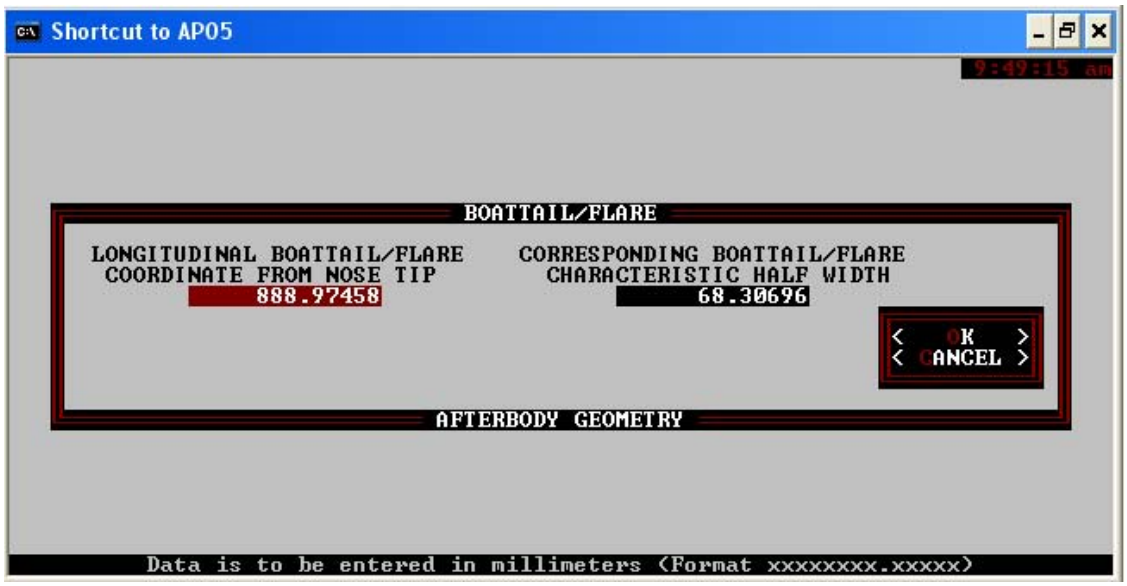

Figure 72. Body-Alone Geometry/Boattail/Flare.

Configuration/Save. Always SAVE the file after every change. In this case, the file is saved under the file name M549.

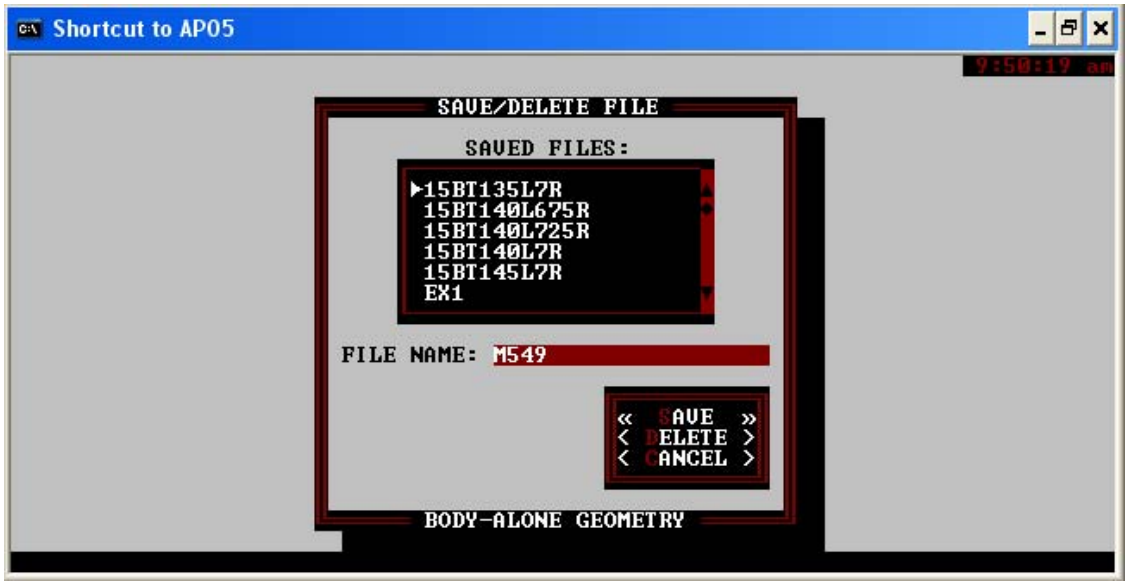

Figure 73. Configuration/Save.

3. Input Aerodynamics Parameters

Edit/Aerodynamics/Free-Stream Conditions. By selecting <Edit> <Aerodynamics> <Free-Stream Conditions>, the aerodynamic parameters like projectile speed in Mach number and angle of attack can be specified.

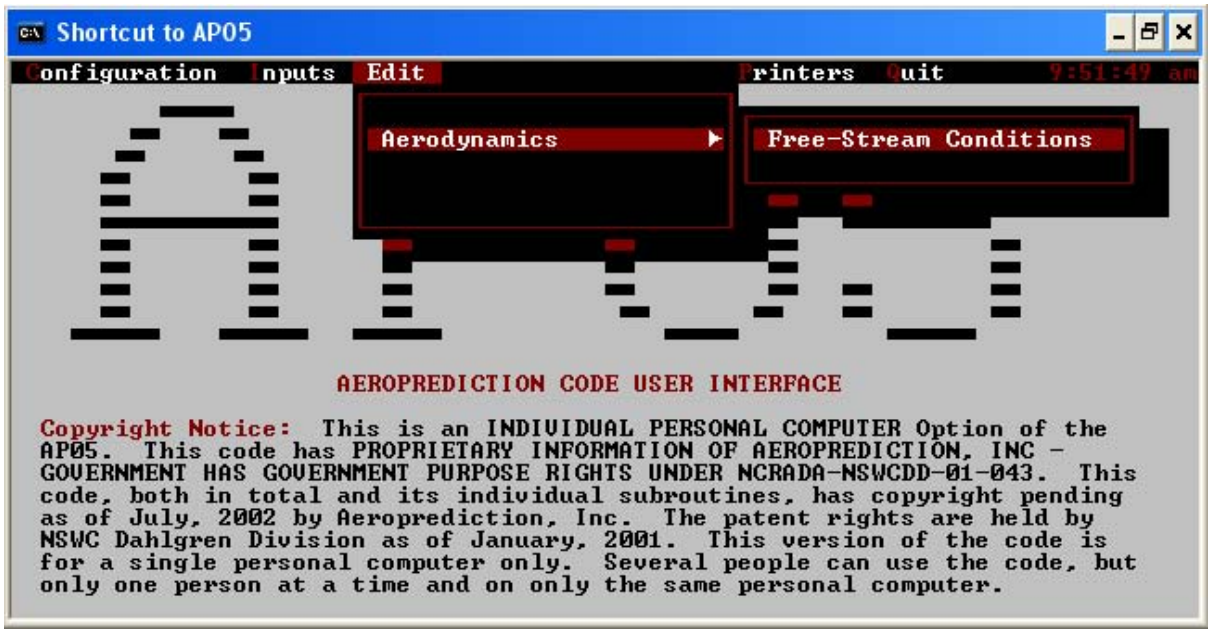

Figure 74. Edit/Aerodynamics/Free-Stream Conditions

Edit/Aerodynamics/Free-Stream Conditions/Alpha Sweep. This menu allows the user to select the initial angle of attack, final angle of attack, interval size between the initial and final angle of attack, Reynolds number and Mach numbers. In this example, the initial angle of attack is set to 0 degree, the final angle of attack is set to 3 degrees with an interval size of 1 degree. The Reynolds number is set by specifying the <Altitude> option with at a height of 30,000 m. The Mach number set is 0.10, 0.20, 0.30, 0.50, 0.60, 0.70, 0.80, 0.90, 1.00, 1.50, 2.00, 3.00, 4.00, 5.00 and 6.00.

Figure 75. Edit/Aerodynamics/Free-Stream Conditions/Alpha Sweep.

Configuration/Save. Always SAVE the file after every change. In this case, the file is saved under the file name M549.

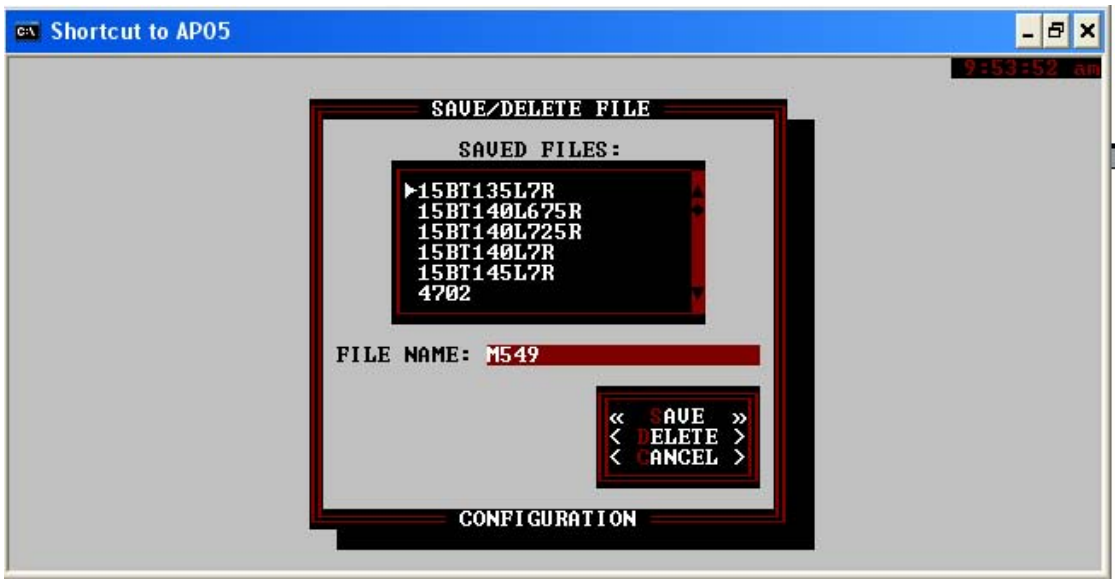

Figure 76. Configuration/Save.

4. Generate Projectile Profile

Generate/Geometry sketch. This option allows AP05 to generate the geometry stretch of the model. In this case, a geometry profile of M549, 155mm artillery projectile is generated.

Figure 77. Generate/Geometry Sketch.

Generate/Aerodynamic Output File. This option allows AP05 to process the aerodynamic output file. The processing time is usually less than a minute and will end with the message stating aerodynamic output file processing completed.

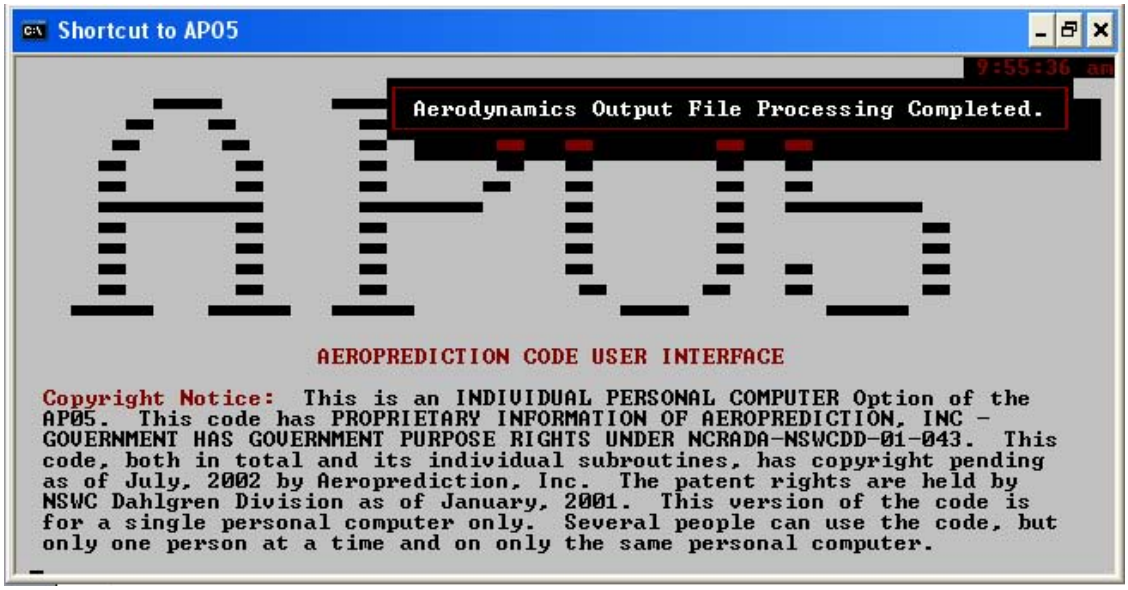

Figure 78. Generate/Aerodynamic Output File.

5. Outputs

Outputs/Aerodynamics. This option allows the aerodynamics output to be displayed, saved, copied or printed. However, the <print> function is not available.

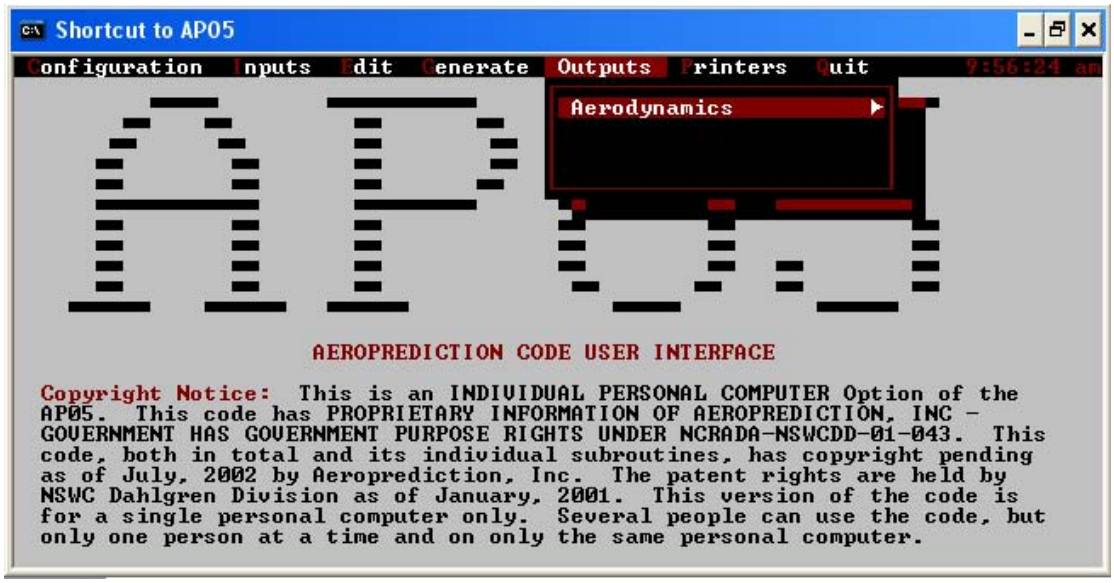

Figure 79. Output/Aerodynamics.

Outputs/Aerodynamics/Aerodynamics Output File. This option allows the aerodynamic output file to be exported out.

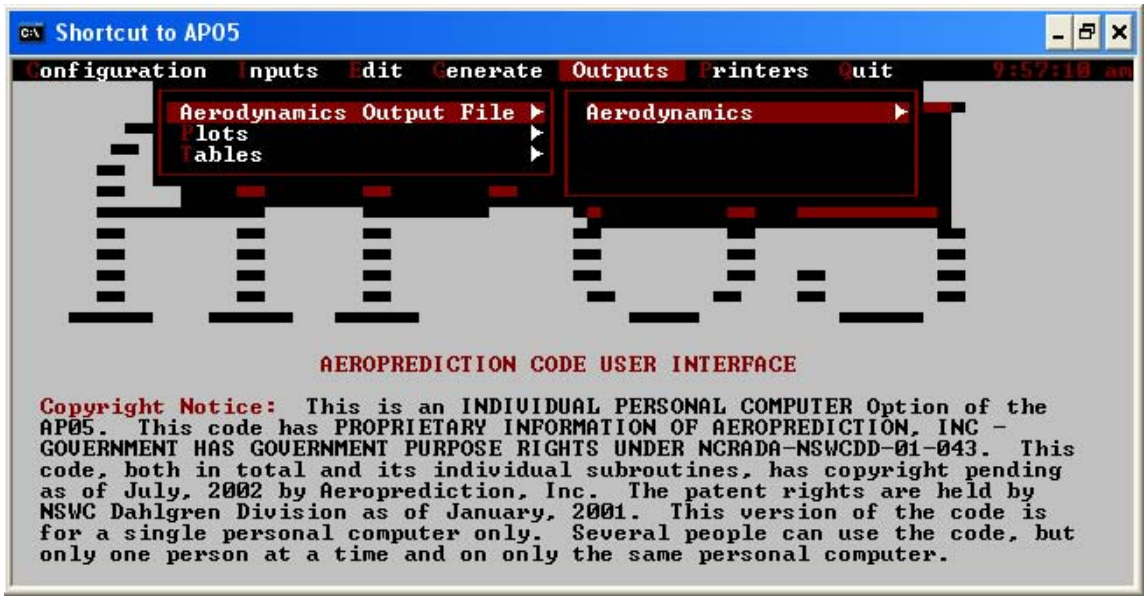

Figure 80. Output/Aerodynamics/Aerodynamic Output File.

Outputs/Aerodynamics/Aerodynamics Output File/Save. There are four options available for the aerodynamic output file to be exported, namely <Save>, <Screen>, <Printer> and <Copy>. The output file is usually <Copy> into a “txt” file. MS Excel is used to plot the data. The <Printer> option is not available.

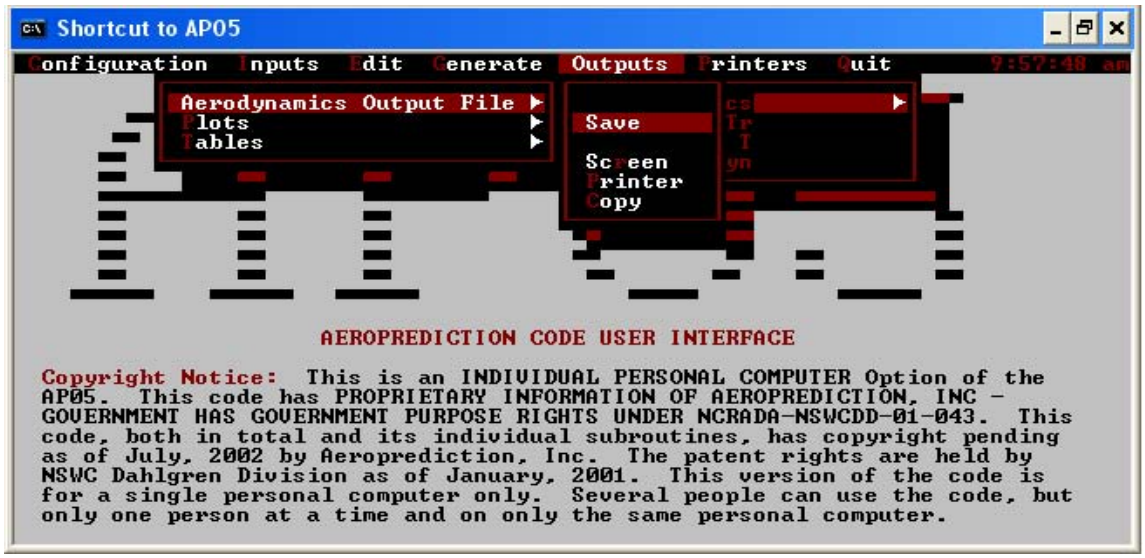

Figure 81. Output/Aerodynamics/Aerodynamic Output File/Save.

Outputs/Aerodynamics/Aerodynamics Output File/Plots/Total Static Aerodynamics. There are two options for the aerodynamics output to be displayed, namely through the use of plots or table.

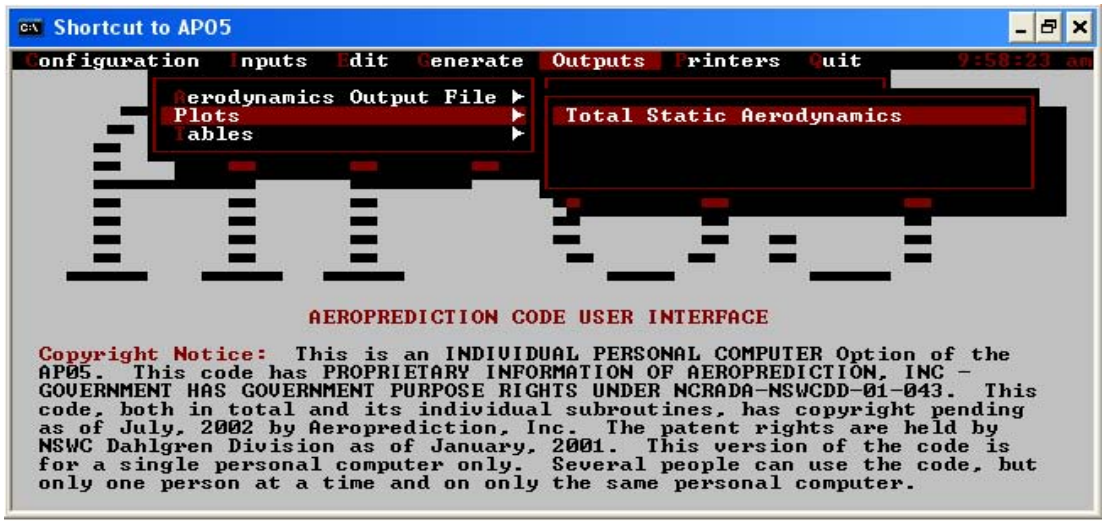

Figure 82. Output/Plots/Total Static Aerodynamics.

Outputs/Aerodynamics/Aerodynamics Output File/Plots/Total Static Aerodynamics. There are various data that AP05 can plot and the user can selected the desired data to be plotted and displayed. This options also allows multiple curve to be plotted overlay on top of one another.

Figure 83. Output/Plots/Total Static Aerodynamics/Select Plot Data.

THIS PAGE INTENTIONALLY LEFT BLANK

INITIAL DISTRIBUTION LIST

1. Defense Technical Information Center
   Ft. Belvoir, Virginia

2. Dudley Knox Library
   Naval Postgraduate School
   Monterey, California

3. Professor and Chairman Knox Millsaps
   Department of Mechanical Engineering and Aeronautical Engineering
   Naval Postgraduate School
   Monterey, California

4. Professor Maximilian Franz Platzer
   Department of Mechanical Engineering and Aeronautical Engineering
   Naval Postgraduate School
   Monterey, California

5. Professor Garth Hobson
   Department of Mechanical Engineering and Aeronautical Engineering
   Naval Postgraduate School
   Monterey, California

6. Professor Anthony Gannon
   Department of Mechanical Engineering and Aeronautical Engineering
   Naval Postgraduate School
   Monterey, California

7. Professor Yeo Tat Soon
   Temasek Defence Systems Institute
   National University of Singapore
   tdshead@nus.edu.sg

8. Ms. Tan Lai Poh
   Temasek Defence Systems Institute
   National University of Singapore